THESIS

SELECTED FACTORS AFFECTING MEASUREMENT OF THE HYDRAULIC CONDUCTIVITY OF GEOSYNTHETIC CLAY LINERS

Submitted by

Monika Aprianti Popang

Department of Civil and Environmental Engineering

In partial fulfillment of the requirements

For the Degree of Master of Science

Colorado State University

Fort Collins, Colorado

Summer 2018

Master's Committee:

Advisor: Joseph Scalia IV
Co-Advisor: Charles D. Shackelford

Michael J. Ronayne

ABSTRACT

SELECTED FACTORS AFFECTING MEASUREMENT OF THE HYDRAULIC CONDUCTIVITY OF GEOSYNTHETIC CLAY LINERS

Geosynthetic clay liners (GCLs) are thin (~7 to 10 mm), factory manufactured hydraulic barriers typically comprising a layer of sodium bentonite sandwiched between two geotextiles. Upon hydration and permeation with water at low effective stress (σ´) (e.g., typically ≤ ~30 kPa [4 psi]), the bentonite in GCLs, which typically is initially in an air-dried condition, swells to form a low hydraulic conductivity (*k*) layer (i.e., *k* of ~2-3×10^{-11} m/s) that is suitable for use as a barrier in hydraulic and chemical containment applications. However, adverse physico-chemical interactions between the bentonite in GCLs and both the hydrating and permeating liquids may yield substantially higher *k* than what is typically acceptable for design (i.e., *k* ≤ 1×10^{-9} m/s). Accordingly, this study pertained to evaluating the effects of the type of permeant liquid and the magnitude of σ´ on the measurement of *k* of two GCLs, a higher grade needle-punched (HGN) GCL and a lower grade needle-punched (LGN) GCL. The permeant liquids included tap water (TW), conservative water (CW), and several calcium chloride ($CaCl_2$) solutions, and the σ´ included 27.3 kPa (4 psi) and 61.7 kPa (9 psi). The resulting measured ratios of final *k* for the HGN GCL relative to the LGN GCL ($k_{f\,HGN}/k_{f\,LGN}$) at ~24-27 kPa (4 psi) were ~28 (1.5 orders of magnitude), ~194 (2.3 orders of magnitude), and ~1975 (3.3 orders of magnitude) based on permeation with 5, 10, and 20 mM $CaCl_2$, respectively. Thus, an increase in the fiber bundles density of the needle-punched fibers of the GCL adversely impacted the *k* of this GCL. Tests using dyed permeant liquids revealed that the high *k* was attributable to preferential flow along the fiber bundles of the GCL. Also, an increase in σ´ from 27.3 kPa (4 psi) to 61.7 kPa (9 psi) did not appreciably impact the measured *k*. Finally, permeation of the HGN GCL with the more dilute liquids (TW, CW, 1 and 2.5 mM $CaCl_2$) resulted in consistently low *k* of ~2×10^{-11} m/s. The results of this study also illustrate the importance of achieving not only hydraulic equilibrium but also chemical equilibrium before terminating the *k* tests, as the measured *k* at hydraulic equilibrium based on the higher ionic strength solutions (i.e., 5, 10, and 20 mM $CaCl_2$) typically were lower and, therefore, more unconservative than the measured *k* at chemical equilibrium.

This study also evaluated the use of different methods to measure the k of the HGN GCL, including the falling headwater, constant tailwater method and the constant rate-of-flow method using a flow pump with pressure transducers. The results indicated that neither method proved substantially effective at achieving chemical equilibrium faster, although employing higher hydraulic gradient (i) was shown to expedite the attainment of chemical equilibrium. This result is associated with flushing action in the intergranular pore spaces that effectively maintaining higher concentration gradient between within and outside the bentonite granules. Also, prehydrating the specimens with the permeant liquid tended to enhance the osmotic swell of the bentonite resulting in a lower k at lower pore volumes of flow. Finally, diffusion of solutes from interlayer to intergranular pore spaces within the GCL specimens permeated with CW was shown to be the rate-limiting mechanism for attaining chemical equilibrium.

ACKNOWLEDGMENTS

This study would not be possible without the scholarship awarded by the Fulbright Program, sponsored by the U.S. government. Immense gratitude to the organizing institutions from both countries, American Indonesian Exchange Foundation (AMINEF) and Institute of International Education (IIE) whose resources have been valuable during the span of my program. Additional awards from Colorado State University and Department of Civil and Environmental Engineering are also greatly acknowledged.

I am sincerely grateful to my Master's committee members, to whom I owe a great deal, as they have been more than helpful during the completion of this thesis. To Dr Joseph Scalia whose knowledge, guidance, and constructive comments has helped me to carry out this research and to write this thesis. To Dr Charles Shackelford for his time, encouragement, and thoughtful criticism over the course of the research and eventually facilitates the betterment of this thesis. To Dr Michael Ronayne for his insightful dialogues and cooperativeness prior to my defense and thereafter.

Special thanks to Mr Joseph Wilmetti and Mr Logan Pokallus for their assistance on the equipment maintenance and troubleshooting.

Thank you to the rest of student members of Geo-Institute at CSU, for their continuous support for the past two years.

Thank you to my family, for their abundant prayers throughout this journey.

TABLE OF CONTENTS

LIST OF TABLES

LIST OF FIGURES

CHAPTER 1 INTRODUCTION

1.1. General Background

The major function of environmental containment systems is to prevent (or minimize) seepage to underlying groundwater. Traditionally, in the United States, compacted clay has been widely employed as a liner material because of the low hydraulic conductivity (k) of compacted clay. In late 1980s, geosynthetic clay liners (GCL) were created as a relatively inexpensive and easy to install alternative to compacted clay liners. Geosynthetic clay liners, are thin (~7 to 10 mm) manufactured hydraulic barrier consisting of bentonite bonded to a layer, or sandwiched between layers, of geosynthetics materials (ASTM D4439-17 2017).

1.2. Problem Statement

Sodium bentonite (Na-bentonite) has the potential for incompatibility when exposed to non-standard solution (viz., solutions other than water). As a result, testing to chemical equilibrium is necessary to determine the anticipated performance of GCL to different leachate solutions prior to use in the field. However, depending on the characteristics of the GCL and permeant liquid, as well as the effective stress applied, the time for a specimen to achieve chemical equilibrium may take months to years. Therefore, there is a need to identify the most expeditious method of determining the k of a GCL to a given chemical solution in the minimum amount of time.

There are several methods available for k testing, include (1) constant head, (2) falling headwater, constant tailwater, (3) falling headwater, rising tailwater, and (4) constant rate-of-flow. Aiban and Znidarcic (1989) assessed the rapidity of k testing of clayey materials via the constant rate-of-flow method (i.e., flow pump) relative to other available methods, and reported that the constant flow method could measure equilibrium k more rapidly. However, Aiban and Znidarcic (1989) did not evaluate k at chemical equilibrium, nor k testing of GCL.

Finally, GCLs are being increasingly used in application in which high shear strength is required. GCLs are engineered to overcome the low strength of Na-bentonite by needle punching bundles of

geosynthetic (polymer) fibers across the profile of the GCL. These fibers act to resist internal shearing failure. To meet the need for high shear strength GCLs, manufacturers are constructing heavily needle-punched GCLs. However, the impact of increasing the needle punching on k has not been reported.

1.3. Objective

This study is divided into two sections. Part one (CHAPTER 2) investigates the k of high shear strength GCL to an array of permeant liquids. Part two (CHAPTER 3) explores factors affecting the time to meet termination criteria for GCL hydraulic compatibility tests. The objectives of this study are as listed as follows,

1. to evaluate the k of high peel-strength GCL permeated with various solutions;
2. to compare k of high peel-strength GCL with a lower peel-strength GCL; and
3. to investigate factors affecting the time to chemical equilibrium in k testing.

CHAPTER 2 HYDRAULIC CONDUCTIVITY OF A HIGH PEEL-STRENGTH GCL UNDER LOW EFFECTIVE STRESS

2.1. Introduction

Geosynthetic clay liners (GCLs) are manufactured hydraulic barriers comprising a clay bound to a layer or layers of geosynthetic materials (see APPENDIX A). Commonly, GCLs comprise two geotextiles, i.e. bottom (carrier) and top (cover) geotextiles, that encase a layer of sodium bentonite. The hydraulic conductivity (k) of a typical GCL permeated with water under low effective stress (σ') of ~27.3 kPa (4 psi) is on the order of $\sim 2 \times 10^{-11}$ m/s (Shackelford et al. 2000). GCLs are typically needle punched or stitched through the bentonite to maintain the integrity of the GCL during transport and installation, and to enhance internal shear strength after installation. For needle-punched GCLs, the cover geotextile component must be non-woven, while the carrier geotextile can be non-woven or woven. Without reinforcing, the friction angle of the hydrated bentonite component of GCLs may be as low as 6° (Shan & Daniel 1991; Trauger et al. 1997), limiting the use of GCLs on side slopes due to concerns for stability. To increase the internal shear strength, GCLs are produced with varying magnitudes of needle punching (Trauger et al. 1997).

Peel-strength is used as an indicator for the internal shear strength of GCLs (Bareither et al. 2018). Higher peel-strength corresponds to greater internal shear strength, typically achieved through increased needle punching in the GCL. High peel-strength GCLs are produced for high shear stress applications, such as in mining operations. For example, in a lined heap leach pad, ore piles may be as high as 100 to 240 m, equivalent to an applied normal stress up to 4 MPa (Lupo 2010). This normal stress equates to a maximum shear stress of 0.12 MPa if the heap leach pad grades at 3% for the purpose of inducing drainage of the leachate.

The potential for incompatibility arises when GCLs are exposed to chemical solutions. In the case where a GCL will be used to contain a chemical solution, k testing with the chemical solution as the permeant liquid is necessary to determine if the GCL will be effective in containing the solution. To assess long-term behavior, measurement of k at chemical equilibrium between the effluent (outflow) and influent (inflow) is necessary. Hydraulic conductivity of high peel-strength GCLs has not been reported in the literature. The

objective of this study is to evaluate the hydraulic behavior of a high peel-strength GCL permeated with a variety of inorganic chemical solutions, and to compare the resulting hydraulic behavior to that of lower peel-strength (standard) GCL.

2.2. Materials and Methods

2.2.1. Liquids

Tap water (TW), conservative water (CW), and calcium chloride ($CaCl_2$) solutions were used as permeant liquids. The properties of these liquids are summarized in Table 2.1. The TW was used as a reference solution, and is recommended as a 'standard' permeant liquid in ASTM D5084-16a (2016). The properties of the TW used in this study were reported by Tong and Shackelford (2016). The measured electrical conductivity (*EC*) and pH of TW were reported as 13 mS/m and 7, respectively. The CW as defined by Scalia and Benson (2010a) and ASTM D5084-16a (2016) was used in this study to mimic pore water that is representative of conservative field hydration and permeation conditions. The CW was prepared by dissolving 15.5 mg NaCl (ACS Grade; Fisher Chemical, Fair Lawn, NJ) and 279.5 mg $CaCl_2 \cdot 2H_2O$ (ACS Grade; Fisher Chemical, Fair Lawn, NJ) into 1 L of de-ionized water (DIW). The $CaCl_2$ solutions, with $CaCl_2$ concentrations ranging from 1 to 20 mM, were used to assess the potential adverse impact on k due to exchange of Ca^{2+} for Na^{+} resulting in reduced bentonite swelling. The concentrations of $CaCl_2$ were selected to allow comparison to previously reported results of tests conducted to evaluate the long-term hydraulic behavior of GCLs (e.g., Jo et al. 2005; Lee & Shackelford 2005b). The *EC* and pH values of permeant liquid batches were measured using benchtop electrodes (Thermo Scientific™, Models 013005MD and 8157BNUMD, Waltham, MA) to ensure that no substantial fluctuation ($\geq \pm 5\%$ from the values reported in Table 2.1) in the liquid chemistry occurred. The range of *EC* for the permeant liquids was within 1.5 orders of magnitude. The measured pH ranged from neutral (TW, DIW) to slightly acidic upon addition of $CaCl_2$ to DIW.

2.2.2. Geosynthetic Clay Liner

A high peel-strength GCL (manufacturer reported peel-strength, MRPS) of 3500 N/m (20 lb/in) manufactured by CETCO® under the trade name BENTOMAT® DN9 was used in this study. The GCL comprised a layer of granular sodium bentonite (Na-bentonite) sandwiched between two non-woven geotextiles reinforced by needle punching without thermal treatment. Detailed properties of this bentonite and GCL are presented in Tables 2.2 and 2.3. The GCL was ~8.9 mm thick in the as-received condition and the mass per unit area of bentonite was ~6.4 kg/m^2 (ASTM D5993-14 2014). Detail on methods to determine needle punching fibers properties are provided by Ghazizadeh and Bareither (submitted 2018; under review).

Particle-size distributions for the Na-bentonite from the GCL are presented in Figure 2.1. Particle-size distributions are reported for both mechanical sieve (air dried) and hydrometer (wet) analyses. Bentonite in the as-received (air dried) condition classified as poorly graded sand, SP (ASTM D2487-17 2017), whereas the hydrated bentonite classified as a high plasticity clay, CH (ASTM D2487-17 2017).

The swell index (*SI*) of the Na-bentonite extracted from the GCL was measured according to ASTM D5890-11 (2011) in each permeant liquid and the resulting values are reported in Table 2.2. As expected, the *SI* was inversely related to the measured *EC* of the permeant liquid (Katsumi et al. 2007).

2.3. Hydraulic Conductivity Tests

A summary of the *k* testing program conducted in this study is provided in Table 2.4. All tests were conducted in flexible-wall permeameters without application of backpressure (Conzelmann et al. 2017). Figure 2.2 contains a schematic of the test setup. All specimens were prehydrated for at least 48 h and subsequently permeated with the same liquid. Tests were not terminated before the hydraulic and chemical termination criteria detailed in ASTM D6766-18 (2018) had been achieved. These criteria include (1) a volumetric ratio of outflow-to-inflow (Q_{out}/Q_{in}) within 1±0.25, (2) *k* within 50 % of the mean *k* of at least three consecutive data points without any indication of an upward or downward trend, and (3) a ratio of outflow-to-inflow *EC* (EC_{out}/EC_{in}) within 1±0.10.

Prior to testing, circular specimens with a diameter, *d*, of 152.4 mm (6 in) were cut with a scalpel blade from a roll of GCL. To prevent loss of bentonite from the GCL during cutting, a small amount of DIW was applied around the rim of the exposed bentonite via a squirt bottle. After the circular specimen was detached from the GCL sheet, any protruding geotextile fibers were trimmed manually with scissors. Each specimen was placed in a flexible-wall permeameter with the cover geotextile facing the inflow (bottom) side between two filter papers (Whatman™, Buckinghamshire, UK) and two fiberglass insulation sheets (mass/area=0.41 kg/m^2) used in lieu of porous stones. The procedure for assembly of GCL within a flexible-wall permeameter was the same as that described by Scalia and Benson (2010a).

After the termination criteria were achieved, inflow and outflow lines were drained, the flexible-wall cell was disassembled, and the specimen was removed. The total weight of the GCL specimen was measured (± 0.01 g), together with measurements of thickness, *L* (± 0.01 mm), with a caliper at six locations around the perimeter of the specimen. The average *L* of the specimen used to calculate k and the pore volume of the specimen (i.e., the thickness of the specimen during permeation was assumed to be the same as the final thickness of the specimen after termination of the test).

Specimens permeated with 5 mM $CaCl_2$ (Test Series 5) and 10 mM $CaCl_2$ (Test Series 6) were subjected to a sequential increase of σ´ from ~27.3 kPa (4 psi) to ~61.7 kPa (9 psi). For these tests, the final thickness of the specimen after termination of the test also was used to calculate the k and pore volumes of the specimen subjected to the lower σ´, i.e., since the thickness of the specimen under the lower σ´ could not be determined. The error associated with the calculated k based on this assumption is considered to be relatively minor. Also, since the specimen likely was the thinnest after termination of the test, use of the final specimen thickness should have resulted in conservative (high) values of k for the specimens at the lower σ´.

2.4. Results and Discussion

The results of all k tests performed at σ´ of ~27.3 kPa (4 psi) are summarized in Table 2.5. Each test result is accompanied by the elapsed time (*t*), pore volumes of flow (PVF), the final degree of saturation (*S*), and the final gravimetric water content (*w*) measured at test completion. Specimens permeated with TW, 1

and 2.5 $CaCl_2$ (Test Series 1, 3, and 4) were terminated prior to achieving chemical equilibrium because the durations of these tests were extensive (83 to 283 d), and no data for similar tests were available in the literature for comparison. Only specimens permeated with CW (Test Series 2) were continued, for future comparison with available results from other GCLs. Thus, the k and PVF values reported in Table 2.5 for these tests represent estimates based on an assumed L of 7.5 mm.

There are three sets of t, PVF, and k values presented in Table 2.5. The values with the 5084 subscript (t_{5084}, PVF_{5084}, k_{5084}) pertain to those based on the hydraulic termination criteria in ASTM D5084-16a (2016). The values with the 6766 subscript (t_{6766}, PVF_{6766}, k_{6766}) pertain to those based on the hydraulic and chemical termination criteria in ASTM D6766-18 (2018). The values with the f subscript (t_f, PVF_f, k_f) pertain to the final values at the end of permeation. The values of S were determined following the procedure described by Conzelmann (2017). Measured S ranged from 92 % to 105 % and are in general agreement with the conclusion by Conzelmann et al. (2017) that specimens with this range in S can be assumed to be saturated at the end of permeation without backpressure. The final w of the bentonite component of the terminated tests ranged from 85 % to 125 %. Generally, GCL specimens permeated with the dilute permeant liquids yielded lower k (~2×10^{-11} m/s), whereas permeation with intermediate strength $CaCl_2$ solutions (5, 10, and 20 mM $CaCl_2$) yielded uncharacteristically high k relative to values previously reported for GCLs permeated with the same $CaCl_2$ solutions (e.g., Jo et al. 2005; Lee & Shackelford 2005b).

2.4.1. Observed Temporal Behavior

The results of Test Series 1 to 7 (TW, CW, 1, 2.5, 5, 10, and 20 mM $CaCl_2$) are shown in Figure 2.3 to Figure 2.9, respectively. Trends observed can be distinguished into two groups based on the strength of the permeant solution and resulting k behavior, viz., dilute solutions and intermediate strength solutions.

Dilute Strength Solutions

Solutions characterized as dilute strength include TW, CW, 1 and 2.5 mM $CaCl_2$. All tests permeated with dilute solutions exhibited an initial steep decrease in k to values ≤ 3×10^{-11} m/s at ≤ 8 PVF (Table 2.5).

Thereafter, k increased minimally due to cation exchange. Despite slight differences in trends between 5 to 8 PVF for Tests 2a and 2b, the values of k with the duplicated tests are within a factor of ~1.9 and, therefore, are considered reproducible (ASTM D6766-18 2018).

The trends exhibited in terms of effluent *EC* also were similar for all tests permeated with dilute solutions. The *EC* values initially were high, then decreased rapidly coincident with decreasing k, and finally decreased slowly towards an *EC* ratio = 1.0±0.1 at low k. For the results of Test Series 2, a unique subsequent slight increase in *EC* ratio was present for both specimens, suggesting some fundamental mechanism for the behavior. However, the reason for this behavior is unknown. For all tests, pH_{out} increased initially and then stabilized at ~1.2pH_{in} for TW and ~1.6pH_{in} for CW, 1, and 2.5 mM $CaCl_2$.

Intermediate Strength Solutions

The temporal trends exhibited by GCL specimens permeated with intermediate strength solutions, i.e., 5, 10, and 20 mM $CaCl_2$, were similar to those described by Shackelford (2008) where the initial k decreased towards a minimum hydraulic conductivity (k_{min}) upon swelling of bentonite granules and eventually increased in response to cation exchange until a state of equilibrium was achieved. For the specimen permeated with 5 mM $CaCl_2$ (Test Series 5), k_{5084} was ~2×10^{-10} m/s, which also represented k_{min}, then k increased to k_{6766} of ~1.1×10^{-9} m/s and subsequently to k_f of ~2.4×10^{-9} m/s. The k_{6766} for the specimens permeated with 10 mM $CaCl_2$ (Test Series 6) were ~1.2×10^{-8} m/s and ~2.9×10^{-8} m/s. The trend in k for Test 6a was similar to that based on the specimen permeated with 5 mM $CaCl_2$, where the k steadily decreased towards k_{5084} and k_{min} of ~5.8×10^{-9} m/s and then increased to k_{6766} of ~1.2×10^{-8} m/s and k_f of ~1.3×10^{-8} m/s at 24 PVF. The trend for Test 6b was also similar to that of Test 6a, although the k_{6766} was somewhat higher at ~2.9×10^{-8} m/s. The k_{6766} for the specimens permeated with 20 mM $CaCl_2$ (Test Series 7) of ~1.6×10^{-7} m/s and ~2.1×10^{-7} m/s were achieved within 8 PVF.

Given these relatively high measured k for the specimens permeated with 5 and 10 mM $CaCl_2$, the σ' for these specimens was sequentially increased from 27.3 kPa (4 psi) to ~61.7 kPa (9 psi). Upon increase of σ', k of specimen permeated with 5 mM $CaCl_2$ (Test Series 5) equilibrated at ~2.3×10^{-10} m/s, or slightly lower

than the k_{min} previously attained under ~27.3 kPa (4 psi), whereas the specimens permeated with 10 mM $CaCl_2$ (Test Series 6) equilibrated to k values of ~8.7×10^{-9} m/s and ~2.1×10^{-8} m/s, which were only marginally lower to the values for k_f of ~1.2×10^{-8} m/s and ~2.9×10^{-8} m/s previously established under ~27.3 kPa (4 psi).

In contrast to the specimens permeated with the dilute solutions, the measured EC_{out}/EC_{in} for the specimens permeated with the intermediate solutions peaked at the beginning of permeation, then reduced rapidly towards EC_{out}/EC_{in} = 1.0±0.1. Also, no subsequent increase in EC_{out}/EC_{in} was observed.

For the specimens permeated with 5 and 10 mM $CaCl_2$, the EC_{out} increased immediately following the increase of σ´. This increase in EC_{out} increased the EC_{out}/EC_{in} to values slightly outside those required for chemical equilibrium that previously had been established. This increase in EC_{out}/EC_{in} likely resulted, in part, from the additional flow of pore water from the specimen due to consolidation resulting from the increase in σ´. However, all tests rapidly re-established chemical equilibrium.

2.4.2. Effect of Increased Needle Punching

In order to explain the uncharacteristically high k associated with the specimens permeated with intermediate strength solutions (Test Series 5 to 7) relative to the k reported in the literature for GCLs permeated with the same solutions and similar σ´, the results of these tests are compared with those for specimens of a lower MRPS GCL reported by Lee and Shackelford (2005b) that were permeated with the same $CaCl_2$ solutions (i.e., 5, 10, and 20 mM $CaCl_2$). Lee and Shackelford (2005b) tested a ~6-mm-thick GCL containing untreated Na-bentonite that was encased between one woven and one non-woven geotextile, affixed together by needle punching and heat bonded (GSE Bentofix® Thermal Lock® NS; MRPS = 440 N/m [2.5 lb/in]). The results from Lee and Shackelford (2005b) corresponding to the GCL with the lower quality bentonite (GCL-LQB) were used for the comparison because the plasticity index (*PI*) and *SI* for the LQB were similar to those for the bentonite of the GCL evaluated in this study. For example, the *PI* and *SI* for the GCL bentonite in this study were 377% and 33.3 mL/2 g (Table 2.2), respectively, whereas the *PI* and *SI* for the LQB bentonite from Lee and Shackelford (2005b) were 393% and 27.5 mL/2 g, respectively. The

k tests in both studies were conducted without backpressure using the falling headwater, constant tailwater method with flexible-wall permeameters. All specimens in both studies were prehydrated for at least 48 h and subsequently permeated with the same liquid. The average σ´ in the middle of the specimen and hydraulic gradient (i) were ~27.3 kPa and ~210 (this study) versus ~23.5 kPa and ~200 (Lee & Shackelford 2005b). The GCL evaluated in this study is referred to hereafter as the GCL with higher grade of needle punching (HGN), whereas the GCL evaluated by Lee and Shackelford (2005b) is referred to hereafter as GCL with lower grade of needle punching (LGN).

The k of the HGN and LGN GCLs are compared in Figure 2.10. Note that, unlike the previous results presented in Section 2.4.1, the elapsed time in Fig. 2.10 does not include the prehydration time of ~48 h to allow for direct comparison of the results between the two studies. Although permeated with a similar range of $CaCl_2$ solutions, the k of HGN GCL were several orders of magnitude higher than the k of the LGN GCL. This difference is hypothesized to be due to the substantially higher quantity of fibers present throughout the HGN GCL (Figure 2.11), which contributed to preferential flow (e.g., see Conzelmann 2017). As a result, measured ratios of final k for the HGN GCL relative to the LGN GCL ($k_{f\,HGN}/k_{f\,LGN}$) for 5 mM $CaCl_2$ was ~28 (1.5 orders of magnitude), $k_{f\,HGN}/k_{f\,LGN}$ for 10 mM $CaCl_2$ was ~194 (2.3 orders of magnitude), and $k_{f\,HGN}/k_{f\,LGN}$ for 20 mM $CaCl_2$ was ~1975 (3.3 orders of magnitude). Hydraulic conductivities reported for the LGN GCL permeated with higher concentration solutions were lower than those for HGN GCL permeated with intermediate concentration solutions. For example, the final k (k_f) of HGN GCL permeated with 5 mM $CaCl_2$ was comparable with that for the LGN GCL permeated with 100 mM $CaCl_2$ (2.4×10^{-9} m/s versus 3.0×10^{-9} m/s), whereas the HGN GCL specimens permeated with 20 mM $CaCl_2$ yielded higher k_f than that for the LGN GCL specimen permeated with 500 mM $CaCl_2$ (1.6×10^{-7} m/s versus 1.2×10^{-8} m/s).

In support of this hypothesis of preferential flow paths, HGN GCL specimens with k higher than 10^{-10} m/s (i.e., those permeated 5, 10, and 20 mM $CaCl_2$ solutions) were permeated with the same solutions tagged with Rhodamine WT dye (Acros Organics, Fair Lawn, NJ), i.e., 20% dye mixed 1:10 by volume with appropriate liquid, after k_{6766} had been established. Rhodamine WT was used due to the distinct bright red

fluorescent color and is commonly used as a visual tracer (Scalia & Benson 2010b). Examples of dyed fiber bundles are shown in Figure 2.12. All dyed specimens were visually confirmed to have preferential flow paths through the needle punching fibers (APPENDIX B).

The HGN GCL permeated with dilute strength solutions (i.e., TW, CW, 1 and 2.5 mM $CaCl_2$) did not yield elevated k (Figure 2.3 to Figure 2.6). Despite a slightly higher *SI* for the bentonite from the HGN GCL relative to that for the bentonite from the LGN GCL (33.3 mL/2 g versus 27.5 mL/2 g), the HGN GCL exhibited k that were orders of magnitude greater when permeated with the intermediate strength solutions. Therefore, *SI* was not an effective indicator of the k for the HGN GCL, since *SI* reflects only the bentonite component of the GCL and, therefore, does not account for preferential flow paths facilitated by the needle-punched fibers. The measured *SI* for the bentonite extracted from the HGN GCL yielded ≥ 15 mL/2 g for all permeant liquids (see Table 2.2), which historically reflects k of at least 10^{-10} m/s (e.g., Lee et al. 2005; Katsumi et al. 2007; Benson & Meer 2009). However, as discussed previously, specimens permeated with as low as 5 mM $CaCl_2$ (*SI* = 22.3 mL/2 g) yielded orders of magnitude higher k than the specimens of the LGN GCL.

A comparison of the difference of time required for HGN and LGN GCLs to reach chemical equilibrium is shown in Figure 2.13. However, the termination criteria for chemical equilibrium imposed in the study by Lee and Shackelford (2005b) were different than those imposed in this study, in that the tests conducted by Lee and Shackelford (2005b) were not terminated until the effluent concentrations of both calcium (Ca^{2+}) and chloride (Cl^-) were within ±10% of those in the influent (source) solutions. As a result, the HGN GCL specimens required considerably less time to achieve chemical equilibrium based on ASTM D6766-18 (2018) than that required for the LGN GCL specimens. This more rapid equilibrium is also hypothesized to have resulted from preferential flow paths and not actual attainment of chemical equilibrium. Permeant liquid that preferentially flows through needle punching fiber bundles does not contact the bentonite within the GCL, and diffusion of ions from the bentonite into the fiber bundle appears to be insignificant relative to the flow through the fiber bundle.

2.4.3. Effect of Termination Criteria Adopted

The k values from Test Series 5, 6, and 7 are compared in Figure 2.14. As shown in Figure 2.14a, k_{5084} based on permeation with the intermediate strength solutions were similar to k_{6766} with exception of Test 5 (5 mM $CaCl_2$) and Test 6a (10 mM $CaCl_2$). The result of Test 5 indicates that, if k was only based on hydraulic equilibrium, k_{min} would be determined as k_{5084}, which is lower and, therefore, less conservative than k_{6766}.

The k_f at ~27.3 kPa (4 psi) are compared versus k_{6766} in Figure 2.14b. The results indicate that, in general, k_{5084} is lower than k_f and, therefore, is unconservative. For the stronger permeant liquids, k_{6766} appears to an adequate measure of k at chemical equilibrium, i.e., $k_{6766} \approx k_f$. Jo et al. (2005) discussed this problem in great detail and recommend a more stringent $EC_{out}/EC_{in} = 1 \pm 0.05$ instead of $EC_{out}/EC_{in} = 1 \pm 0.1$ to provide appropriate and representative k, although the more stringent criterion likely will require longer test durations to achieve.

2.4.4. Effect of Effective Stress

The σ´ of specimens permeated with 5 and 10 mM $CaCl_2$ was increased to ~61.7 kPa (9 psi) after establishing k_f under ~27.3 kPa (4 psi). This sequential increase of σ´ was performed to test whether increased σ´ would overcome the effect of preferential flow along needle punching fiber bundles within HGN GCL. Increased σ´ has been shown to offset the deleterious effects of leachate chemistry on k of GCLs, due to shrinkage of available flow paths (i.e., decrease in void ratio) within the bentonite layer (e.g., Fernandez & Quigley 1991; Petrov & Rowe 1997; Rowe 1998; Daniel 2000; Shackelford et al. 2000; Marcial et al. 2002; Bouazza 2002).

Bradshaw and Benson (2014) reported that allowing the specimen to reach chemical equilibrium at lower σ´ and then subsequently increasing the stress and thereafter allowing the specimen to re-equilibrate (i.e., sequential method) yielded a similar, but slightly higher k (< 5.3×) than initially permeating the specimen to chemical equilibrium under the higher stress. The authors suggested that the increase in k due to cation exchange is mitigated due to higher applied stress.

The impact on k resulting from the sequential increase of σ´ is shown in Figure 2.15. The individual results were previously described in Section 2.4.1. Upon increase of σ´, specimens permeated with 10 mM $CaCl_2$ essentially had no change in k, whereas specimen permeated with 5 mM $CaCl_2$ exhibited an approximately one order of magnitude decrease in k. This result indicates that doubling the σ´ may not be sufficient to overcome the effect of needle punching. Of note, HGN GCLs are designed for applications that require high internal shearing resistance, which will generally occur under high normal stresses. Thus, the range of σ´ evaluated in this study is unlikely to match the stresses intended for this product. Further study is needed on the HGN GCLs under higher σ´.

2.4.5. Effect of Permeant Liquid

The effect of the *EC* of permeant liquid is illustrated in Figure 2.16. The k of HGN GCL increased markedly upon permeation with solutions with *EC* > 62 mS/m. In contrast, k of specimens permeated with solutions with *EC* < 62 mS/m (i.e., TW, CW, 1 and 2.5 mM $CaCl_2$) were all comparable at ~2×10^{-11} m/s.

The results for the LGN GCL are also included in Figure 2.16 for comparison. However, as previously noted, chemical equilibrium in this study was based only on *EC*.

Table 2.1. Properties of permeant liquids

Solution	Parameter			
	Ionic strength, *I* (mM)	**Ratio of monovalent-to-divalent cations, *RMD* ($mM^{½}$)[a]**	**Electrical conductivity, *EC* (mS/m)**	**pH**
Tap Water (TW)[b]	106.7	697.4	13	7.00
Conservative Water (CW)[c]	6	6.1	51	5.74
1 mM $CaCl_2$	3	-	26	5.68
2.5 mM $CaCl_2$	7.5	-	62	5.58
5 mM $CaCl_2$	15	-	122	5.16
10 mM $CaCl_2$[d]	30	-	236	5.12
20 mM $CaCl_2$	60	-	438	5.44

[a]As described in Kolstad et al. (2004)

[b]As described in Tong and Shackelford (2016)

[c]As described in Scalia and Benson (2010)

[d]Standard water in ASTM D5084-16a

Table 2.2. Properties of bentonite

Property		Value
Mineralogy	Montmorillonite (%)	85 - 91
	Quartz (%)	2 - 4
	Augite (%)	0 - 5
	etc.	< 3
Cation Exchange Capacity, *CEC* (meq/100 g)		78
Atterberg Limits (ASTM D4318)	Liquid Limit, *LL* (%)	411
	Plastic Limit, *PL* (%)	34
	Plasticity Index, *PI* (%)	377
Particle Size (ASTM D422)	% Fines (<75 μm)	95
	% <5 μm	86
	% <2 μm	74
Activity, *A*		5.1
Swell Index[a], *SI* (mL/2 g)	Tap Water (ASTM D5890)	33.3
	Conservative Water	31.6
	1 mM $CaCl_2$	32.3
	2.5 mM $CaCl_2$	26.3
	5 mM $CaCl_2$	22.3
	10 mM $CaCl_2$	17.3
	20 mM $CaCl_2$	15.0

[a]Values reported are averages of three measurements

Table 2.3. Properties of GCL

Property		Value
Initial air-dried (off roll) water content (%)		2.9
Initial (off roll) thickness (mm)		8.86 (SD=0.67, n=40)
Average bentonite mass/area (kg/m^2)	Oven dried (ASTM D5993)	6.36 (SD=0.32, n=10)
	Air dried	6.55 (SD=0.32, n=10)
Carrier Geotextile (ASTM D5291)	Type	Non-woven
	Mass (kg/m^2)	0.36 (SD=0.05, n=10)
Cover Geotextile (ASTM D5291)	Type	Non-woven
	Mass (kg/m^2)	0.28 (SD=0.03, n=10)
Structure and Reinforcement	Needle-punched	Yes
	Thermally treated	No
Bundle size (mm)		1.09 (SD=0.24, n=10)
No. of bundles/area ($bundles/m^2$)		146,300 (SD=1,240, n=40)
No. of monofilament/bundle		42 (SD=6.39, n=20)
Percentage area covered by bundles		13.6
Manufacturer reported peel strength, MRPS	N/mm	3500
	lb/in	20

Table 2.4. Testing program

Test Series	Permeant liquid[a]	Effective Stress, σ´ (kPa [psi])
1	TW	27.3 [4]
2	CW	27.3 [4]
3	1 mM $CaCl_2$	27.3 [4]
4	2.5 mM $CaCl_2$	27.3 [4]
5	5 mM $CaCl_2$	27.3 [4]; 61.7 [9]
6	10 mM $CaCl_2$	27.3 [4]; 61.7 [9]
7	20 mM $CaCl_2$	27.3 [4]

[a]See Section 2.2.1 for description and properties of each permeant liquid

Table 2.5. (Color) Summary of the results of the hydraulic conductivity tests

Test Series	Test Number[a]	Permeant liquid[b]	Values at termination criteria										
			ASTM D5084-16a (2016)			ASTM D6766-18 (2018)			Final			*w*	*S*
			t_{5084} (d)[c]	PVF_{5084}	k_{5084} (m/s)	t_{6766} (d)[c]	PVF_{6766}	k_{6766} (m/s)	t_f (d)[c]	PVF_f	k_f (m/s)	(%)	(%)
1	1	TW	31.94 [5]	4.7	1.6×10^{-11}				283.86 [5]	14.3	1.6×10^{-11}	125	103
2	2a	CW	36.2 [5]	5.8	1.4×10^{-11}	[5]			[5]				
	2b	CW	24.7 [6]	6.4	2.6×10^{-11}	[6]			[6]				
3	3	1 mM $CaCl_2$	35.97 [6]	4.2	1.3×10^{-11}				83.47 [6]	6.5	1.5×10^{-11}	106	92
4	4	2.5 mM $CaCl_2$	25.73 [6]	7.8	1.4×10^{-11}				98.03 [3]	13.0	1.7×10^{-11}	105	103
5	5	5 mM $CaCl_2$	2.62 [3]	11.5	2.0×10^{-10}	4.49 [3]	18.7	1.1×10^{-9}	6.15 [3]	44.5	2.4×10^{-9}	85	104
6	6a	10 mM $CaCl_2$	0.247 [3]	13.0	5.8×10^{-9}	0.399 [3]	20.8	1.2×10^{-8}	0.441 [3]	24.0	1.3×10^{-8}	87	104
	6b	10 mM $CaCl_2$	0.011 [3]	2.2	3.4×10^{-8}	0.059 [3]	10.9	2.9×10^{-8}	0.097 [3]	17.8	3.1×10^{-8}	89	95
7	7a	20 mM $CaCl_2$	0.007 [6]	2.4	8.6×10^{-8}	0.018 [6]	8.3	1.6×10^{-7}	0.019 [6]	9.0	1.6×10^{-7}	96	104
	7b	20 mM $CaCl_2$	0.011 [6]	2.3	1.5×10^{-7}	0.018 [6]	8	2.1×10^{-7}	0.019 [6]	9.0	2.1×10^{-7}	99	105

[a]Green color indicate tests are still running and have not meet chemical equilibrium criteria; thus, PVF (gray) is an estimated value

[b]See Section 2.2.1 for description and properties of each permeant liquid

[c]Reported time at which termination criteria was met elapsed since permeation, values in brackets are approximate time spent for hydration

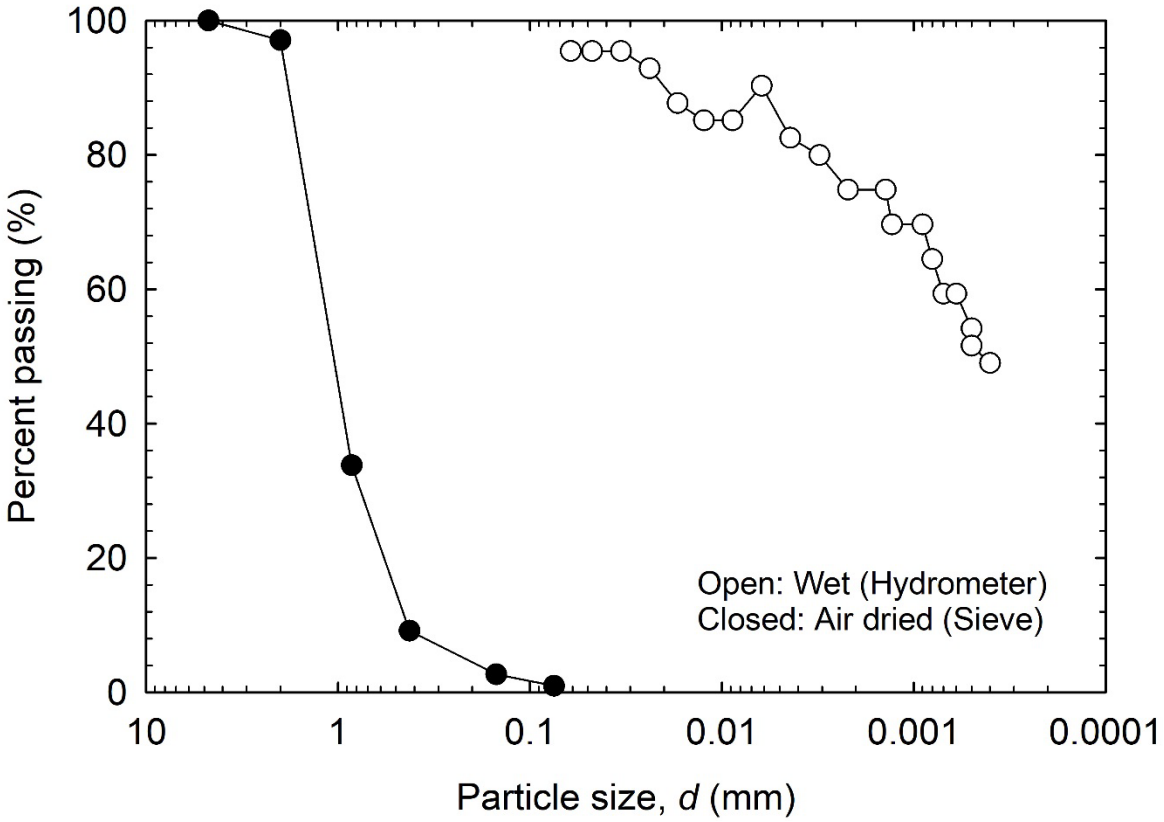

Figure 2.1. Particle-size distributions for bentonite extracted from the GCL based on mechanical sieve (air dried) and hydrometer (wet) analyses

NOT TO SCALE

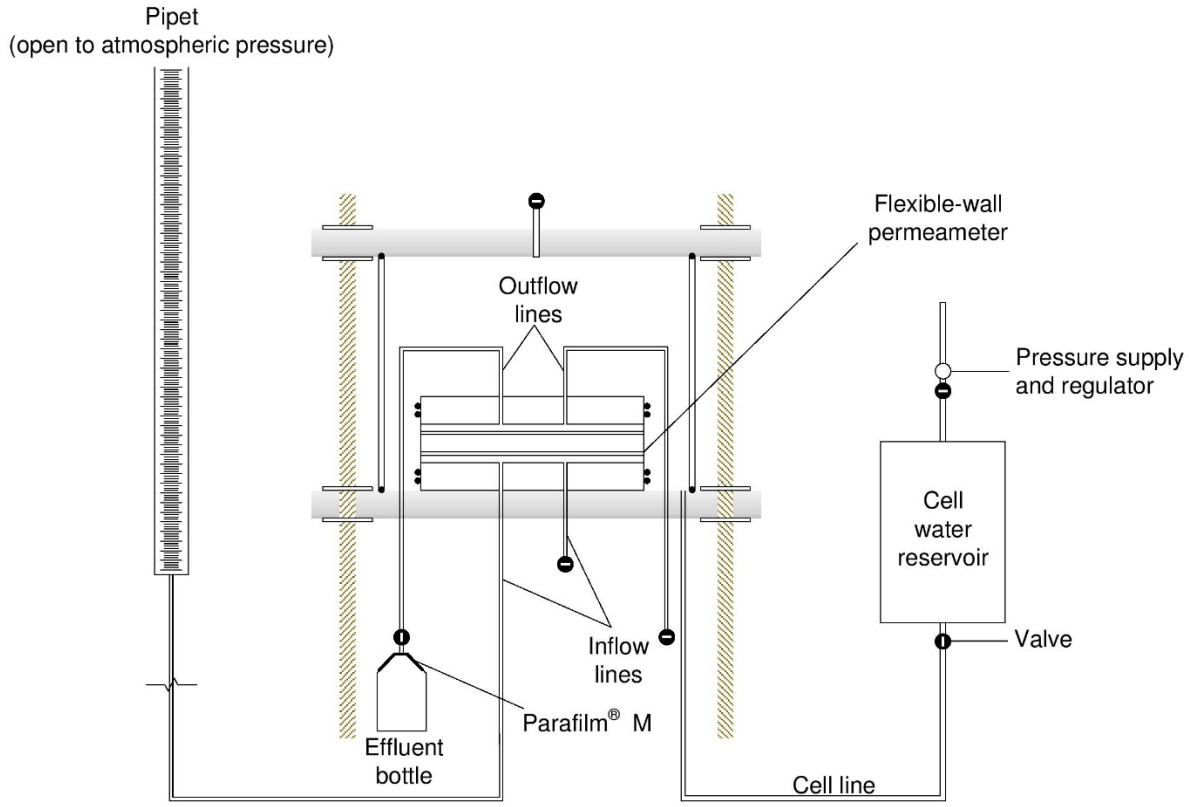

Figure 2.2. Schematic of the test setup for hydraulic conductivity testing by falling headwater, constant tailwater method

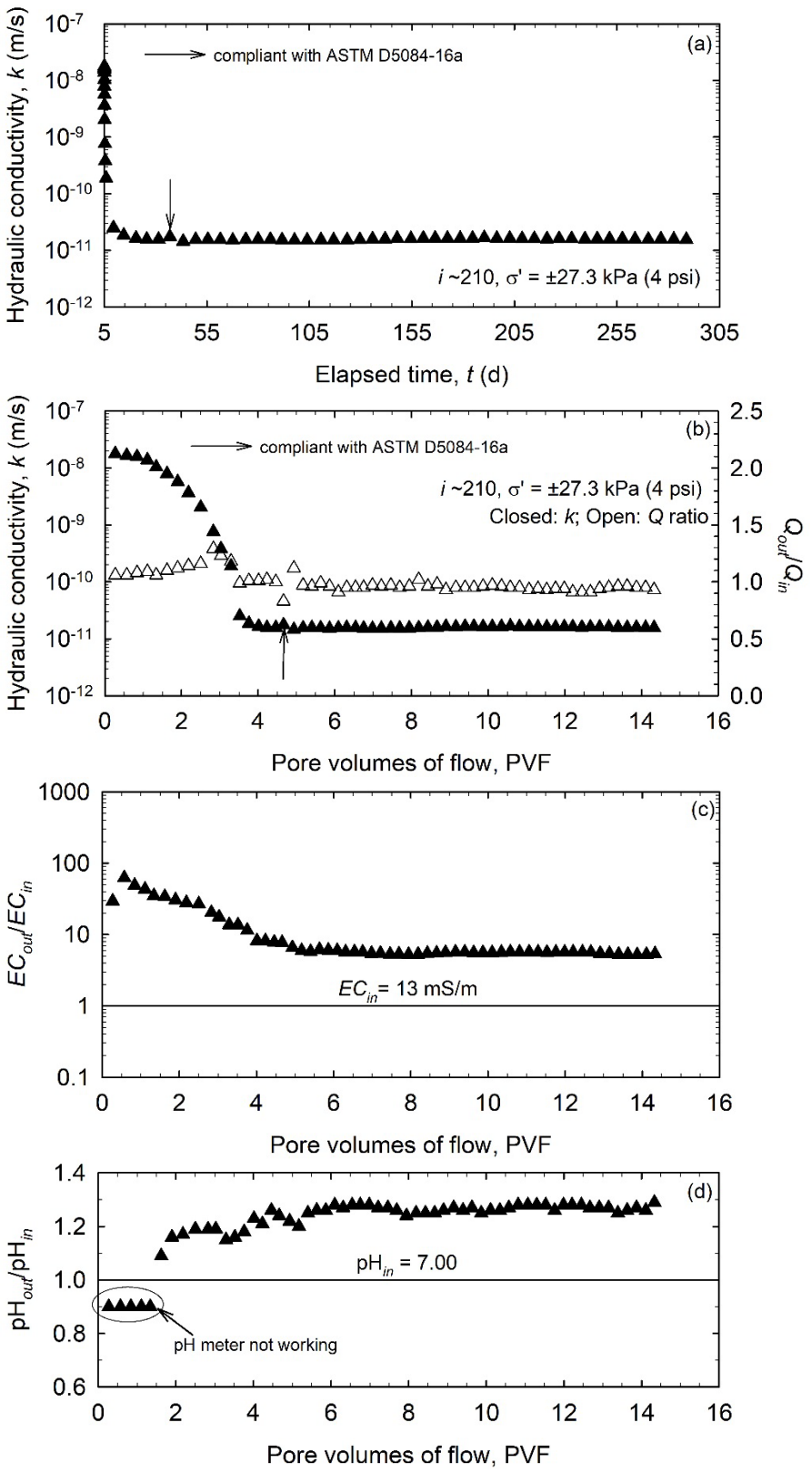

Figure 2.3. Test results for specimen permeated with tap water (Test Series 1): (a) hydraulic conductivity versus elapsed time; (b) hydraulic conductivity and flow ratio versus pore volumes of flow; (c) electrical conductivity; and (d) pH

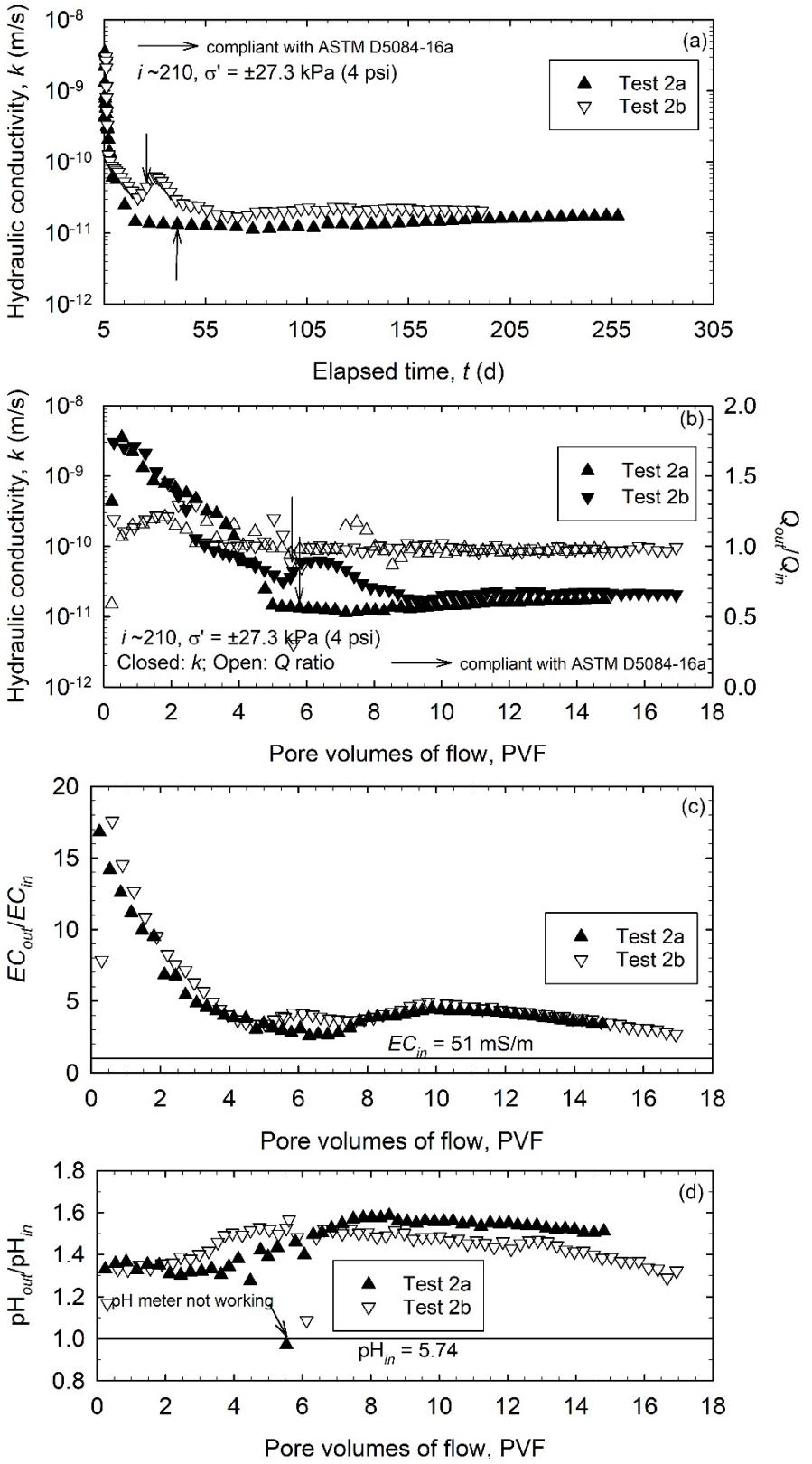

Figure 2.4. Test results for specimen permeated with conservative water (Test Series 2): (a) hydraulic conductivity versus elapsed time; (b) hydraulic conductivity and flow ratio versus pore volumes of flow; (c) electrical conductivity; and (d) pH

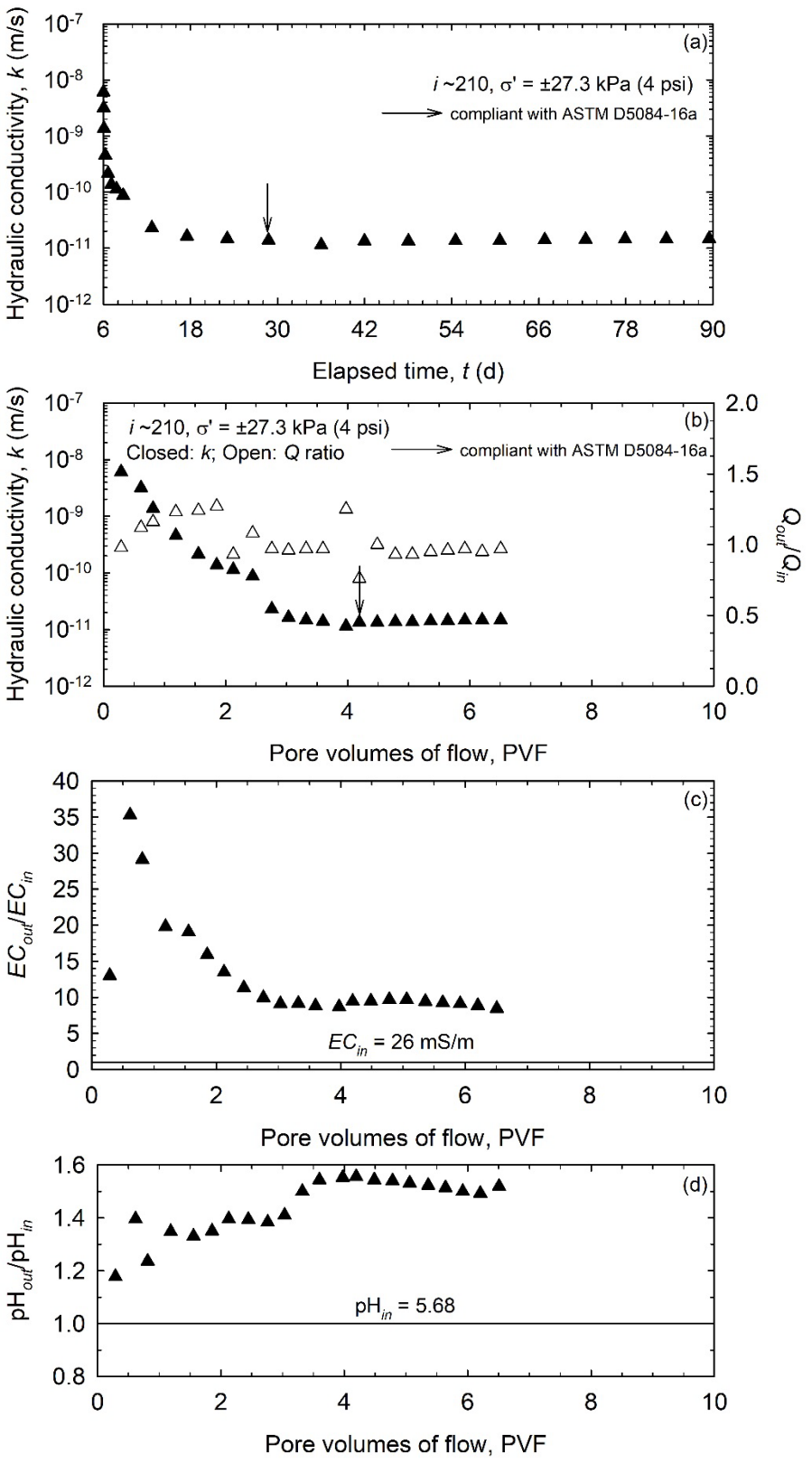

Figure 2.5. Test results for specimen permeated with 1 mM $CaCl_2$ (Test Series 3): (a) hydraulic conductivity versus elapsed time; (b) hydraulic conductivity and flow ratio versus pore volumes of flow; (c) electrical conductivity; and (d) pH

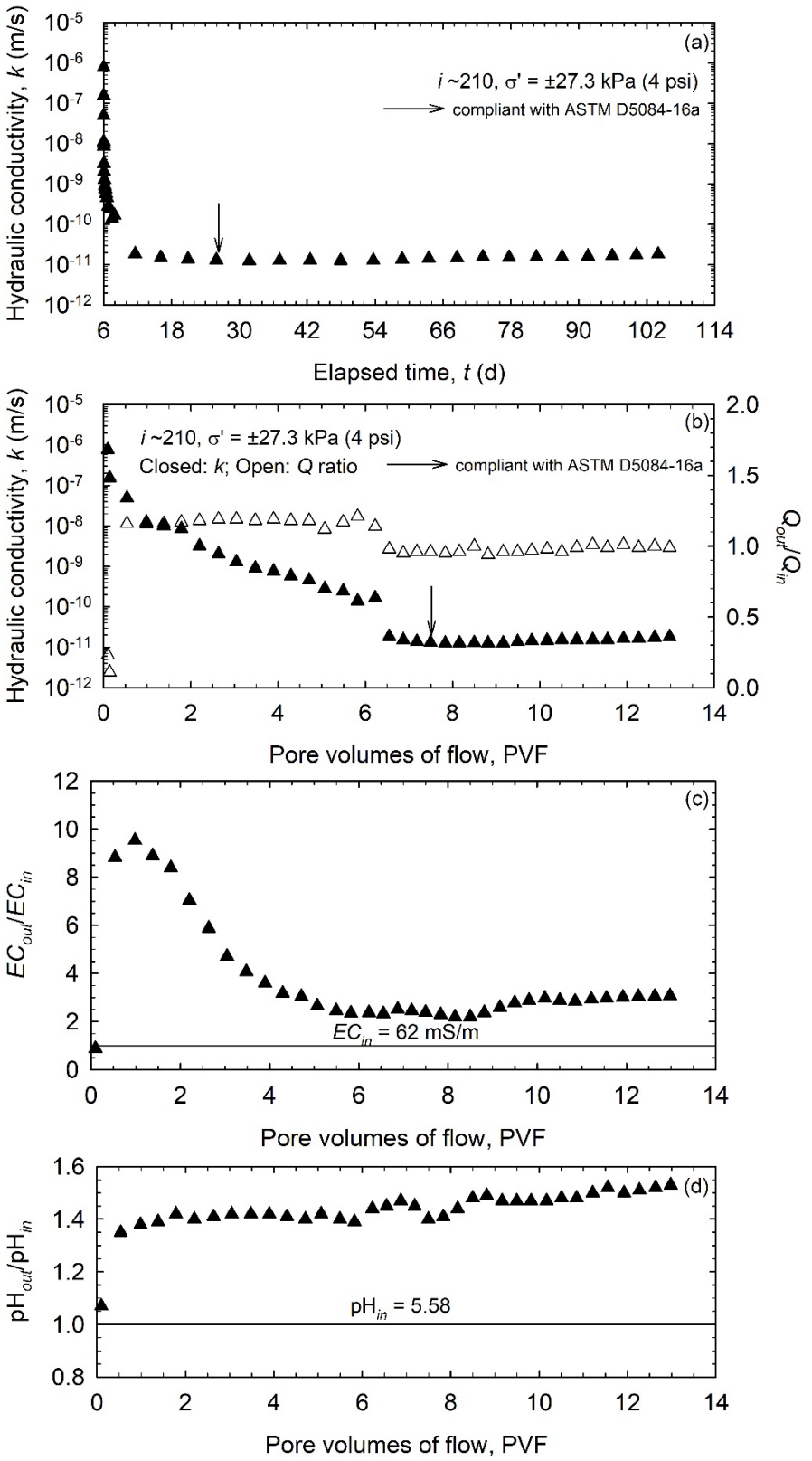

Figure 2.6. Test results for specimen permeated with 2.5 mM $CaCl_2$ (Test Series 4): (a) hydraulic conductivity versus elapsed time; (b) hydraulic conductivity and flow ratio versus pore volumes of flow; (c) electrical conductivity; and (d) pH

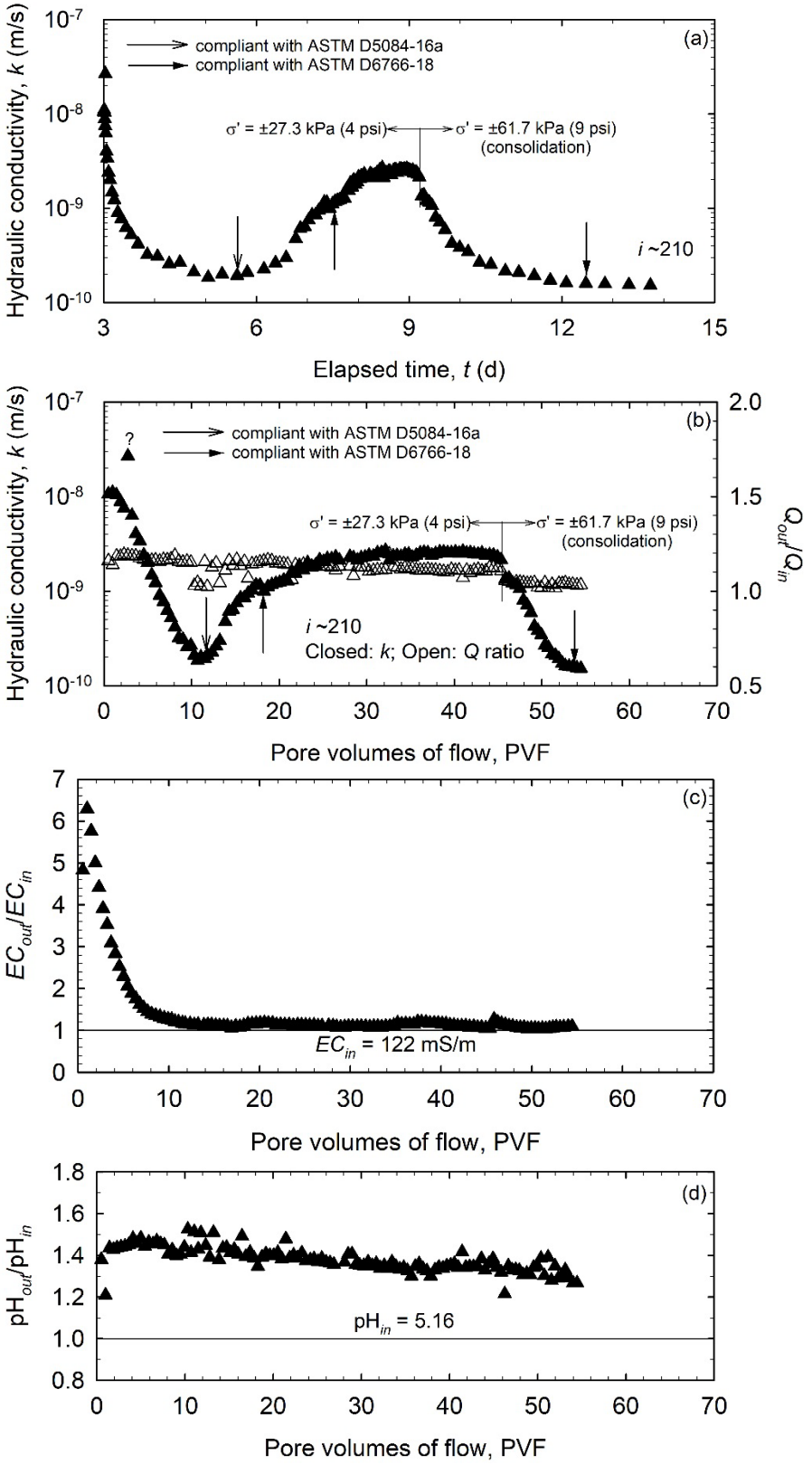

Figure 2.7. Test results for specimen permeated with 5 mM $CaCl_2$ (Test Series 5): (a) hydraulic conductivity versus elapsed time; (b) hydraulic conductivity and flow ratio versus pore volumes of flow; (c) electrical conductivity; and (d) pH

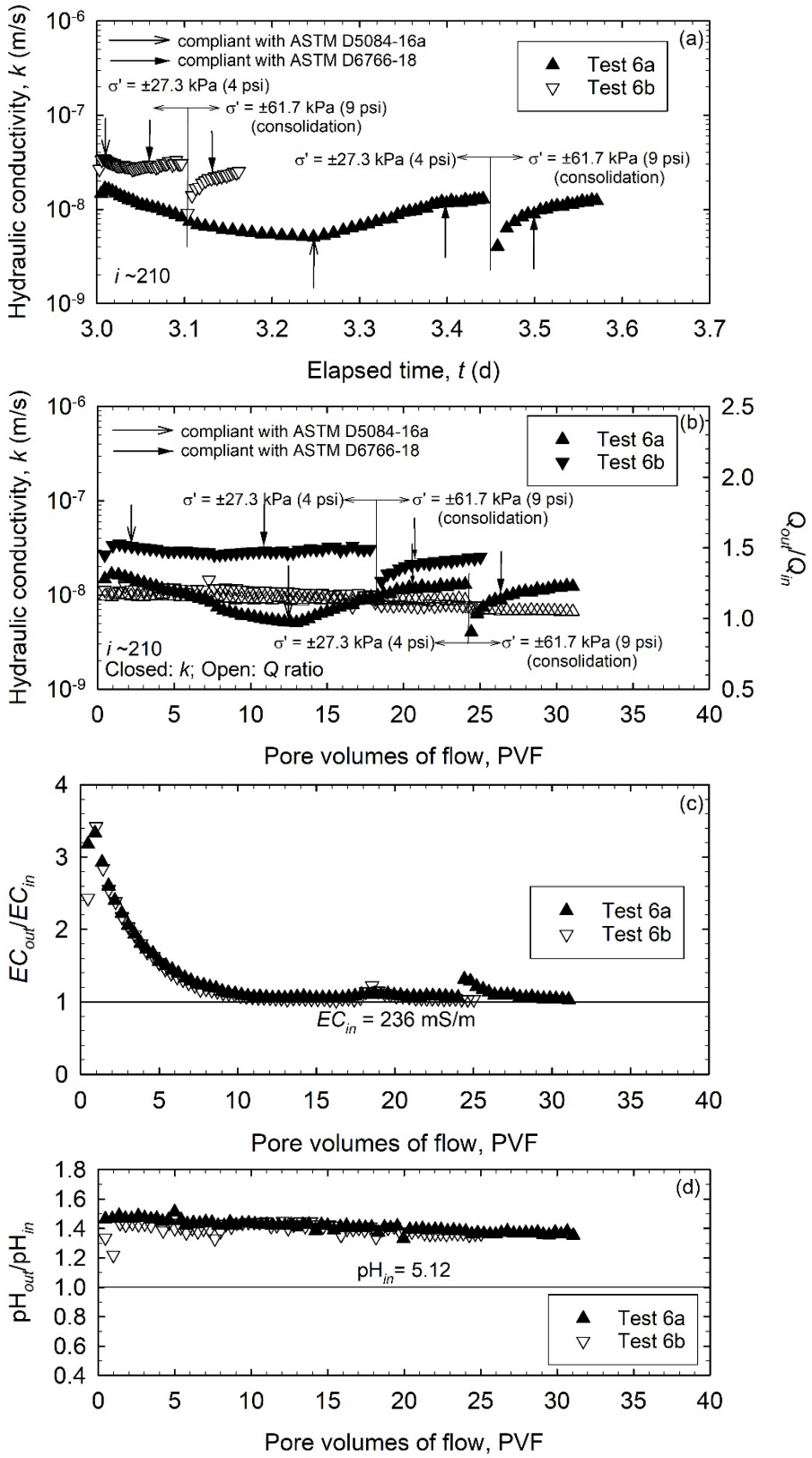

Figure 2.8. Test results for specimen permeated with 10 mM $CaCl_2$ (Test Series 6): (a) hydraulic conductivity versus elapsed time; (b) hydraulic conductivity and flow ratio versus pore volumes of flow; (c) electrical conductivity; and (d) pH

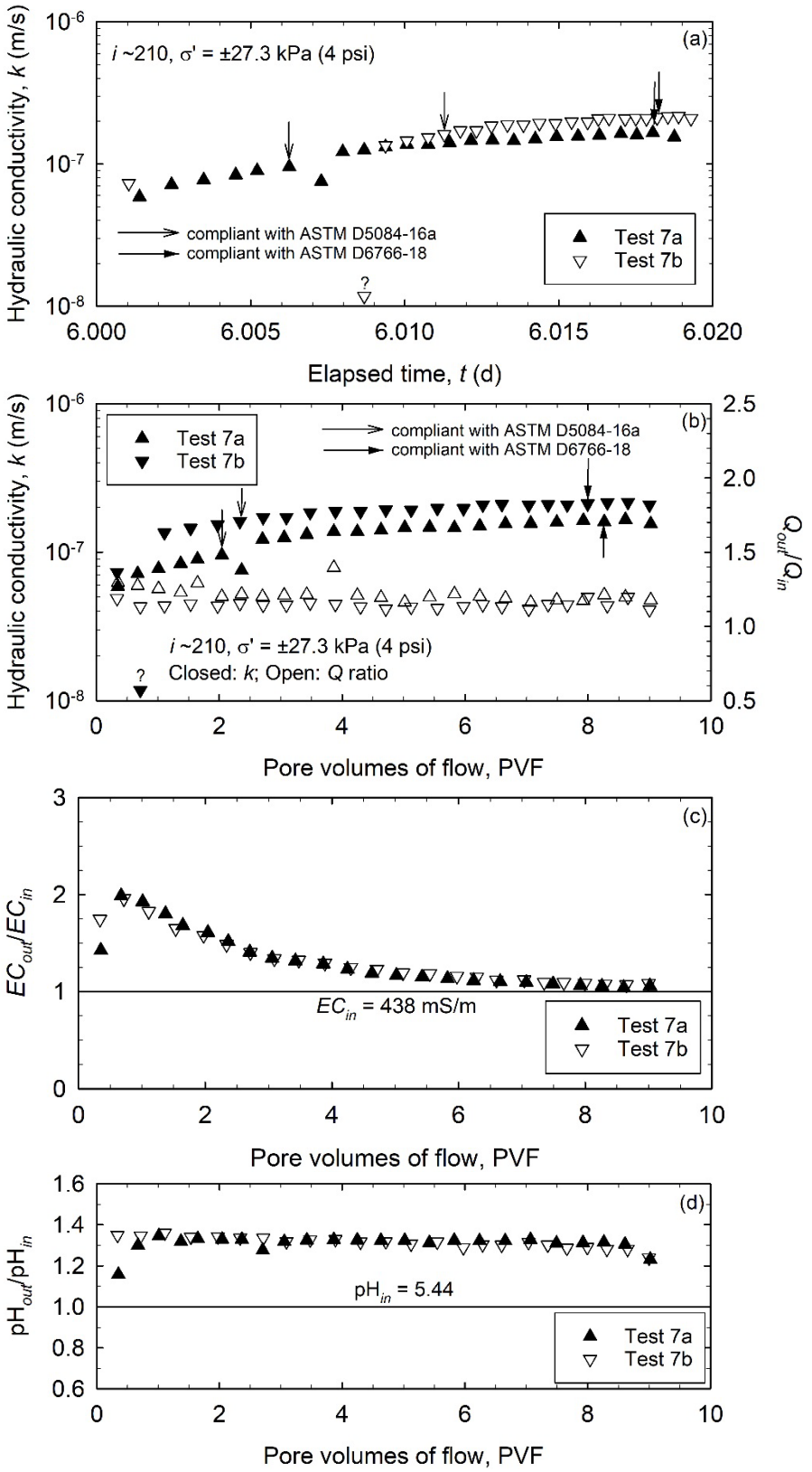

Figure 2.9. Test results for specimen permeated with 20 mM $CaCl_2$ (Test Series 7): (a) hydraulic conductivity versus elapsed time; (b) hydraulic conductivity and flow ratio versus pore volumes of flow; (c) electrical conductivity; and (d) pH

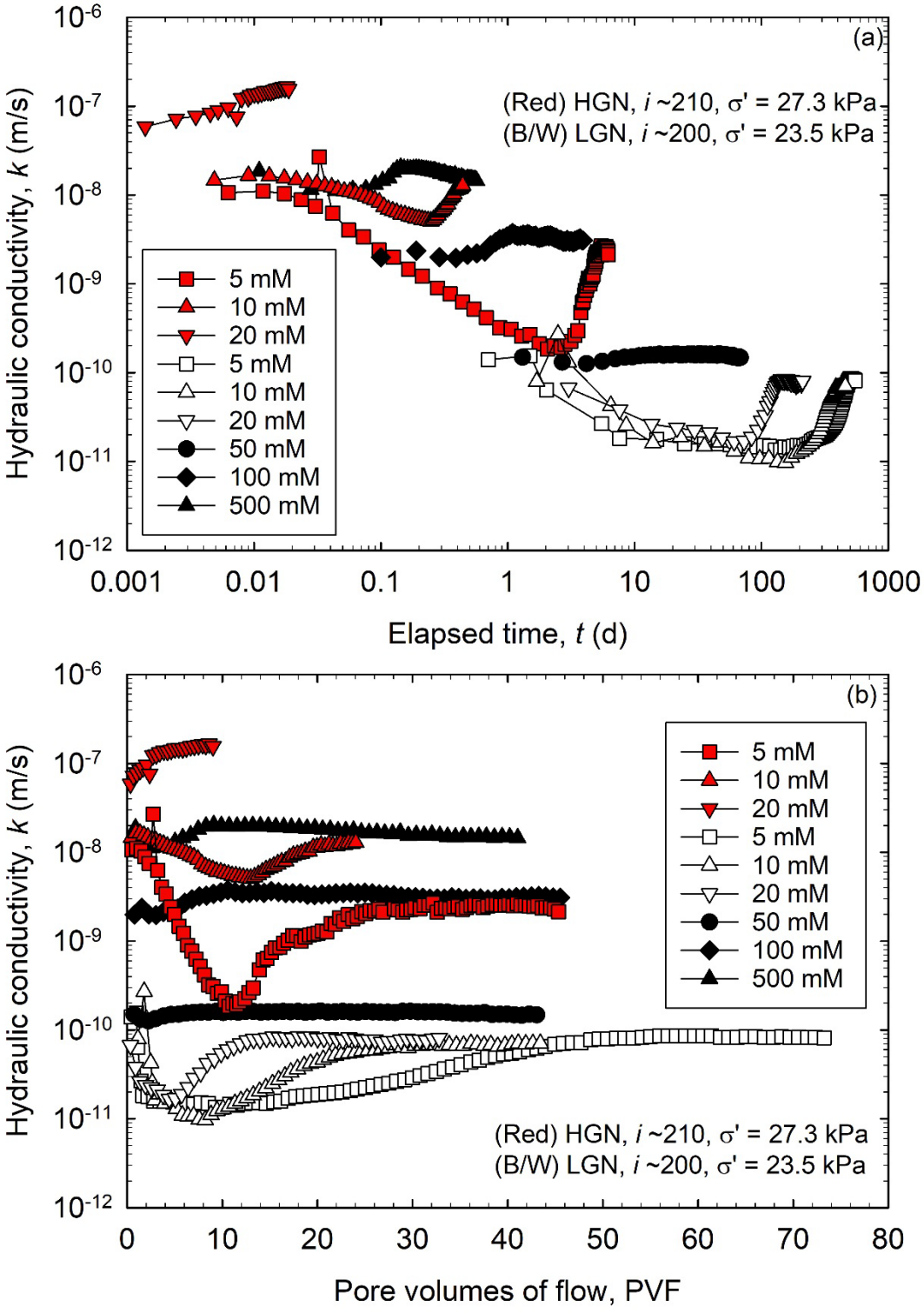

Figure 2.10. (Color) Comparison of hydraulic conductivity of GCLs based on permeation with $CaCl_2$ solutions for higher grade needle punching (HGN [from this study, red]) versus lower grade needle punching (LGN [from Lee and Shackelford (2005b), black and white, B/W]): (a) hydraulic conductivity with respect to time in log scale and (b) hydraulic conductivity with respect to pore volumes of flow

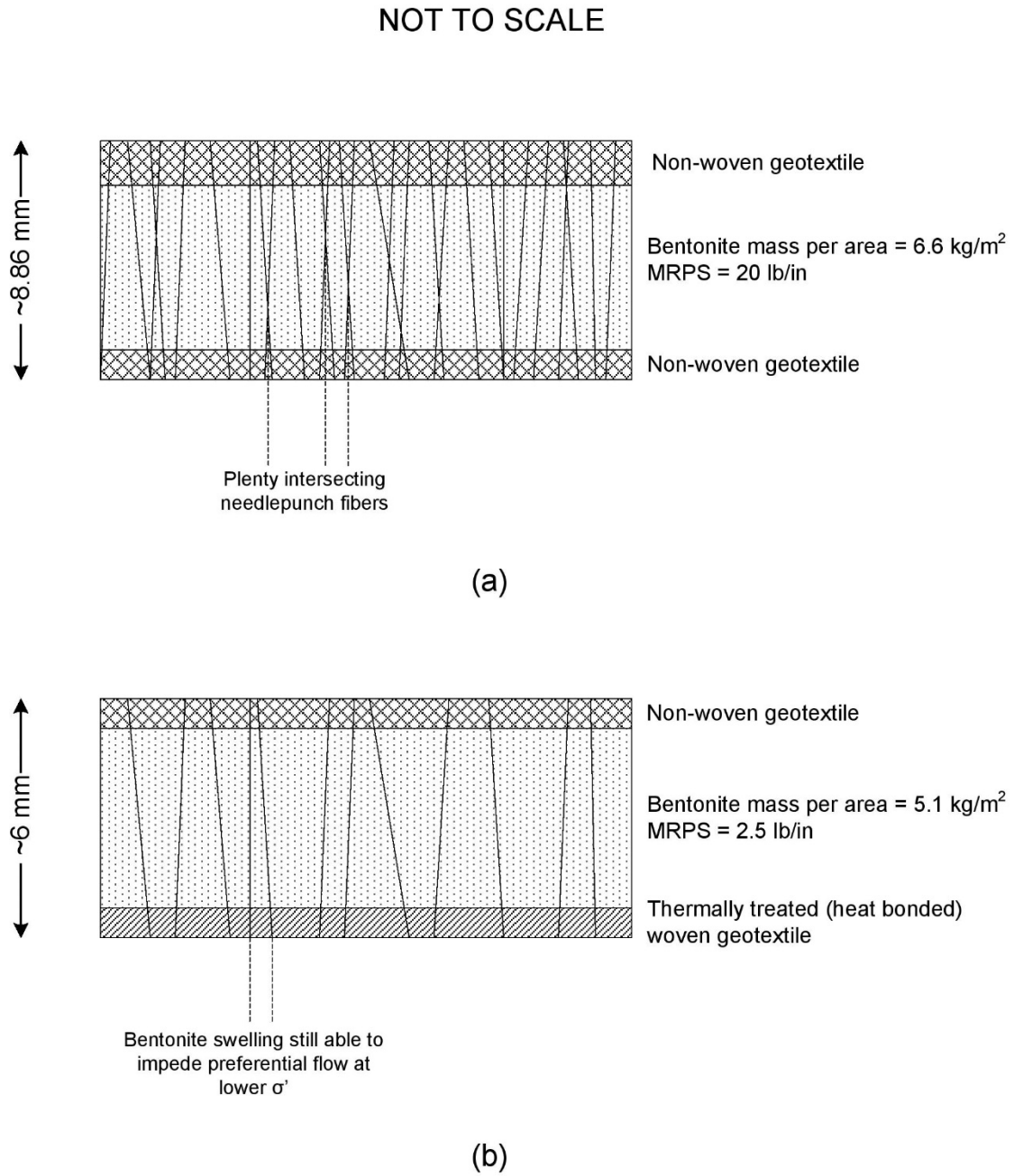

Figure 2.11. Cross section illustrating difference between: (a) higher grade needle punching, HGN GCL and (b) lower grade needle punching, LGN GCL

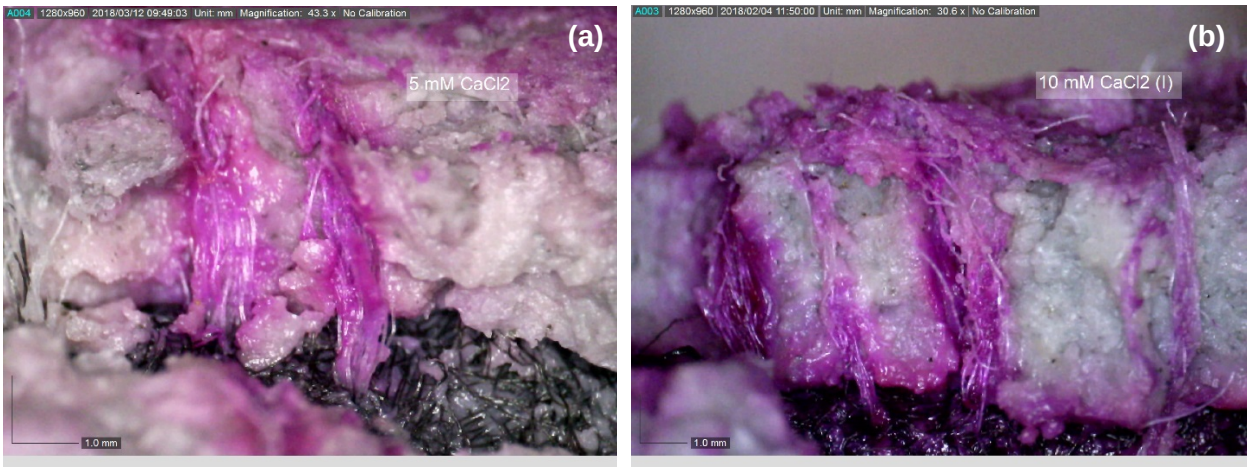

Figure 2.12. (Color) Preferential flow path in dyed higher grade needle punching (HGN) specimens: (a) 5 mM $CaCl_2$ and (b) 10 mM $CaCl_2$

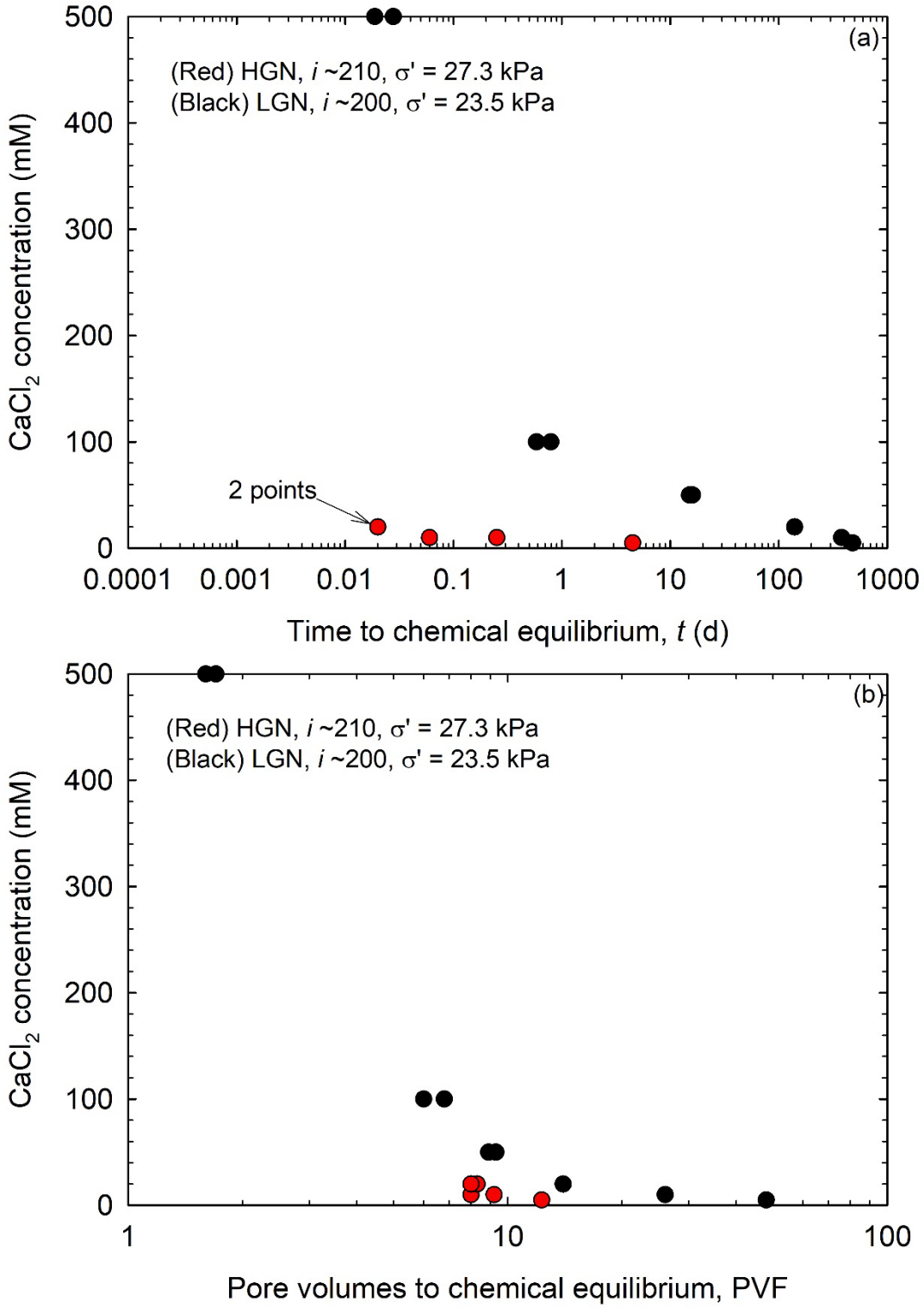

Figure 2.13. (Color) (a) Elapsed time and (b) pore volumes of flow required to achieve chemical equilibrium for higher grade needle punching (HGN [from this study, red]) versus lower grade needle punching (LGN [from Lee and Shackelford (2005b), black]) based on permeation with $CaCl_2$ solutions

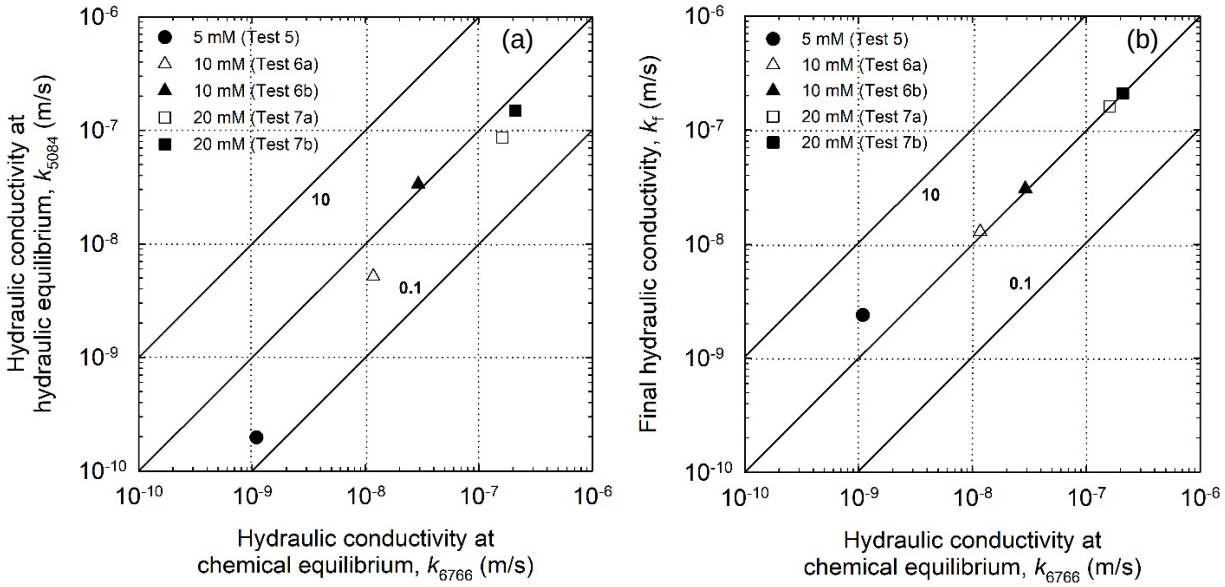

Figure 2.14. Hydraulic conductivity based on the function of termination criteria adopted: (a) k_{6766} versus k_{5084} and (b) k_{6766} versus k_f

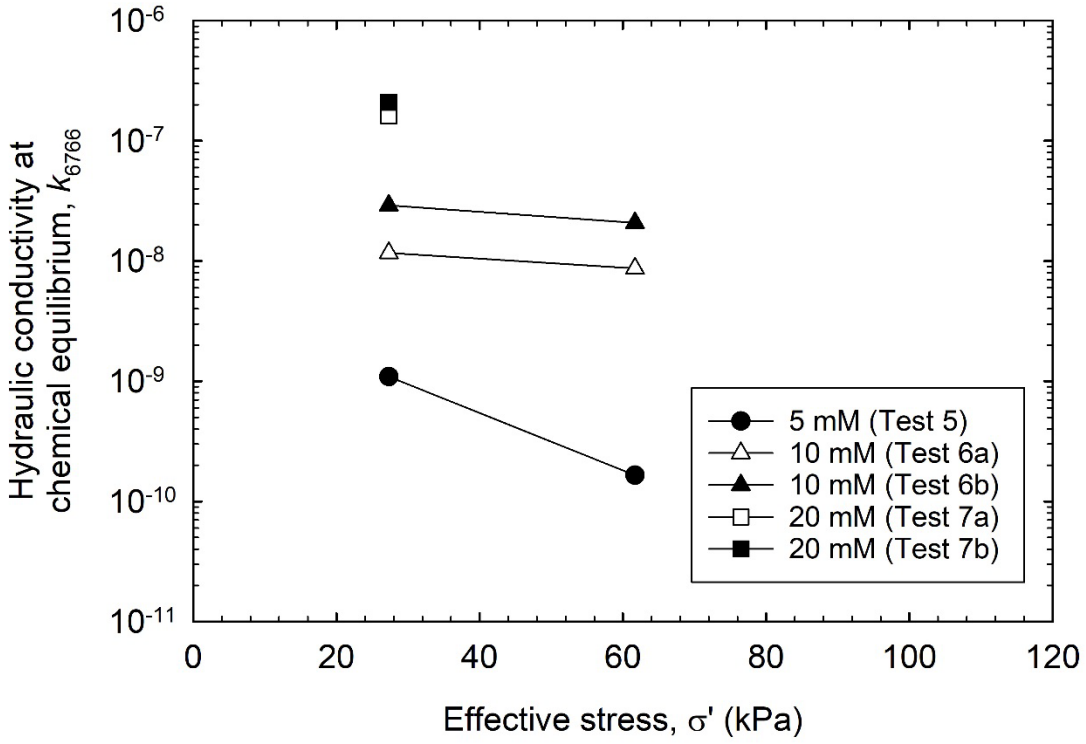

Figure 2.15. Hydraulic conductivity based on the function of effective stress on HGN GCL permeated with $CaCl_2$

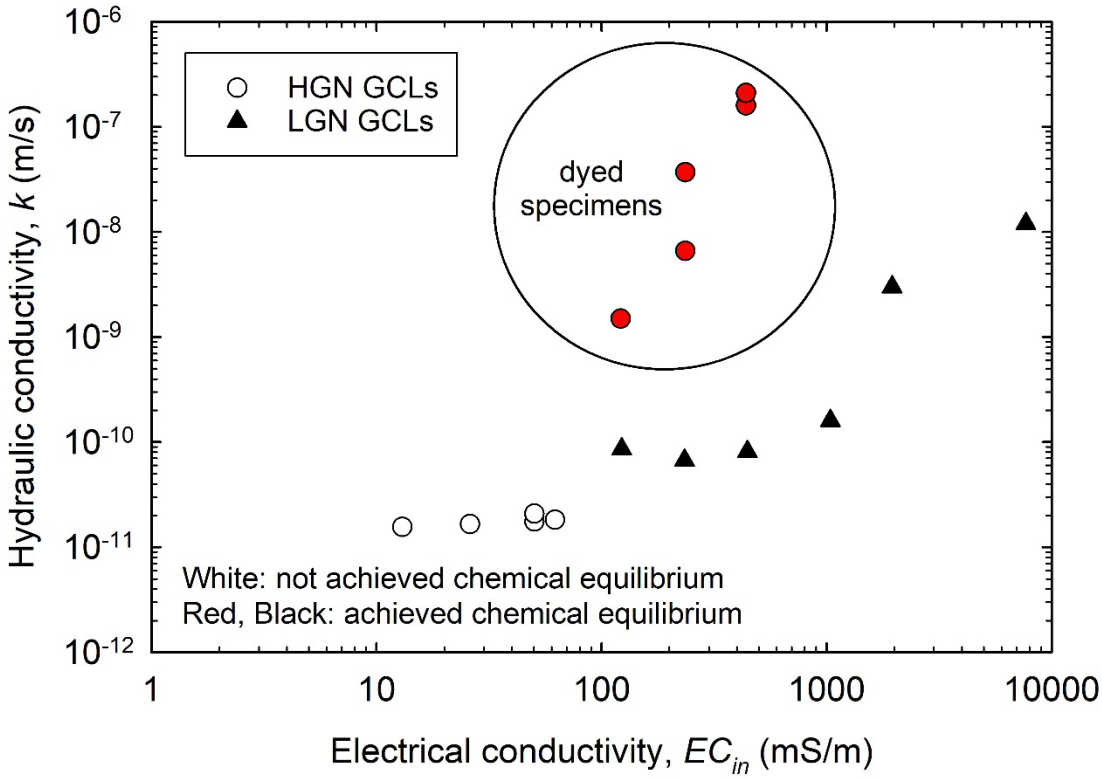

Figure 2.16. (Color) Effect of permeant liquid electrical conductivity on hydraulic conductivity of higher grade needle punching (HGN [from this study, ○]) versus lower grade needle punching (LGN [from Lee and Shackelford (2005b), ▲]) at low effective stress (σ' = ~24-27 kPa [4 psi])

CHAPTER 3 SELECTED FACTORS AFFECTING THE TIME TO MEET TERMINATION CRITERIA FOR GCL HYDRAULIC COMPATIBILITY TESTS

3.1. Introduction

Geosynthetic clay liners (GCLs) are manufactured hydraulic barriers comprising a clay bound to a layer or layers of geosynthetic materials (see APPENDIX A). Commonly, GCLs comprise two geotextiles [i.e. bottom (carrier) and top (cover) geotextile] that encase a layer of sodium bentonite (Na-bentonite). Binding of the GCL is accomplished by needle punching, stitching, chemical adhesives, or other methods. GCLs are used in containment systems because of the low hydraulic conductivity (k) of the Na-bentonite component, typically ~2×10^{-11} m/s when permeated with water. However, there are wide range of mechanical/structure and physico-chemical factors that can affect the k of high plasticity clays such as Na-bentonite (Mesri & Olson 1971b).

Bentonites are natural clays with a mineralogical composition dominated by montmorillonite, which is a member of the smectite group of phyllosilicates, although the content of montmorillonite in different bentonites can vary (Lee & Shackelford 2005b). Bentonites are further characterized by the dominant bound cation that satisfies the cation exchange capacity (*CEC*) of the clay. In GCLs, Na-bentonite is typically used (Shackelford et al. 2000), because of the greater swelling of Na-bentonite relative to calcium (Ca-) or magnesium (Mg-) bentonites (Mesri & Olson 1971a; Gleason et al. 1997; Likos & Lu 2006). Sodium activated bentonites (e.g., Norotte et al. 2004) and chemically enhanced bentonites (e.g., Ashmawy et al. 2002; Di Emidio et al. 2011; Scalia et al. 2018) also can be used in GCLs to enhance the hydraulic performance of the bentonite layer.

Although Na-bentonite has a low k when permeated with water, permeation with electrolyte solutions may yield incompatibility (Shackelford & Sample-Lord 2014). Incompatibility, in the context of clays used for barriers, is the suppression (from a dry state) or reduction (from a swollen state) in the swelling of the clay due to adverse physico-chemical interactions with the permeant solution. The result of incompatibility is a higher k than the same material under the same conditions permeated with water (Mitchell

& Madsen 1987; Shackelford 1994; Rad et al. 1994; Shackelford et al. 2000; Osicki et al. 2004; Guyonnet et al. 2005; Gates et al. 2011).

The concentration and composition of inorganic electrolyte solutions play major role in dictating the k of GCLs. In this regard, chemical solutions are often characterized in terms of ionic strength (I), defines as follows:

$$I = \frac{1}{2}\sum_i M_i Z_i^2 \quad (1)$$

where M is the molar concentration of ion species i and Z is the valence (charge) of ion species i. The k of Na-bentonite has been shown to increase non-linearly with increasing I, all other factors being equal (Jo et al. 2001). At low I (< 50 mM), the k of GCLs also has been shown to be dependent on the ratio of monovalent-to-divalent cations (*RMD*) in solution (Kolstad et al. 2004), where *RMD* is defined as follows:

$$RMD = \frac{M_M}{\sqrt{M_D}} \quad (2)$$

where M_M is the total molarity of monovalent cations and M_D is the total molarity of divalent cations present in the mixture. When there is a higher relative abundance of divalent cations in the solution (i.e., low *RMD*), k tends to be higher (Kolstad et al. 2004).

The k of GCLs is dependent on whether the bentonite hydrates (swells) before permeation with chemical solution, which is known as a first exposure or prehydration effect (e.g., Shan & Daniel 1991; Daniel et al. 1993; Shackelford 1994; Petrov et al. 1997b; Quaranta et al. 1997; Ruhl & Daniel 1997; Lin & Benson 2000; Shan & Lai 2002). Specimens that do not adequately swell, or are non-prehydrated, tend to yield higher k than prehydrated specimens (all other factors being equal). Shackelford (2008) noted that the temporal trend of k for specimens permeated with $CaCl_2$ solutions tend to reflect different stages, reflected by an initial decrease in k to a minimum value (k_{min}) upon swelling, followed by a rapid and then more gradual increase in

k resulting from compression of the diffuse double layer of osmotically hydrated montmorillonite due to cation exchange until an equilibrium exchange condition was achieved resulting in a final, steady state k. Prehydration of GCLs with water results in a higher degree of initial osmotic swelling and, thus, a lower k_{min} (Petrov & Rowe 1997). Lee and Shackelford (2005a) noted that the effect of prehydration with water was more pronounced for GCLs permeated with solutions containing > 100 mM $CaCl_2$ and less pronounced for specimens permeated with solutions containing < 50 mM $CaCl_2$.

Since GCLs are often used to contain inorganic chemical solutions, the potential problem of incompatibility is common. As a result, site-specific k testing is necessary to predict representative k at chemical equilibrium (i.e., under long-term conditions). Depending on site-specific characteristics, such as the specific GCL, the stress conditions, the hydration conditions, and the permeant solution; the time for a GCL specimen to achieve chemical equilibrium can vary considerably, from only a few minutes for very high ionic strength solutions (i.e., I > 1 M) to one or more years for solutions with low ionic strength (e.g., I < 5 mM) (Jo et al. 2005). Thus, understanding the long-term k of a candidate GCL can be problematic in practice.

The objective of this study was to investigate factors affecting the time to chemical equilibrium in k testing, and to determine if an alternative test method could be used to expedite hydraulic compatibility test on a higher grade needle-punching GCL. Two different test methods were evaluated, including the falling headwater, constant tailwater tests and constant rate-of-flow tests, both of which were performed on prehydrated (baseline condition) GCL specimens.

3.2. Background

3.2.1. Methods for Measuring GCL Hydraulic Conductivity

ASTM D6766-18 (2018) recommends four alternative methods for measuring the k of GCLs with potentially incompatible solutions: constant head (*Method A*), falling headwater, constant tailwater (*Method B*), falling headwater, increasing tailwater (*Method C*), and constant rate-of-flow (*Method D*). All methods are performed using flexible-wall permeameters. *Methods A*, *B*, and *C* rely on imposing a hydraulic gradient (i) across the specimen, and measuring the volumetric flow (Q), to determine k. *Method D* relies on imposing a

constant volumetric flow rate (q) and measuring i to determine k. *Methods B* and *C* are commonly used to measure the k of GCLs (Shackelford et al. 2000). *Method B* and *Method D* are employed in this study.

3.2.1.1. Falling Headwater, Constant Tailwater Method

The falling headwater, constant tailwater method (*Method B*) is frequently used to measure the k of GCLs (e.g., Jo et al. 2001; Jo et al. 2004; Kolstad et al. 2004; Jo et al. 2005; Lee & Shackelford 2005a; Lee & Shackelford 2005b; Jo et al. 2006; Bradshaw & Benson 2014; Conzelmann & Scalia 2016; Conzelmann et al. 2017). This method requires determination of head loss across the specimen based on boundary conditions and allows for easy and accurate monitoring of Q. The equation to calculate k with this method is as follows:

$$k = \frac{a \cdot L}{A \cdot \Delta t} \ln\left(\frac{h_i}{h_f}\right) \tag{3}$$

where a is the cross sectional area of the influent pipet, L is the specimen thickness (determined at the end of testing), A is the cross sectional area of the specimen, and h_i and h_f are the initial and final head, respectively, during any given time interval Δt.

3.2.1.2. Constant Flow Method

The i that arises due to an applied q, is defined in terms of the difference in pore-water pressure (Δu) across a specimen of length L as follows:

$$i = \frac{\Delta u}{\gamma_w \cdot L} \tag{4}$$

where γ_w is the unit weight of the permeant liquid. The k is then calculated via Darcy's law as follows:

$$Q = q \cdot \Delta t = k \cdot i_{ss} \cdot A \quad (5)$$

where i_{ss} is the steady state i generated from the imposed q.

An advantage of the constant flow method is the ability impose small q (the flow pump used in this study allowed for application of q as low as 0.55 mL/d) and highly accurate measurement of Δu with digital pressure transducers. The ability to accurately measure k with minimal flow through the test specimen allowed for more rapid determination of k at hydraulic equilibrium (i.e., as defined in ASTM D5084-16a 2016; Aiban & Znidarcic 1989) relative to the falling headwater, constant tailwater method which required > 0.5 mL of inflow/outflow volume for each reading. However, the equipment (e.g., flow pump, digital pressure transducer, and data acquisition system) required to perform a constant rate-of-flow test makes this method more complicated and more expensive to perform.

Historical usage of flow pump for geotechnical applications

The application of constant flow can be accomplished using either with a commercially available flow pump or a stepper motor actuator paired with displacement gauge. Several common usages of flow pump are: (1) to measure k (e.g., Olsen 1966; Olsen et al. 1985; Fernandez & Quigley 1985; Quigley et al. 1987; Aiban & Znidarcic 1989; Abu-Hejleh et al. 1993; Kashir & Yanful 1997; Petrov et al. 1997a; McCartney & Znidarcic 2010; Lee & Znidarcic 2013), (2) to perform column testing (e.g., Redmond & Shackelford 1994; Shackelford & Redmond 1995; Hong & Shackelford 2017a; Hong & Shackelford 2017b), (3) to maintain constant concentration along boundaries of the specimen in membrane testing (e.g., Malusis et al. 2001; Malusis & Shackelford 2002; Kang & Shackelford 2009; Kang & Shackelford 2010; Bohnhoff & Shackelford 2013; Meier & Shackelford 2017; Sample-Lord & Shackelford 2018), and (4) to provide constant suction in low-stress consolidation on soft materials (e.g., Abu-Hejleh et al. 1996; Fox & Baxter 1997; Tian 2017; Herweynen et al. 2017). These examples demonstrate the ability of flow pump to accurately and consistently apply low q.

3.2.2. Termination Criteria

ASTM D5084-16a (2016) describes standard termination criteria for measurement of k at hydraulic equilibrium of saturated porous material using a flexible-wall permeameter. In the case of low k material (k < 1×10^{-10} m/s), the criteria are: (1) the ratio of outflow-to-inflow volumetric flow (Q_{out}/Q_{in}) within 1±0.25 and (2) k within 50 % of the mean k of at least four consecutive data points without any indication of an upward or downward trend. Daniel (1994) recommends that permeation with non-standard liquids be continued until at least two pore volumes of flow has passed through the specimen and the chemical composition of influent and effluent is similar. Pore volumes of flow (PVF) is defined as the cumulative volume of outflow, Q_{out}, through the void volume of the porous specimen (V_v), or:

$$PVF = \frac{Q_{out}}{V_v} = \frac{q_{out} \cdot t}{n \cdot A \cdot L} \tag{6}$$

where t is the elapsed time since the start of permeation, n is the porosity of the specimen, A is the cross-sectional area of the specimen, and L is the thickness of the specimen. The use of the total porosity in Eq. 6 implies that all the pore space within the specimen is available to conduct flow. In the case of prehydration, usually with water, a net PVF, PVF_{net}, may be used to exclude permeation with the hydrating liquid as follows (Shackelford & Redmond 1995):

$$PVF_{net} = PVF - PVF_{hl} \tag{7}$$

where PVF_{hl} is the number of pore volumes of flow with only the hydrating liquid.

Shackelford et al. (1999) recommends using electrical conductivity (EC) to characterize chemical composition of the inflow and outflow solutions. The use of EC to measure chemical equilibrium is included in ASTM D6766-18 (2018), which is specific to the measurement of k of GCLs. The hydraulic termination criteria in ASTM D6766-18 (2018) are the same as those in ASTM D5084-16a (2016) except that only the last three (or more) consecutive data points should be considered. Additional termination criteria related to the

establishment of chemical equilibrium are also included. Chemical equilibrium is determined as a ratio of outflow *EC* to inflow *EC* (EC_{out}/EC_{in}) within 1±0.10. Previous studies have also measured the rate of sodium (Na) elution and compared the major ion concentrations between effluent and influent to determine whether chemical equilibrium had been established (e.g., Quaranta et al. 1997; Jo et al. 2004; Jo et al. 2005; Lee & Shackelford 2005a; Lee & Shackelford 2005b; Benson et al. 2010; Mazzieri et al. 2013).

ASTM D6766-18 (2018) does not include equilibrium in pH as a termination criterion. Several studies have reported that pH_{out} may not equal pH_{in} despite the attainment of equilibrium in terms of k and *EC* (e.g., Jo et al. 2005; Lee & Shackelford 2005a; Lee & Shackelford 2005b).

3.3. Materials and Methods

3.3.1. Liquids

Tap water (TW) and conservative water (CW) solutions were used as permeant liquids. The properties of these liquids are summarized in Table 3.1. The TW was used as a reference solution, and is recommended as a 'standard' permeant liquid in ASTM D5084-16a (2016). The properties of the TW used in this study were reported by Tong and Shackelford (2016). The measured *EC* and pH of TW were reported as 13 mS/m and 7, respectively. The CW as defined by Scalia and Benson (2010a) and ASTM D5084-16a (2016), was used in this study to mimic pore water that is representative of conservative field hydration and permeation conditions. The CW was prepared by dissolving 15.5 mg NaCl (ACS Grade; Fisher Chemical, Fair Lawn, NJ) and 279.5 mg $CaCl_2 \cdot 2H_2O$ (ACS Grade; Fisher Chemical, Fair Lawn, NJ) into 1 L of deionized water (DIW). The *EC* and pH of permeant liquid batches were measured using benchtop electrodes (Thermo Scientific™, Models 013005MD and 8157BNUMD, Waltham, MA) ensuring no substantial fluctuation (≥ ±5% from the values reported in Table 3.1) in the liquid chemistry occurred.

3.3.2. Geosynthetic Clay Liner

A high peel-strength GCL (manufacturer reported peel-strength, MRPS) of 3500 N/m (20 lb/in) manufactured by CETCO® under the trade name BENTOMAT® DN9 was used in this study. The GCL

comprised a layer of natural granular Na-bentonite sandwiched between two non-woven geotextiles reinforced by needle punching without thermal treatment. Detailed properties of the bentonite and GCL are presented in Tables 3.2 and 3.3. The GCL was ~8.9 mm thick in the as-received condition and the mass per unit area of bentonite was ~6.4 kg/m^2 (ASTM D5993-14 2014). Detail on methods to determine needle punching fibers properties are provided by Ghazizadeh and Bareither (submitted 2018; under review). Particle-size distributions for the Na-bentonite from the GCL are presented in Figure 3.1. Particle-size distributions are reported for both mechanical sieve (air dried) and hydrometer (wet) analyses. Bentonite in the as-received (air dried) condition classified as poorly graded sand, SP (ASTM D2487-17 2017), whereas the hydrated bentonite classified as a high plasticity clay, CH (ASTM D2487-17 2017). The swell index (*SI*) of Na-bentonite extracted from the GCL was measured according to ASTM D5890-11 (2011) in each permeant liquid (see Table 3.2).

3.3.3. Hydraulic Conductivity Tests

A summary of the *k* testing program conducted in this study is provided in Table 3.4. The *k* tests were performed by two methods: (1) the falling headwater, constant tailwater (ASTM D6766-18 2018; *Method B*) and (2) the constant rate-of-flow method (ASTM D6766-18 2018; *Method D*). All tests were performed in flexible-wall permeameters without application of backpressure. The effluent was analyzed for *EC*, which was used as an indicator for chemical equilibrium as per ASTM D6766-18 (2018).

Circular GCL specimens were cut with a scalpel blade from GCL roll with diameters, *d*, of 101.6 mm (4 in) for constant rate-of-flow tests and 152.4 mm (6 in) for falling headwater, constant tailwater tests. To prevent loss of bentonite from the GCL during cutting, a small amount of DIW was applied along the rim of the exposed bentonite via a squirt bottle. Larger cross-sectional area specimens were used for the falling headwater, constant tailwater method to enable greater volumes of liquid to pass through the specimen (i.e., greater Q_{out}) for *EC* and pH measurement (electrode probes used in this study required at least 15-20 mL of effluent for optimum measurement). After the circular specimen was detached from the sheet, any protruding geotextile fibers were trimmed. Specimens were placed in a flexible-wall permeameter with cover geotextile

facing the inflow (bottom) side between two filter papers (Whatman™, Buckinghamshire, UK) and two fiberglass insulation sheets (mass/area=0.41 kg/m^2) used in lieu of porous stones. The procedure for assembly of GCL specimens within a flexible-wall permeameter was as the same as that described by Scalia and Benson (2010a).

After the termination criteria were achieved, inflow and outflow lines were drained, the flexible-wall cell was disassembled, and the specimen was removed. The total weight of the GCL specimen was measured (± 0.01 g), together with measurements of thickness, L (± 0.01 mm), with a caliper at six locations around the perimeter of the specimen. The average L of the specimen used to calculate k and the pore volume of the specimen (i.e., the thickness of the specimen during permeation was assumed to be the same as the final thickness of the specimen after termination of the test).

3.3.3.1. Simplified Falling Headwater, Constant Tailwater Tests

A falling headwater, constant tailwater method without backpressure saturation was used in this study to measure k, and is referred hereafter as the 'simplified method'. This method, which is advantageous in terms of advantage the convenient collection of effluent samples for *EC* and pH measurement, has been used in prior studies involving GCL and/or bentonite composite materials (e.g., Ruhl & Daniel 1997; Jo et al. 2001; Vasko et al. 2001; Jo et al. 2004; Jo et al. 2005; Lee & Shackelford 2005b; Scalia et al. 2014; Conzelmann & Scalia 2016). Conzelmann et al. (2017) showed that backpressure is not necessary to saturate a GCL during k testing.

A schematic of the simplified falling head test, which was similar to the testing setup described by Conzelmann and Scalia (2016), is provided in Figure 3.2. An average effective stress (σ´) of 27.3 kPa (4 psi) and average i of ~210 was applied. Generally, the magnitude of i is an important factor affecting the measurement of k (Daniel 1994; Shackelford 1994), and maximum i for different measured k are prescribed in ASTM D5084-16a (2016). However, Shackelford et al. (2000) showed that the measured k of GCL specimen is practically independent of i over a broad range in i ($17 \leq i \leq 546$) provided the mean σ´ in the

specimen is the same. In this study, the simplified setup was adapted to accommodate two different GCL specimen conditions, viz., prehydrated (P) and non-prehydrated (NP) specimens.

Prehydrated (P) specimens

Prehydrated (P) specimens are specified for use in ASTM D6766-18 (2018) and as such determined as the baseline condition. Herein, prehydrated refers to a specimen that is initially exposed to the permeant liquid without permeation for at least 48 h.

Non-prehydrated (NP) specimens

Tests were also performed on non-prehydrated (NP) (air dried) specimens. For these tests, the air-dried specimens were permeated immediately after setup in the flexible-wall cell with the permeant liquid. These specimens typically required up to 1000 mL of solution during the first week. The NP test concluded when hydraulic termination criteria in ASTM D5084-16a (2016) were achieved. The objective of the non-prehydrated tests was to quantify the number of pore volumes of flow (PVF) required prior to attainment of low k. To provide a continuous supply of influent solution during the initial stages of non-prehydrated tests, a Mariotte bottle was attached to the inflow system (see Figure 3.2) to provide a sufficient supply of permeant (approximately 3 L). During this initial stage of the test, the constant head method was used (ASTM D6766-18 2018; *Method A*). Once the flow reduced to a sufficiently low q such that accurate measurement of influent was difficult, the Mariotte bottle was disconnected, and a pipet was used to supply inflow in a falling headwater, constant tailwater condition. Non-prehydrated tests with mock GCL specimens (bulk Na-bentonite) were also performed to investigate if there was a distinct behavior between GCL with and without needle punching, the results are presented in APPENDIX C.

3.3.3.2. Constant Flow Method Tests

Constant rate-of-flow tests were performed by pumping permeant liquid at a constant q, through a test specimen with a flow pump (Harvard Apparatus, Model 944, Holliston, MA). The test setup is illustrated

in Figure 3.3. Only prehydrated (P) specimens were tested using this method of permeation. As with the simplified method, prehydration in flow pump was performed without backpressure. A separate inflow reservoir filled with solution was connected to the inflow side (bottom) of the specimen for at least 48 h. The flow pumps used included two parallel tracks double-chamber infusion-withdrawal stainless steel syringes. The calibration for the flow pump is described in APPENDIX D. A differential pressure transducer (Omegadyne Inc., Model MMDWB030BIV10P4A0T3A5CE, Sunbury, OH) or two in-line pressure transducers (Omegadyne Inc., Model PXM209-1.60G10V, Sunbury, OH) were connected to the inflow and outflow lines to measure the difference in pore-water pressure (Δu) across the specimen. Pressure transducers were connected to a data acquisition system (National Instruments, Model NI USB-6009, Austin, TX) using the LabVIEW computer software (National Instruments, Austin, TX).

A complication of the constant flow method is determining the q to apply (given k is not known *a priori*), so that the steady state pore-water pressure difference (Δu_{ss}) does not exceed the confining cell pressure to ensure contact between membrane and the specimen, but needs to be sufficiently high to ensure the test is completed in reasonable time frame (Daniel 1994; Hong & Shackelford 2017a). Permeation was continued until hydraulic and chemical termination criteria required by ASTM D6766-18 (2018) was established.

Two sets of duplicate constant rate-of-flow tests were performed by different methods, viz., (1) infusing liquid into the inflow side while simultaneously withdrawing liquid from the outflow side (Test Series 11 in Table 3.2), and (2) only infusing liquid into the inflow side (Test Series 12 in Table 3.2). Each test series pair shared an influent supply reservoir and 60 mL polyethylene narrow mouth bottles were used on the outflow side of each test to collect the effluent for *EC* and pH measurement. The influent supply reservoir and effluent containers were covered with Parafilm® M (Bemis Company Inc., Oshkosh, WI) to avoid potential changes in liquid chemistry resulting from evaporation. The small pin hole was punctured through the film to maintain atmospheric pressure boundary conditions.

3.4. Results

The results of all k tests are summarized in Table 3.5. Each test result is accompanied by the elapsed time (t), PVF, the final degree of saturation (S), and the final gravimetric water content (w) measured at test completion. The elapsed time is defined as time spent for both hydration (without flow) and permeation (with flow).

All the prehydrated (P) tests (Test Series 1, 2, 11, and 12) have not achieved chemical equilibrium by the time of writing. In these cases, for specimen permeated with CW, the k and PVF reported in Table 3.5 for these tests represent estimates based on an assumed L of 7.5 mm whereas specimen permeated with TW (Test Series 1) was terminated prior to achieving chemical equilibrium because the duration of this test was extensive (283 d). Meanwhile non-prehydrated (NP) tests (Test Series 8) were not extended until the attainment of chemical equilibrium as discussed in Section 3.3.3.1.

There are two sets of t, PVF, and k values presented in Table 3.5. The values with the 5084 subscript (t_{5084}, PVF_{5084}, k_{5084}) pertain to those based on the hydraulic termination criteria in ASTM D5084-16a (2016). The values with the f subscript (t_f, PVF_f, k_f) pertain to those at the end of permeation. The values of S were determined following the procedure described by Conzelmann (2017). Measured S ranged from 103 % to 110 % and are in general agreement with Conzelmann et al. (2017) that specimens in this range in S can be assumed to be saturated at the end of permeation without backpressure. The final w of the bentonite component of the terminated tests ranged from 106 % to 126 %.

The results for individual test are presented in Figure 3.4 through Figure 3.8. At the time of writing, k for all tests were $< 3\times10^{-11}$ m/s. The temporal behavior of each test method is described subsequently.

3.4.1. Simplified Method Tests

3.4.1.1. Prehydrated (P) Tests

The results of simplified method test on prehydrated specimen permeated with TW and CW are shown in Figure 3.4 and Figure 3.5, respectively. Test 2b was a replicate of Test 2a and exhibited similar behavior; only Test 2a shown herein for brevity, Test 2b is shown in APPENDIX E. Specimens initially

exhibited a steep decline of k to values of ~1.6×10^{-11} m/s for TW and ~1.4×10^{-11} m/s for CW after 32 days of permeation (4.7 PVF) for TW and 36 days (5.8 PVF) for CW. The k stayed constant since the attainment of hydraulic equilibrium for specimen permeated with TW, whereas for specimen permeated with CW, thereafter, k increased minimally due to cation exchange.

The trends of effluent *EC* were similar. The peak of *EC* ratio occurred at the onset of permeation (EC_{out} = 813 mS/m for TW and 841 mS/m for CW) and then reduced rapidly corresponding to reductions in k. A unique subsequent slight increase in *EC* ratio then occurred at the onset of low k (> 7 PVF) in specimens permeated with CW, corresponding to back diffusion of soluble salts and exchanged cations (Ca^{2+} for Na^{+}; discussed in Section 3.5.2). Meanwhile, in all tests, pH_{out} increased with time towards a constant value at ~$1.2pH_{in}$ for TW and ~$1.6pH_{in}$ for CW.

3.4.1.2. Non-prehydrated (NP) Tests

The results for simplified method test on non-prehydrated specimen are presented in Figure 3.6. Test 8b was a replicate of Test 8a and exhibited similar behavior; only Test 8a shown herein for brevity, Test 8b is shown in APPENDIX E. Initial k was high (~6×10^{-8} m/s) as expected from poorly graded sand material during the initial stage of granule wetting, hydration, and swelling. The k reduced towards k_{5084} of ~2.1×10^{-10} m/s. Time needed to reach k_{5084} was 3 days (6.8 PVF). The k versus PVF graph illustrates a distinct behavior attributed to the continuous hydration process on dry specimen.

A temporary plateau in k versus time (or versus PVF) was observed at which k_{5084} was achieved. This plateau is hypothesized to result from water filling intergranular pores (at $Q_{in} > Q_{out}$) subsequently migrating by rate-limited osmosis into interparticle and interlayer pore spaces (at $Q_{in} \approx Q_{out}$), yielding swelling, and then further reducing k. The test was continued for several additional PVF until clear peak of *EC* ratio trend was obtained. The k_f was comparable to k_{5084} obtained from prehydrated specimen (~2.5×10^{-11} m/s). This decrease in k after attainment k_{5084} was observed near the peak *EC* ratio at t = 4 day. Effluent *EC* progressed from $EC_{out} \approx EC_{in}$ initially, to a peak *EC* ratio at k_{5084} then finally decreased to a diffusion

dominated *EC* ratio similar to prehydrated tests. Measured pH progressed upwards to a constant value of ~1.4pH$_{in.}$

3.4.2. Constant Flow Method Tests

The results of flow pump tests (Test Series 11 and 12) with prehydrated specimens are shown in Figure 3.7 and Figure 3.8. The results of Test 11a are presented in Figure 3.7 (Test 11b was a replicate of Test 11a and exhibited similar behavior; only Test 11a shown herein for brevity, Test 11b is shown in APPENDIX E). The results of Test 12a are presented in Figure 3.8 (Test 12b was a replicate of Test 12a and exhibited similar behavior; only Test 12a shown herein for brevity, Test 12b is shown in APPENDIX E).

The results of measured Δu, and therefore calculated k, exhibited initial erratic behavior at the onset of permeation (t < 60 days). This apparent erratic behavior is hypothesized to have resulted from specimen saturation. The inadequacy of the external prehydration setup for flow pump test had influenced the state of hydration of the specimen (i.e., not thoroughly hydrated).

Constant flow specimens achieved k_{5084} at < 8 PVF (k_{5084} = 5.7×10^{-11} m/s for Test 11a and 4.6×10^{-11} m/s for Test 12a). These k_{5084} values were higher than the k obtained after saturation (3.7×10^{-11} m/s for Test 11a and 2.2×10^{-11} m/s for Test 12a). This discrepancy is hypothesized to have occurred due to limited osmosis at interparticle and interlayer pores as liquid was supplied into the specimen at a limited q (although the intergranular pore spaces had been filled, as Q_{out}/Q_{in} was immediately within termination criterion). Saturation is interpreted to have occurred at t > 60 days, when Δu trends smoothed. This saturation process took longer time (27 PVF for Test 11a and 22 PVF for Test 12a) than Simplified NP test (6 PVF) presumably due to lower q being applied to the specimens. At PVF ≥ 22 (saturated condition) k increased minimally with time (and PVF) due to cation exchange.

A difference was observed in the Q_{out}/Q_{in} trend before and after saturation, where after saturation was achieved the Q_{out} consistently exceeded the Q_{in} (although still within 25 % allowable threshold). However, Test 11a exhibited a return to $Q_{out}/Q_{in} \approx 1$ after 220 d (47 PVF). This difference likely resulted from physico- (due to change of Δu) and chemico- (due to cation exchange) consolidation (Shackelford et al. 2018;

manuscript in progress) of the specimens. The obtained k values were similar regardless type of method employed to apply the continuous flow.

3.5. Discussion

3.5.1. Osmosis within Bentonite Granules

The effect of osmosis is illustrated in Figure 3.9 by comparing the results of Simplified P test (Test 2a) and Simplified NP test (Test 8a). Elapsed time in Figure 3.9 was normalized so that t = 0 d corresponds to the initiation of bentonite wetting (Test 2a hydrated for ~5 days). Simplified P test had noticeably steeper decrease in k with time. The k at the onset of permeation, for Simplified P test was ~4×10^{-9} m/s, one order of magnitude lower than Simplified NP test at ~6×10^{-8} m/s.

The difference of temporal behavior between Simplified P and Simplified NP tests (see Figure 3.6) can be explained by three-compartment model from Jo et al. (2006), as illustrated in Figure 3.10. Equally, Aitchison et al. (1965) explained the potential of soil water was divided into gravitational potential, matrix or capillary potential, and osmotic (or solute) potential. At the onset of permeation, when $Q_{in} >> Q_{out}$, the intergranular pores are initially filled with permeant solution. Once $Q_{in} \approx Q_{out}$, osmosis within interparticle and interlayer pore spaces progresses through crystalline and osmotic swelling regimes. Throughout permeation, excess soluble salts are flushed out. This process lasts until peak effluent EC (marked with red arrows in Figure 3.9), corresponding to when the GCL achieved k of ~2×10^{-10} m/s at which k transport within the bentonite is dominated by diffusion (Shackelford 2014). However, this trend was not observed in Simplified P tests (see Figure 3.5). Hydration without inducing flow through the specimen allowed soluble salts to equilibrate within the intergranular pore spaces until permeation commenced. Hence in Simplified P tests, the peak EC ratio (EC_{out}/EC_{in}) was observed at the onset of permeation and finally decreased to a lower rate controlled by diffusion. Discussion regarding diffusion can be found in the subsequent section.

As described in Section 3.4.1.2, the k of Simplified NP test exhibited a temporary plateau at ~2×10^{-10} m/s (6 PVF) before k decreased further. This trend was not observed in Simplified P test. The k_{5084} attained

for all three methods were the highest for Simplified NP (Test 8a) specimen, then Flow Pump P (Tests 11a and 12a), and the lowest for Simplified P (Test 2a).

Bowders (1991) and Shackelford (1994) discussed the effect of i on pore fluid as 'retention time.' High i results in a lower retention time during which the permeant liquid can interact with the specimen. ASTM D6766-18 (2018) calls for 48 h period under backpressure from both ends (under zero gradient) "to allow saturation, hydration, swell, and consolidation to occur." This duration (or retention time) appears adequate to promote faster chemical process (osmosis).

Prior hydration enables the bentonite in Simplified P specimen to swell and reach a lower k with less PVF than Simplified NP specimen. However, with regard to elapsed time, Simplified NP attained k_{5084} (highest q through the specimen) the fastest. However, the k_{5084} obtained from this method is one order of magnitude higher than prehydrated tests either with constant rate-of-flow or simplified method.

3.5.2. Diffusion as Primary Factor Affecting Time to Chemical Equilibrium

The effect of diffusion on time to chemical equilibrium is evaluated by comparing the *EC* measurements from the Simplified P (Test 2a), Simplified NP (Test 8a), and Flow Pump P (Tests 11a and 12a) specimens, as presented in Figure 3.11. The results of pH measurements are also presented for completeness but are not discussed. Diffusion, as opposed to advection, becomes the dominant transport process at $k < 2\text{-}3\times10^{-10}$ m/s (Shackelford 2014). All prehydrated specimens exhibited a unique subsequent slight increase in *EC* ratio after low k was established. For the Simplified P test, this increase was hypothesized to be an indication of rate limited back diffusion of soluble salts; although i was kept relatively constant, the rate of salt egress was not constant due to varying permeant solution contact time governed by increasing k. This change of k may affect the magnitude of chemical gradient between intergranular and intergranular pores.

Multiple subsequent slight increase in *EC* ratio were also observed in Flow Pump P tests (Figure 3.11). These unique subsequent slight increase in *EC* ratio were prompted by the decrease in the q imposed by the flow pump (to 5.2 mL/d) to avoid membrane blowout after specimen saturation ($\Delta u_{ss} < \sigma_c = 69$ kPa

[10 psi]). The three-compartment model illustrated in Figure 3.10 again provides a framework for interpreting these results. The outward egress of salt is dependent on the rate at which cations diffuse out from interparticle and interlayers pore spaces to intergranular pores. The rate of cation exchange (i.e., ion exchange reaction kinetics) is relatively quick, if not rapid (e.g., Ogwada & Sparks 1986; Crooks et al. 1993; Tang & Sparks 1993). However, as the results of the constant rate-of-flow tests illustrate, the rate of diffusion limits the establishment of chemical equilibrium.

Based on the results presented in Figure 3.11, the Flow Pump P tests are projected to reach $EC_{out} \approx EC_{in}$ in a shorter time than the Simplified P test by the virtue of maintaining higher q during the diffusion-dominated portion of the test. Higher q allowed for greater mass transfer of soluble salts from intergranular pores after these salts have diffused out from the interlayer then interparticle pore spaces. This flushing action maintained the concentration gradient between interlayer pore spaces and the intergranular pore spaces through at which the bulk of advection occurs.

The difference between k determined based on hydraulic (ASTM D5084-16a 2016) or chemical (ASTM D6766-18 2018) equilibrium is that the *EC* criterion requires sufficient time and flow through the specimen to allow for cation exchange and back diffusion of soluble salts to occur. Thus, although use of flow pump enabled rapid measurement of k_{5084}, the method did not yield a more rapid path to chemical equilibrium (except that, in this study, flow pump tests used a higher q and thus higher i, which increased the rate of salt flushing). A higher q across the falling head test specimens (by i) may be useful to achieve chemical equilibrium faster, although higher i generally requires higher σ'. An additional tradeoff testing with an elevated i is that test results may yield unrealistic retardation factors. Shackelford and Redmond (1995) noted that at a sufficiently low flow rate, longer retention time enabled the solute to adsorb within the bentonite and as a result increased the retardation factor. Thus, testing with high i does not provide a perfect solution to more rapidly attaining chemical equilibrium.

Table 3.1. Properties of permeant liquids

Solution	Parameter			
	Ionic strength, *I* (mM)	**Ratio of monovalent-to-divalent cations, *RMD* ($mM^{½}$)[a]**	**Electrical conductivity, *EC* (mS/m)**	**pH**
Tap Water (TW)[b]	106.7	697.4	13	7.00
Conservative Water (CW)[c]	6	6.1	51	5.74

[a]As described in Kolstad et al. (2004)

[b]As described in Tong and Shackelford (2016)

[c]As described in Scalia and Benson (2010)

Table 3.2. Properties of bentonite

Property		Value
Mineralogy	Montmorillonite (%)	85 - 91
	Quartz (%)	2 - 4
	Augite (%)	0 - 5
	etc.	< 3
Cation Exchange Capacity, *CEC* (meq/100 g)		78
Atterberg Limits (ASTM D4318)	Liquid Limit, *LL* (%)	411
	Plastic Limit, *PL* (%)	34
	Plasticity Index, *PI* (%)	377
Particle Size (ASTM D422)	% Fines (<75 μm)	95
	% <5 μm	86
	% <2 μm	74
Activity, *A*		5.1
Swell Index[a], *SI* (mL/2 g)	Tap Water (ASTM D5890)	33.3
	Conservative Water	31.6

[a]Values reported are averages of three measurements

Table 3.3. Properties of GCL

Property		Value
Initial air-dried (off roll) water content (%)		2.9
Initial (off roll) thickness (mm)		8.86 (SD=0.67, n=40)
Average bentonite mass/area (kg/m^2)	Oven dried (ASTM D5993)	6.36 (SD=0.32, n=10)
	Air dried	6.55 (SD=0.32, n=10)
Carrier Geotextile (ASTM D5291)	Type	Non-woven
	Mass (kg/m^2)	0.36 (SD=0.05, n=10)
Cover Geotextile (ASTM D5291)	Type	Non-woven
	Mass (kg/m^2)	0.28 (SD=0.03, n=10)
Structure and Reinforcement	Needle-punched	Yes
	Thermally treated	No
Bundle size (mm)		1.09 (SD=0.24, n=10)
No. of bundles/area ($bundles/m^2$)		146,300 (SD=1,240, n=40)
No. of monofilament/bundle		42 (SD=6.39, n=20)
Percentage area covered by bundles		13.6
Manufacturer reported peel strength, MRPS	N/mm	3500
	lb/in	20

Table 3.4. Testing program

Test Series		Test Type	Permeant liquid[a]
1	Simplified Method	Prehydrated (P)	TW
2			CW
8		Non-prehydrated (NP)	CW
11	Constant flow	Simultaneous infuse-withdrawal (P)	CW
12		Infuse only (P)	CW

[a]See Section 3.3.1 for description and properties of each permeant liquid

Table 3.5. (Color) Summary of the results of the hydraulic conductivity tests

	Test Series	Test number[a]	Test type	Permeant liquid[b]	Values at termination criteria							
					ASTM D5084-16a (2016)			Final			*w*	*S*
					t_{5084} (d)[c]	PVF_{5084}	k_{5084} (m/s)	t_f (d)[c]	PVF_f	k_f (m/s)	(%)	(%)
Simplified Method	1	1	Prehydrated (P)	TW	31.94 [5]	4.7	1.6×10^{-11}	283.86 [5]	14.3	1.6×10^{-11}	125	103
	2	2a		CW	36.2 [5]	5.8	1.4×10^{-11}	[5]				
		2b		CW	24.7 [6]	6.4	2.6×10^{-11}	[6]				
	8	8a	Non-prehydrated (NP)	CW	2.8 [0]	6.8	2.1×10^{-10}	21.86 [0]	8.8	2.5×10^{-11}	106	110
		8b		CW	5.2 [0]	10.7	2.4×10^{-10}	28.79 [0]	14.1	3.2×10^{-11}	126	109
Constant flow	11	11a	Simultaneous infuse-withdrawal (P)	CW	16.4 [3]	5.2	5.7×10^{-11}	[3]				
		11b		CW				[3]				
	12	12a	Infuse only (P)	CW	14.4 [3]	7.1	4.6×10^{-11}	[3]				
		12b		CW	14.4 [3]	7.4	8.1×10^{-11}	[3]				

[a]Green color indicate tests are still running and have not meet chemical equilibrium criteria; thus, PVF (gray) is an estimated value

[b]See Section 3.3.1 for description and properties of each permeant liquid

[c]Reported time at which termination criteria was met elapsed since permeation, values in brackets are approximate time spent for hydration

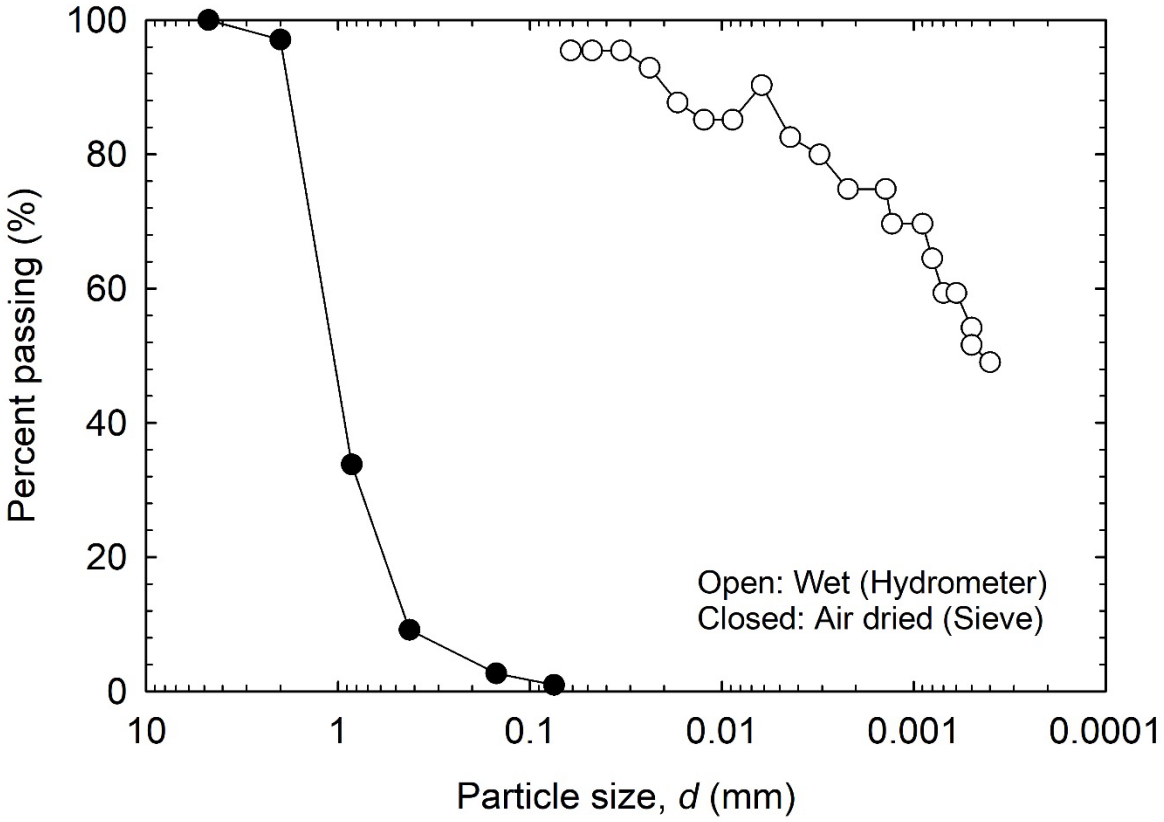

Figure 3.1. Particle-size distributions for bentonite extracted from the GCL based on mechanical sieve (air dried) and hydrometer (wet) analyses

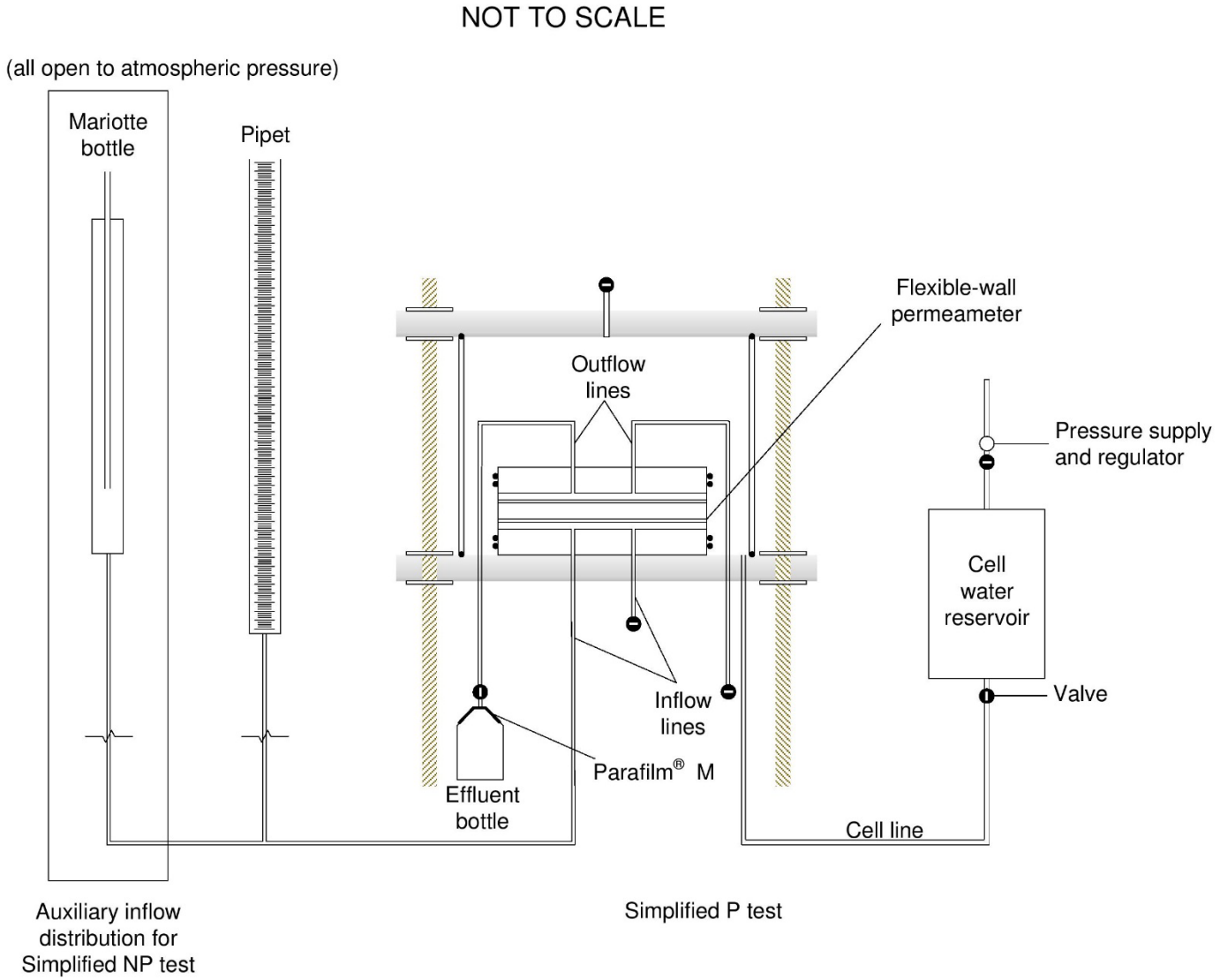

Figure 3.2. Schematic of the test setup for hydraulic conductivity testing by falling headwater, constant tailwater method (for prehydrated 'P' specimens) and constant head method (for non-prehydrated 'NP' specimens)

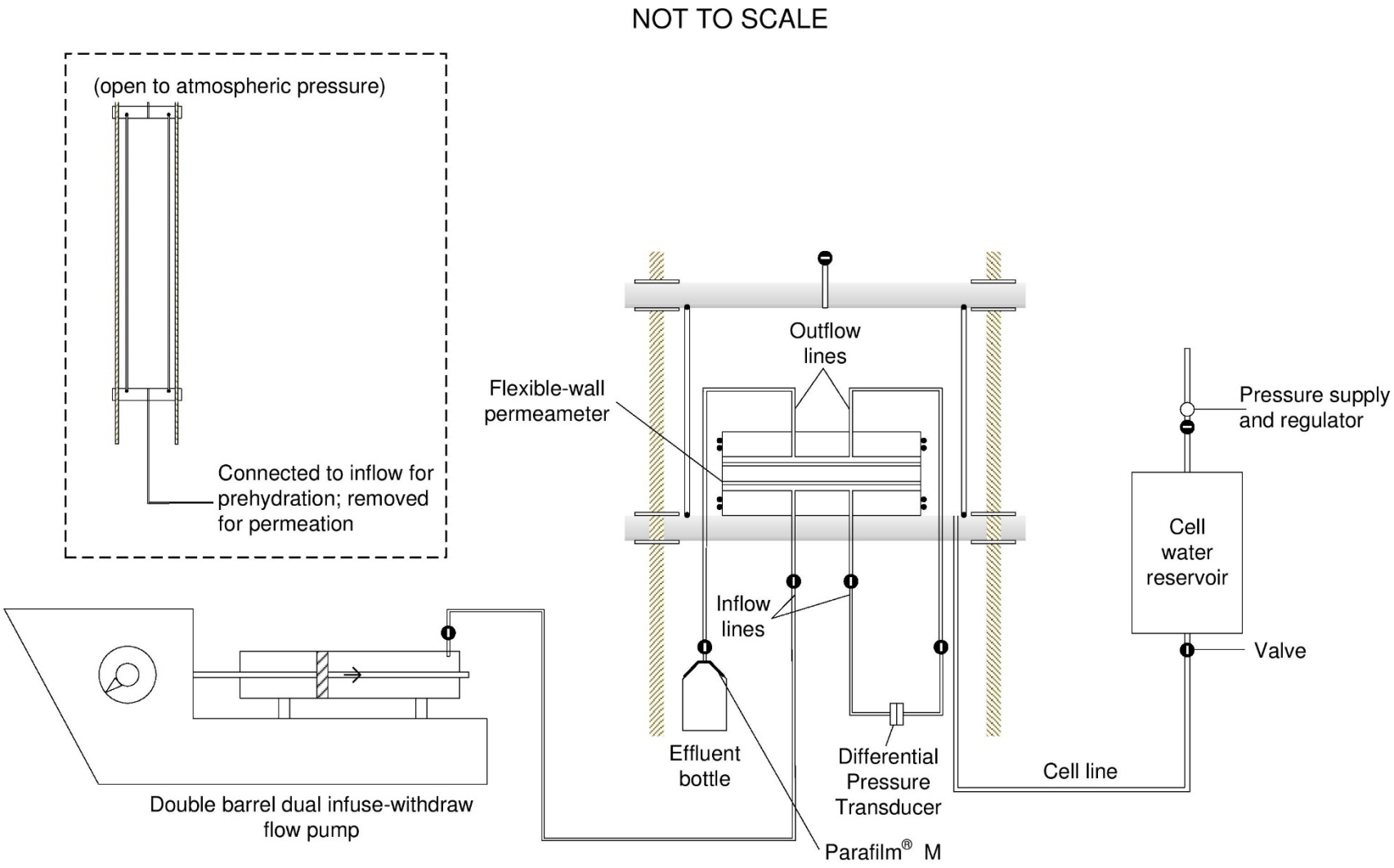

Figure 3.3. Schematic of the test setup for hydraulic conductivity testing by constant rate-of-flow method (flow pump) including the apparatus used for prehydration stage

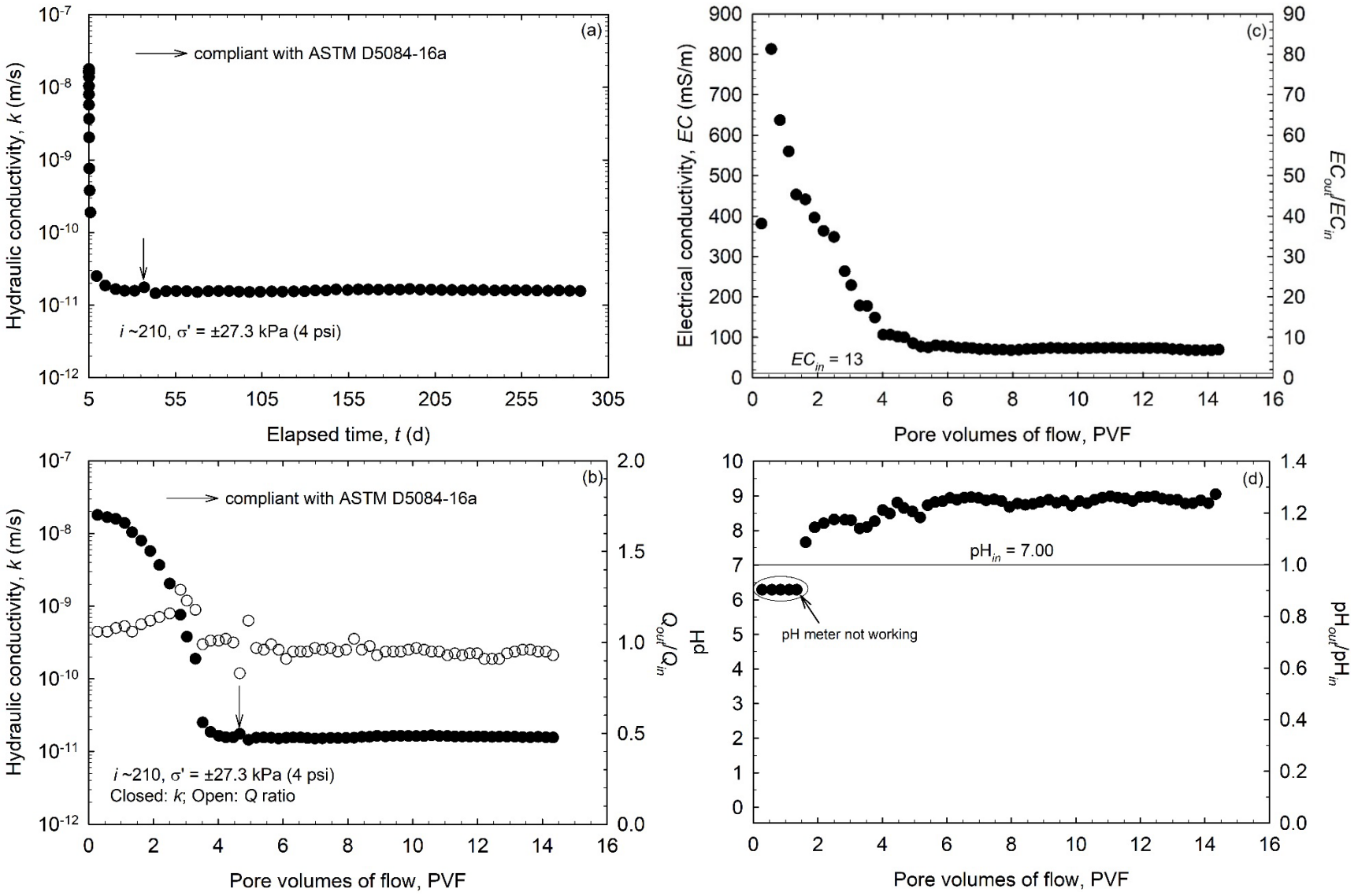

Figure 3.4. Test results for falling headwater, constant tailwater method for prehydrated (Simplified P) test with tap water (Test 1): (a) hydraulic conductivity with respect to elapsed time, (b) hydraulic conductivity with respect to pore volumes of flow, (c) electrical conductivity, and (d) pH

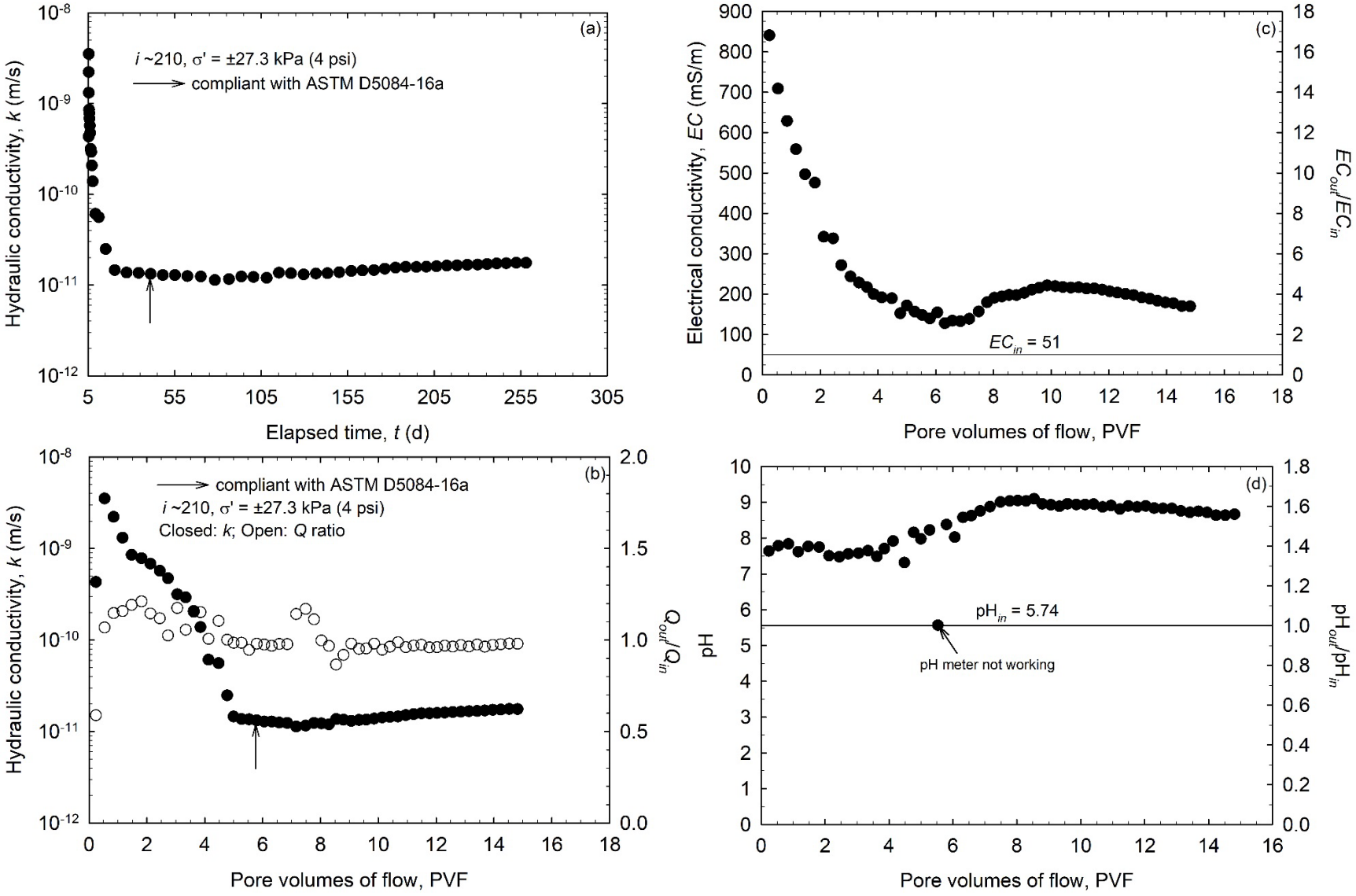

Figure 3.5. Test results for falling headwater, constant tailwater method for prehydrated (Simplified P) test with conservative water (Test 2a): (a) hydraulic conductivity with respect to elapsed time, (b) hydraulic conductivity with respect to pore volumes of flow, (c) electrical conductivity, and (d) pH

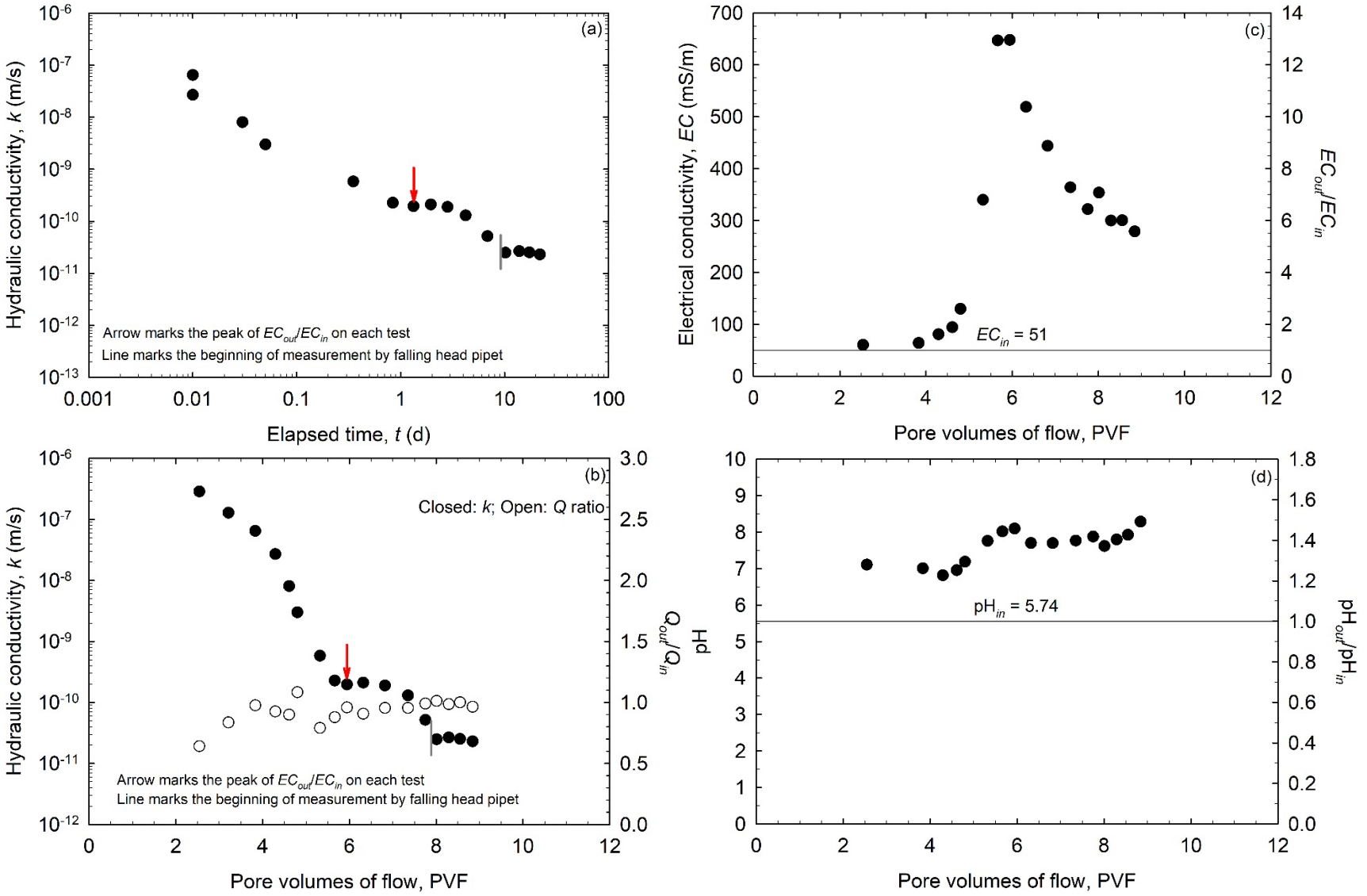

Figure 3.6. (Color) Test results for non-prehydrated (Simplified NP) test with conservative water (Test 8a): (a) hydraulic conductivity with respect to elapsed time on log scale, (b) hydraulic conductivity with respect to pore volumes of flow, (c) electrical conductivity, and (d) pH

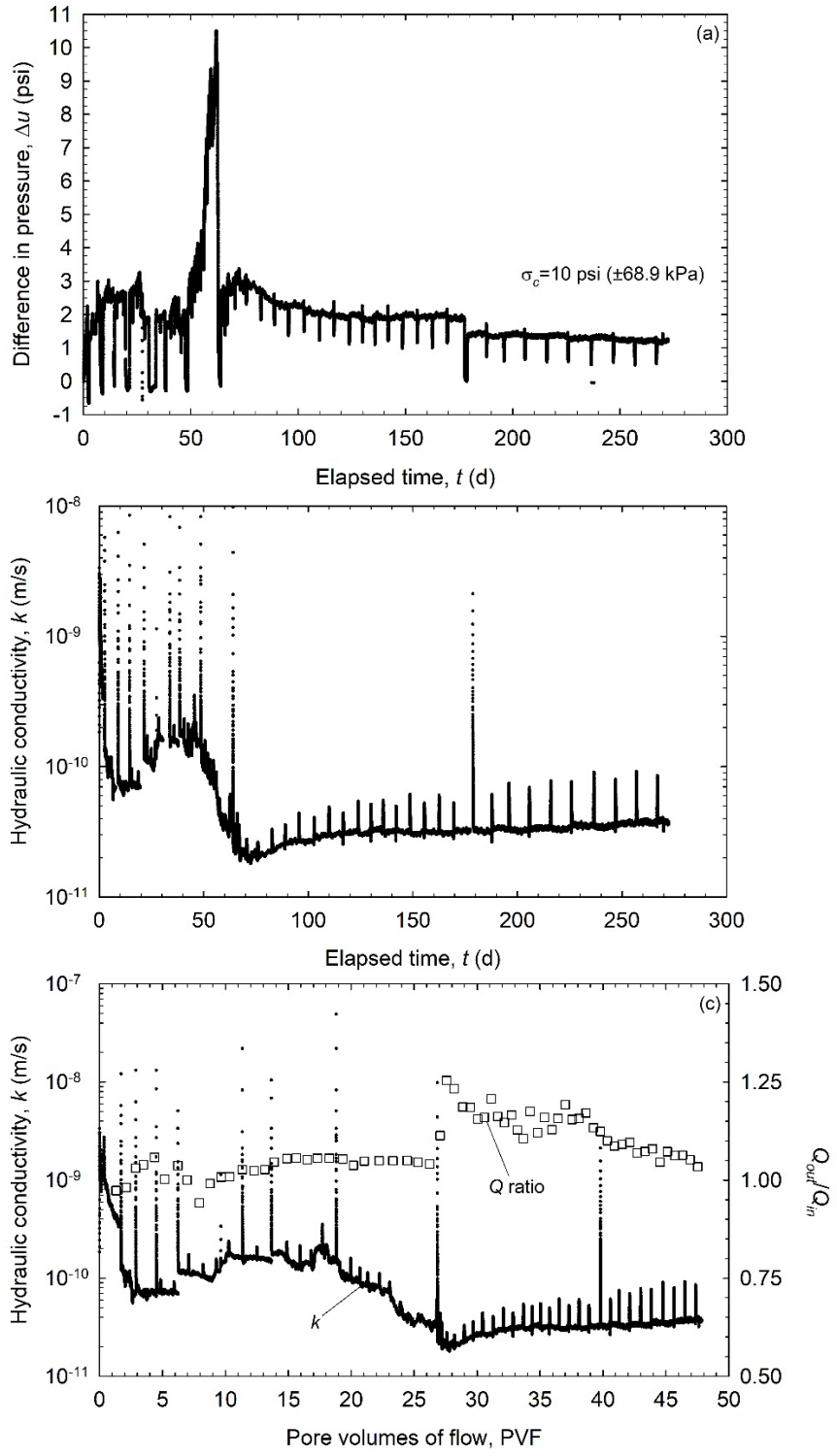

Figure 3.7. Test results for constant rate-of-flow for prehydrated (Flow Pump P) test with conservative water by simultaneous infusing influent and withdrawing effluent (Test 11a): (a) difference in pore-water pressure with respect to elapsed time, (b) hydraulic conductivity and cell water reading with respect to elapsed time, and (c) hydraulic conductivity and volumetric flow ratio with respect to pore volumes of flow

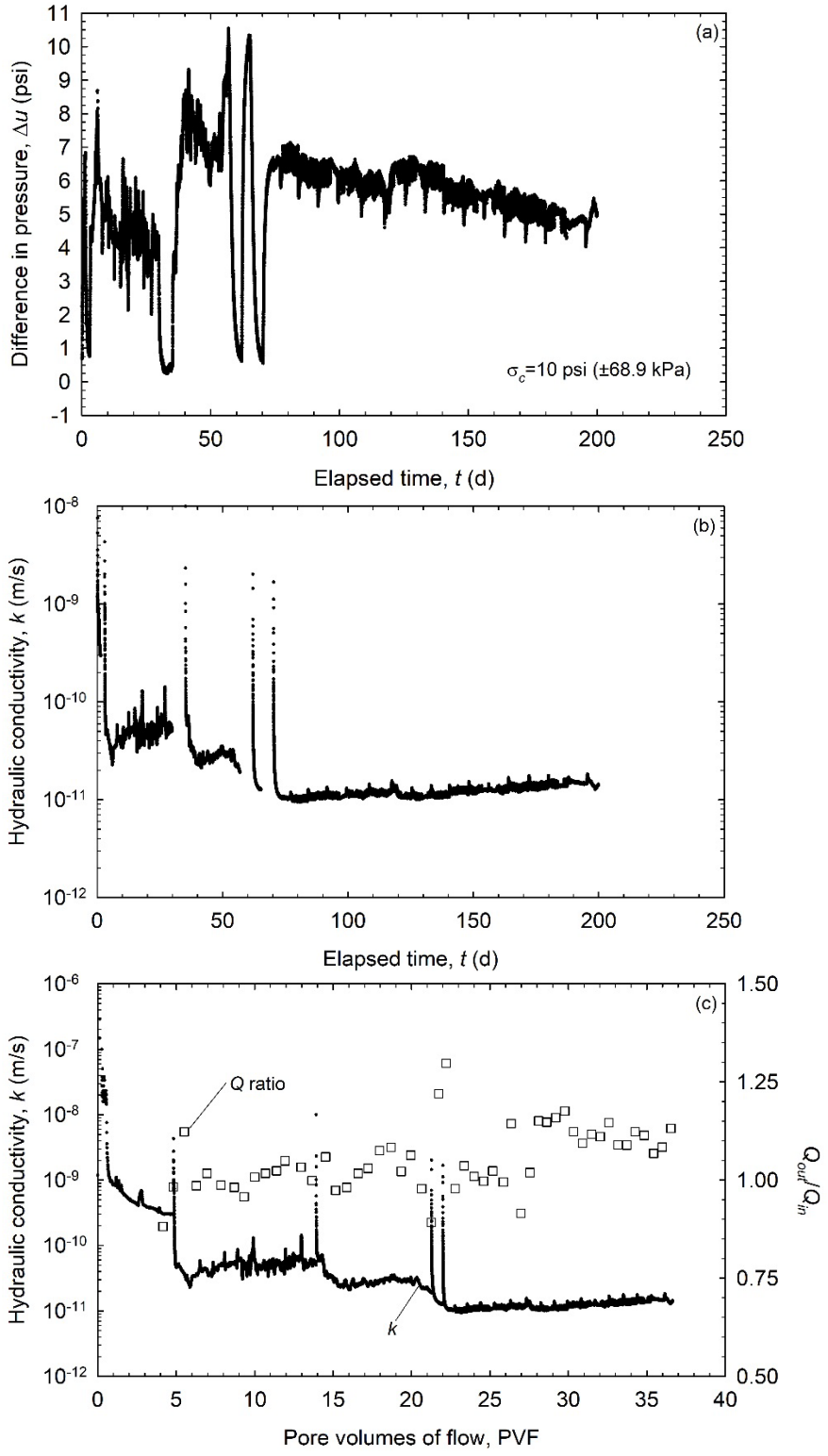

Figure 3.8. Test results for constant rate-of-flow for prehydrated (Flow Pump P) test with conservative water by infusing influent only (Test 12a): (a) difference in pore-water pressure with respect to elapsed time, (b) hydraulic conductivity and cell water reading with respect to elapsed time, and (c) hydraulic conductivity and volumetric flow ratio with respect to pore volumes of flow

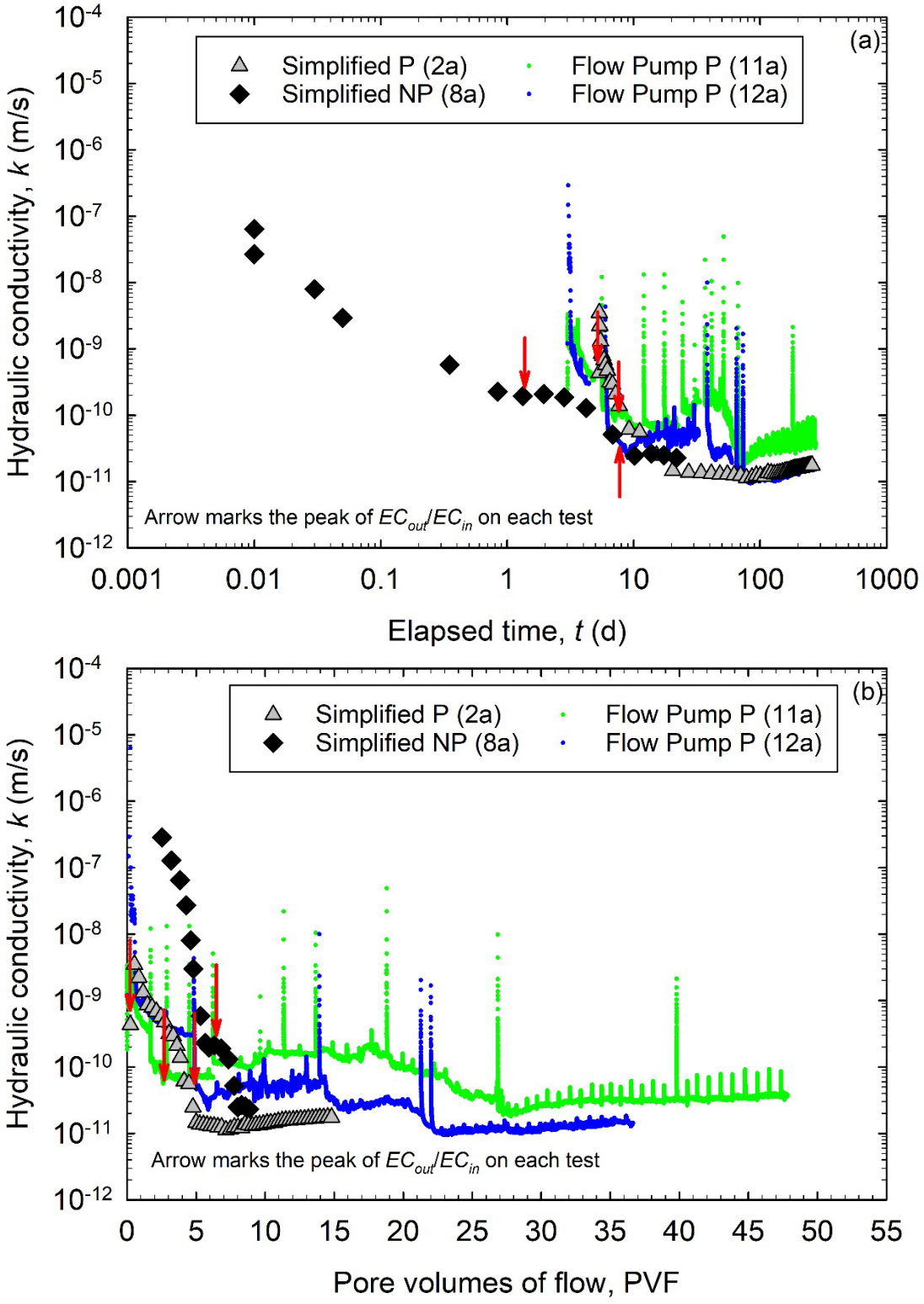

Figure 3.9. (Color) Comparison of hydraulic conductivity from all test methods: (a) hydraulic conductivity with respect to elapsed time in log scale, (b) hydraulic conductivity with respect to pore volumes of flow

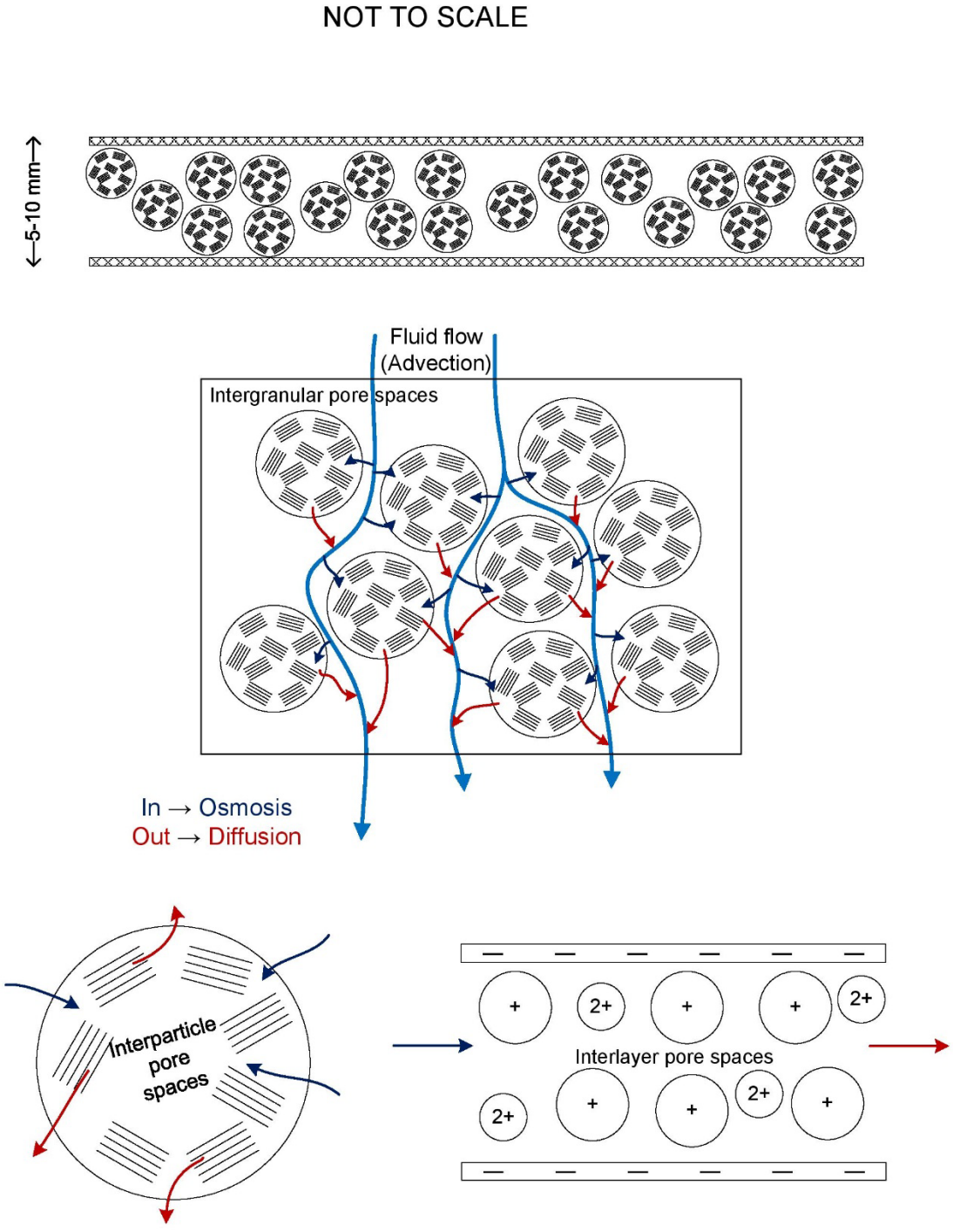

Figure 3.10. (Color) Concept of three compartment model within GCL (redrawn after Jo et al. 2006)

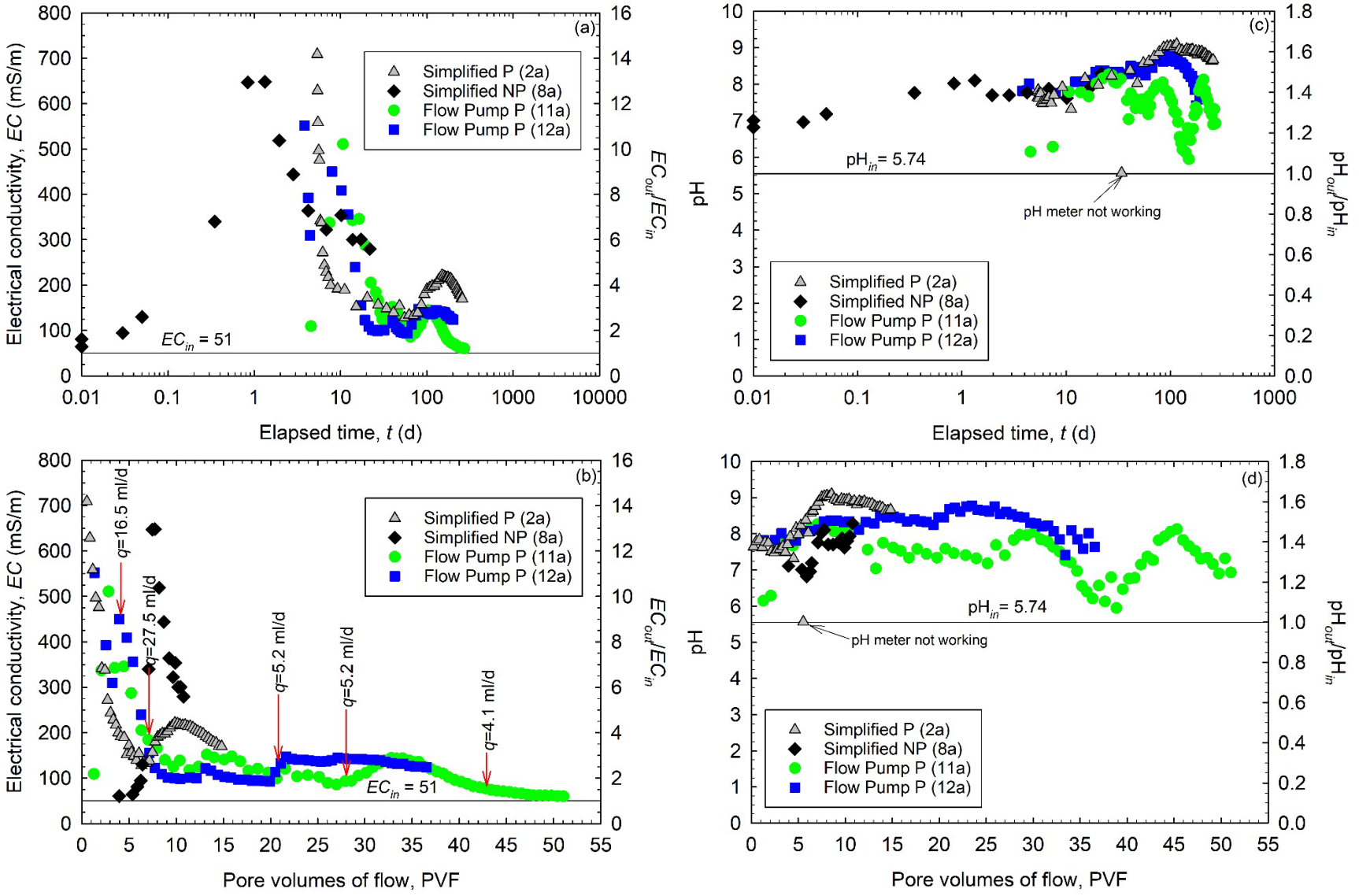

Figure 3.11. (Color) Effect of diffusion illustrated by: (a) electrical conductivity versus elapsed time in log scale and (b) electrical conductivity versus pore volumes flow. Data on corresponding pH measurement provided in (c) and (d) for completeness

CHAPTER 4 CONCLUSION AND RECOMMENDATION

This study was divided into two sections, as defined in CHAPTER 1. CHAPTER 2 focused on the effect of the grade of needle punching of the GCL on hydraulic conductivity (k), by evaluating the k of a high peel-strength GCL permeated with various solutions, and compared the results with a lower peel-strength GCL. CHAPTER 3 investigated potential means to expedite the achievement of chemical equilibrium during GCL compatibility test by evaluating two different test methods. Conclusions and recommendations from this study are provided below.

The k of a high peel-strength GCL, designated as higher grade needle punching (HGN) GCL, was assessed under low effective stress (σ') of ~27.3 kPa (4 psi) with a range of inorganic chemical solutions. The tests were performed by a falling headwater, constant tailwater method without application of backpressure. All specimens were prehydrated for at least 48 h and subsequently permeated with the same liquid. Specimens permeated with dilute strength solutions (tap water, TW; conservative water, CW; 1 and 2.5 mM $CaCl_2$) were conducted until hydraulic equilibrium was reached, but at the time of writing, chemical equilibrium (defined in terms of electrical conductivity, EC, ratio = 1.0±0.1) had not been attained. Whereas specimens permeated with intermediate strength solutions (5, 10, and 20 mM $CaCl_2$) had achieved hydraulic and chemical equilibrium. Once specimens permeated with 5 and 10 mM $CaCl_2$ had reached chemical equilibrium and established final k, the σ' was sequentially increased to ~61.7 kPa (9 psi), and the tests were continued until equilibrium were re-established.

HGN GCL permeated with solutions EC > 62 mS/m (i.e., intermediate strength solutions) produced uncharacteristically high k relative to the k reported in the literature for lower grade needle punching (LGN) GCL—up to three orders of magnitude for specimen permeated with 20 mm $CaCl_2$. This result is attributed to the preferential flow paths through the GCL fiber bundles. The time of permeation required to achieve chemical equilibrium was faster for tests conducted on HGN GCL compared to LGN GCL. This result is hypothesized not to be an actual attainment of chemical equilibrium, due to the aforementioned preferential flow in fiber bundles, although attainment of true chemical equilibrium is anticipated to result in an even

higher k. HGN GCL produced low k (~2-3×10^{-11} m/s) when permeated with dilute strength solutions (EC ≤ 62 mS/m). The sequential increase of σ´ to ~61.7 kPa (9 psi) indicated that HGN GCL was unable to overcome the effect of needle punching. Therefore these products may be unsuitable for use in lower σ´ applications with the intent of enabling future expansion/higher stress. Future research should test HGN GCL at higher σ´ range to characterize the k property if HGN GCL used as intended, and explore the effect of HGN GCL k if prehydrated with a dilute strength solution prior to permeation with intermediate strength solutions.

Compatibility of the HGN GCL was assessed by long-term k tests planned until attainment of chemical equilibrium. However, at the time of writing, the tests had not met chemical equilibrium—although currently available results can be used to infer future behavior. Tests were performed by two methods described in ASTM D6766-18 (2018): (1) falling headwater, constant tailwater (*Method B*) and (2) constant rate-of-flow (*Method D*). To mimic the pore water that is representative of conservative field hydration and permeation conditions, all specimens were tested with conservative water (CW) with varying hydration state of the GCL (viz., prehydrated versus non-prehydrated).

The effect of diffusion as the limiting process to attainment of chemical equilibrium was evident from effluent EC measurements. Fluctuating flow pump rate (q) to prevent membrane blowout (i.e., steady state pore-water pressure, Δu_{ss} > cell pressure, σ_c) provided evidence that hydraulic gradient (i) directly impacts the flushing of soluble salts. Diffusion occurred concurrently into and from (removing exchanged cations and soluble salts) interparticle and interlayer to intergranular pore spaces and then out from the GCL. Faster duration to chemical equilibrium can be attained by increasing the i as means to maintain a high concentration gradient between intergranular pore space and within bentonite granules thus maximize the rate of diffusion. These findings are consistent with the three-compartment model for GCL compatibility.

The trend of k and EC measurements were dependent on the manner (i and hydration state) at which the tests were performed. Permeating non-prehydrated (dry) GCL did not yield greater elution of soluble salts than permeating prehydrated (i.e., in-permeameter hydrated) specimens.

REFERENCES

Abu-Hejleh, A.N., Znidarcic, D. & Barnes, B.L., 1996. Consolidation characteristics of phosphatic clays. *Journal of Geotechnical Engineering*, 122(4), pp.295–301. Available at: https://doi.org/10.1061/(ASCE)0733-9410(1996)122:4(295).

Abu-Hejleh, A.N., Znidarcic, D. & Illangasekare, T.H., 1993. Permeability determination for unsaturated soils. In S. L. Houston & W. K. Wray, eds. *Unsaturated Soils (GSP 39)*. Dallas, Texas, USA, pp. 163–174.

Aiban, S.A. & Znidarcic, D., 1989. Evaluation of the flow pump and constant head techniques for permeability measurements. *Geotechnique*, 39(4), pp.655–666. Available at: https://doi.org/10.1680/geot.1989.39.4.655.

Aitchison, G.D., Russam, K. & Richards, B.G., 1965. Engineering concepts of moisture equilibrium and moisture changes in soils. In G. D. Aitchison, ed. *Moisture Equilibria and Moisture Changes in Soils Beneath Covered Areas*. Sydney, Australia: Butterworths, pp. 7–21.

Ashmawy, A.K., El-Hajji, D., Sotelo, N. & Muhammad, N., 2002. Hydraulic performance of untreated and polymer-treated bentonite in inorganic landfill leachates. *Clays and Clay Minerals*, 50(5), pp.546–552.

ASTM D2487-17, 2017. Standard Practice for Classification of Soils for Engineering Purposes (Unified Soil Classification System). *ASTM International, West Conshohocken, PA*, pp.1–10. Available at: https://doi.org/10.1520/D2487-17.

ASTM D4439-17, 2017. Standard Terminology for Geosynthetics. *ASTM International, West Conshohocken, PA, USA*, pp.1–6. Available at: https://doi.org/10.1520/D4439-17.

ASTM D5084-16a, 2016. Standard Test Methods for Measurement of Hydraulic Conductivity of Saturated Porous Materials Using a Flexible Wall Permeameter. *ASTM International, West Conshohocken, PA, USA*, pp.1–24. Available at: https://doi.org/10.1520/D5084-16A.

ASTM D5890-11, 2011. Standard Test Method for Swell Index of Clay Mineral Component of Geosynthetic Clay Liners. *ASTM International, STP1142*, pp.1–7. Available at: https://doi.org/10.1520/D5890-11.

ASTM D5993-14, 2014. Standard Test Method for Measuring Mass Per Unit of Geosynthetic Clay Liners. *ASTM International, West Conshohocken, PA*, pp.1–4. Available at: https://doi.org/10.1520/D5993-14.

ASTM D6766-18, 2018. Standard Test Method for Evaluation of Hydraulic Properties of Geosynthetic Clay Liners Permeated with Potentially Incompatible Aqueous Solutions. *ASTM International, West Conshohocken, PA, USA*, pp.1–9. Available at: https://doi.org/10.1520/D6766-18.

Bareither, C.A., Soleimanian, M.R. & Ghazizadeh, S., 2018. Direct shear testing of GCLs at elevated temperature and in a non-standard solution. *Geosyntethics International*. Available at: https://doi.org/10.1680/jgein.18.00014.

Benson, C.H. & Meer, S.R., 2009. Relative abundance of monovalent and divalent cations and the impact of desiccation on geosynthetic clay liners. *Journal of Geotechnical and Geoenvironmental Engineering*, 135(3), pp.349–358. Available at: https://doi.org/10.1061/(ASCE)1090-0241(2009)135:3(349).

Benson, C.H., Ören, A.H. & Gates, W.P., 2010. Hydraulic conductivity of two geosynthetic clay liners permeated with a hyperalkaline solution. *Geotextiles and Geomembranes*, 28(2), pp.206–218. Available at: http://dx.doi.org/10.1016/j.geotexmem.2009.10.002.

Bohnhoff, G.L. & Shackelford, C.D., 2013. Improving membrane performance via bentonite polymer nanocomposite. *Applied Clay Science*, 86, pp.83–98. Available at: http://dx.doi.org/10.1016/j.clay.2013.09.017.

Bouazza, A., 2002. Geosynthetic clay liners. *Geotextiles and Geomembranes*, 20(2), pp.3–17.

Bowders Jr., J.J., 1991. Permeability of clays under organic permeants (Discussion). *Journal of Geotechnical Engineering*, 115(1), pp.1278–1280. Available at: https://doi.org/10.1061/(ASCE)0733-9410(1991)117:8(1278.2).

Bradshaw, S.L. & Benson, C.H., 2014. Effect of municipal solid waste leachate on hydraulic conductivity and exchange complex of geosynthetic clay liners. *Journal of Geotechnical and Geoenvironmental Engineering*, 140(4), p.04013038. Available at: https://doi.org/10.1061/(ASCE)GT.1943-5606.0001050.

Conzelmann, J.T., 2017. *Hydraulic and Chemical Properties of Geosynthetic Clay Liners in Mining Applications*. MS

Thesis: Colorado State University.
Conzelmann, J.T. & Scalia IV, J., 2016. Method and equipment for hydraulic conductivity measurement of geosynthetic clay liners with mine waste leachates. In *Proceedings of Tailings and Mine Waste 2016*. Keystone, Colorado, USA: UBC Studios, University of British Columbia, Vancouver, pp. 643–653.
Conzelmann, J.T., Scalia IV, J. & Shackelford, C.D., 2017. Effect of backpressure saturation on the hydraulic conductivity of GCLs. In *Geotechnical Frontiers (GSP 276)*. pp. 227–235.
Crooks, J.E., El-Daly, H., El-Sheikh, M.Y., Habib, A.-F.M & Zaki, A.B., 1993. Kinetics of ion- exchange on montmorillonite clays. *International Journal of Chemical Kinetics*, 25(3), pp.161–168. Available at: https://doi.org/10.1002/kin.550250304.
Daniel, D.E., 2000. Hydraulic durability of geosynthetic clay liners. In *Proceedings of the GRI-14 Conference on "Hot Topics in Geosynthetics - I."* GII Publications, pp. 116–135.
Daniel, D.E., 1994. State-of-the-Art: Laboratory hydraulic conductivity tests for saturated soils. *Hydraulic Conductivity and Waste Contaminant Transport in Soil, ASTM STP 1142*, pp.30–78.
Daniel, D.E., Shan, H.-Y. & Anderson, J.D., 1993. Effects of partial wetting on the performance of the bentonite component of a geosynthetic clay liners. In *Geosynthetics '93*. Vancouver, Canada, pp. 1483–1496.
Di Emidio, G., Van Impe, W.F. & Verastegui-Flores, R.-D., 2011. Advances in geosynthetic clay liners: Polymer enhanced clays. In *Geo-Frontiers*. ASCE, pp. 1931–1940.
Fernandez, F. & Quigley, R.M., 1991. Controlling the destructive effects of clay - organic liquid interactions by application of effective stresses. *Canadian Geotechnical Journal*, 28(3), pp.388–398. Available at: https://doi.org/10.1139/t91-049.
Fernandez, F. & Quigley, R.M., 1985. Hydraulic conductivity of natural clays permeated with simple liquid hydrocarbons. *Canadian Geotechnical Journal*, 22(2), pp.205–214. Available at: https://doi.org/10.1139/t85-028.
Fox, P.J. & Baxter, C.D.P., 1997. Consolidation properties of soil slurries from hydraulic consolidation test. *Journal of Geotechnical and Geoenvironmental Engineering*, 123(8), pp.770–776. Available at: https://doi.org/10.1061/(ASCE)1090-0241(1997)123:8(770).
Gates, W.P., Hines, P. & Bouazza, A., 2011. SEM study of mineralogical changes to GCLs following permeation by strongly alkaline leachates. In J. Han & D. E. Alzamora, eds. *Geo-Frontiers*. Dallas, Texas, USA: ASCE, pp. 2021–2030.
Ghazizadeh, S. & Bareither, C.A., 2018. Micro-scale shear analysis of needle-punched reinforced GCLs subjected to elevated temperature.
Gleason, M.H., Daniel, D.E. & Eykholt, G.R., 1997. Calcium and sodium bentonite for hydraulic containment applications. *Journal of Geotechnical and Geoenvironmental Engineering*, 123(5), pp.438–445. Available at: https://doi.org/10.1061/(ASCE)1090-0241(1997)123:5(438).
Guyonnet, D., Gaucher, E., Gaboriau, H., Pons, C.-H., Clinard, C., Norotte, V. & Didier G., 2005. Geosynthetic clay liner interaction with leachate: Correlation between permeability, microstructure, and surface chemistry. *Journal of Geotechnical and Geoenvironmental Engineering*, 131(6), pp.740–749. Available at: https://doi.org/10.1061/(ASCE)1090-0241(2005)131:6(740).
Herweynen, W., Bareither, C.A. & Scalia IV, J., 2017. Salinity effects on the consolidation behavior of kaolin. In G. W. Wilson, D. C. Sego, & N. A. Beier, eds. *Proceedings of Tailings and Mine Waste*. Banff, Alberta, Canada: University of Alberta, pp. 166–173.
Hong, C.S. & Shackelford, C.D., 2017a. Long-term column testing of zeolite-amended backfills. I: Testing methodology and chemical compatibility. *Journal of Geotechnical and Geoenvironmental Engineering*, 143(9). Available at: https://doi.org/10.1061/(ASCE)GT.1943-5606.0001733.
Hong, C.S. & Shackelford, C.D., 2017b. Long-term column testing of zeolite-amended backfills. II : Solute transport properties. *Journal of Geotechnical and Geoenvironmental Engineering*, 143(9), pp.1–16. Available at: https://doi.org/10.1061/(ASCE)GT.1943-5606.0001734.
Jo, H.Y., Katsumi, T., Benson, C.H. & Edil, T.B., 2001. Hydraulic conductivity and swelling of nonprehydrated GCLs permeated with single-species salt solutions. *Journal of Geotechnical and Geoenvironmental Engineering*, 127(7), pp.557–567. Available at: https://doi.org/10.1061/(ASCE)1090-0241(2001)127:7(557).

Jo, H.Y. Benson, C.H., Shackelford, C.D., Lee, J.-M. & Edil, T.B., 2005. Long-term hydraulic conductivity of a geosynthetic clay liner permeated with inorganic salt solutions. *Journal of Geotechnical and Geoenvironmental Engineering*, 131(4), pp.405–417. Available at: https://doi.org/10.1061/(ASCE)1090-0241(2005)131:4(405).

Jo, H.Y., Benson, C.H. & Edil, T.B., 2004. Hydraulic conductivity and cation exchange in non-prehydrated and prehydrated bentonite permeated with weak inorganic salt solutions. *Clays and Clay Minerals*, 52(6), pp.661–679. Available at: https://doi.org/10.1346/CCMN.2004.0520601.

Jo, H.Y., Benson, C.H. & Edil, T.B., 2006. Rate-limited cation exchange in thin bentonitic barrier layers. *Canadian Geotechnical Journal*, 43(4), pp.370–391. Available at: https://doi.org/10.1139/t06-014.

Kang, J. & Shackelford, C.D., 2009. Clay membrane testing using a flexible-wall cell under closed-system boundary conditions. *Applied Clay Science*, 44, pp.43–58. Available at: http://dx.doi.org/10.1016/j.clay.2009.01.006.

Kang, J. & Shackelford, C.D., 2010. Membrane behavior of compacted clay liners. *Journal of Geotechnical and Geoenvironmental Engineering*, 136(10), pp.1368–1382. Available at: https://doi.org/10.1061/(ASCE)GT.1943-5606.0000358.

Kashir, M. & Yanful, E.K., 1997. A flow pump system for assessing clay barrier-permeant compatibility. *Geotechnical Testing Journal*, 20(2), pp.179–190. Available at: https://doi.org/10.1520/GTJ10737J.

Katsumi, T., Ishimori, H., Ogawa, A., Yoshikawa, K., Hanamoto, K. & Fukagawa, R., 2007. Hydraulic conductivity of nonprehydrated geosynthetic clay liners permeated with inorganic solutions and waste leachates. *Soils and Foundations*, 47(1), pp.79–96.

Kolstad, D.C., Benson, C.H. & Edil, T.B., 2004. Hydraulic conductivity and swell of nonprehydrated geosynthetic clay liners permeated with multispecies inorganic solutions. *Journal of Geotechnical and Geoenvironmental Engineering*, 130(12), pp.1236–1249.

Lee, J.-M., Shackelford, C.D., Benson, C.H., Jo, H.-Y. & Edil T.B., 2005. Correlating index properties and hydraulic conductivity of geosynthetic clay liners. *Journal of Geotechnical and Geoenvironmental Engineering*, 131(11), pp.1319–1329. Available at: https://doi.org/10.1061/(ASCE)1090-0241(2005)131:11(1319).

Lee, J.-M. & Shackelford, C.D., 2005a. Concentration dependency of the prehydration effect for a geosynthetic clay liner. *Soils and Foundations*, 45(4), pp.27–41. Available at: https://doi.org/10.3208/sandf.45.4_27.

Lee, J.-M. & Shackelford, C.D., 2005b. Impact of bentonite quality on hydraulic conductivity of geosynthetic clay liners. *Journal of Geotechnical and Geoenvironmental Engineering*, 131(1), pp.64–77. Available at: https://doi.org/10.1061/(ASCE)1090-0241(2005)131:1(64).

Lee, J. & Znidarcic, D., 2013. Flow pump system for unsaturated soils: Measurement of suction response and the soil-water retention curve. *Geotechnical Testing Journal*, 36(5), pp.695–706. Available at: https://doi.org/10.1520/GTJ20120027.

Likos, W.J. & Lu, N., 2006. Pore scale analysis of bulk volume change from crystalline interlayer swelling in Na+- and Ca2+- smectite. *Clays and Clay Minerals*, 54(4), pp.516–529.

Lin, L. & Benson, C.H., 2000. Effect of wet-dry cycling on swelling and hydraulic conductivity of GCLs. *Journal of Geotechnical and Geoenvironmental Engineering*, 126(1), pp.40–49. Available at: https://doi.org/10.1061/(ASCE)1090-0241(2000)126:1(40).

Lupo, J.F., 2010. Liner system design for heap leach pads. *Geotextiles and Geomembranes*, 28(2), pp.163–173. Available at: http://dx.doi.org/10.1016/j.geotexmem.2009.10.006.

Malusis, M.A. & Shackelford, C.D., 2002. Chemico-osmotic efficiency of a geosynthetic clay liner. *Journal of Geotechnical and Geoenvironmental Engineering*, 128(2), pp.97–106. Available at: https://doi.org/10.1061/(ASCE)1090-0241(2002)128:2(97).

Malusis, M.A., Shackelford, C.D. & Olsen, H.W., 2001. A laboratory apparatus to measure chemico-osmotic efficiency coefficients for clay soils. *Geotechnical Testing Journal*, 24(3), pp.229–242. Available at: https://doi.org/10.1520/GTJ11343J.

Marcial, D., Delage, P. & Cui, Y.J., 2002. On the high stress compression of bentonites. *Canadian Geotechnical Journal*, 39(4), pp.812–820. Available at: https://doi.org/10.1139/t02-019.

Mazzieri, F., Di Emidio, G., Fratalocchi, E., Di Sante, M., & Pasqualini, E., 2013. Permeation of two GCLs with an acidic metal-rich synthetic leachate. *Geotextiles and Geomembranes*, 40, pp.1–11.

McCartney, J.S. & Znidarcic, D., 2010. Testing system for hydraulic properties of unsaturated nonwoven geotextiles. *Geosynthetics International*, 17(5), pp.355–363. Available at: https://doi.org/10.1680/gein.2010.17.5.355.

Meier, A.J. & Shackelford, C.D., 2017. Membrane behavior of compacted sand-bentonite mixture. *Canadian Geotechnical Journal*, 54(9), pp.1284–1299. Available at: https://doi.org/10.1139/cgj-2016-0708.

Mesri, G. & Olson, R.E., 1971a. Consolidation characteristics of montmorillonite. *Geotechnique*, 21(4), pp.341–352. Available at: https://doi.org/10.1680/geot.1971.21.4.341.

Mesri, G. & Olson, R.E., 1971b. Mechanisms controlling the permeability of clays. *Clays and Clay Minerals*, 19(3), pp.151–158.

Mitchell, J.K. & Madsen, F.T., 1987. Chemical effects on clay hydraulic conductivity. In R. D. Woods, ed. *Proceedings of Geotechnical Practice for Waste Disposal '87*. ASCE, pp. 87–116.

Norotte, V., Didier, G., Guyonnet, D. & Gaucher, E., 2004. Evolution of GCL hydraulic performance during contact with landfill leachate. *Advances in Geosynthetic Clay Liner Technology: 2nd Symposium*, pp.41–52. Available at: https://doi.org/10.1520/STP12197S.

Ogwada, R.A. & Sparks, D.L., 1986. Kinetics of ion exchange on clay minerals and soil: II. Elucidation of rate-limiting steps. *Soil Science Society of America Journal*, 50(5), pp.1162–1166.

Olsen, H.W., 1966. Darcy's law in saturated kaolinite. *Water Resources Research*, 2(2), pp.287–295.

Olsen, H.W., Nichols, R.W. & Rice, T.L., 1985. Low gradient permeability measurement in a triaxial system. *Geotechnique*, 35(2), pp.145–157. Available at: https://doi.org/10.1680/geot.1985.35.2.145.

Osicki, R.S., Fleming, I.R. & Haug, M.D., 2004. A simple compatibility testing protocol for bentonite-based barrier systems. *Advances in Geosynthetic Clay Liner Technology: 2nd Symposium*, pp.31–40. Available at: https://doi.org/10.1520/STP12196S.

Petrov, R.J. & Rowe, R.K., 1997. Geosynthetic clay liner (GCL) - chemical compatibility by hydraulic conductivity testing and factors impacting its performance. *Canadian Geotechnical Journal*, 34(6), pp.863–885. Available at: https://doi.org/10.1139/t97-055.

Petrov, R.J., Rowe, R.K. & Quigley, R.M., 1997a. Comparison of laboratory-measured GCL hydraulic conductivity based on three permeameter types. *Geotechnical Testing Journal*, 20(1), p.49. Available at: https://doi.org/10.1520/GTJ11420J.

Petrov, R.J., Rowe, R.K. & Quigley, R.M., 1997b. Selected factors influencing GCL hydraulic conductivity. *Journal of Geotechnical and Geoenvironmental Engineering*, 123(8), pp.683–695. Available at: https://doi.org/10.1061/(ASCE)1090-0241(1997)123:8(683).

Quaranta, J.D., Gabr, M.A. & Bowders, J.J., 1997. *First-exposure performance of the bentonite component of a GCL in a pow-pH, calcium-enriched environment*, West Conshohocken, PA: ASTM International. Available at: https://doi.org/10.1520/STP11801S.

Quigley, R.M., Fernandez, F., Yanful, E., Helgason, T. & Margaritis, A., 1987. Hydraulic conductivity of contaminated natural clay directly below a domestic landfill. *Canadian Geotechnical Journal*, 24(3), pp.377–383. Available at: https://doi.org/10.1139/t87-048.

Rad, N.S., Jacobson, B.D. & Bachus, R.C., 1994. Compatibility of geosynthetic clay liners with organic and inorganic permeants. In G. P. Karunaratne, S. H. Chew, & K. S. Wong, eds. *Proceedings of the Fifth International Conference on Geotextiles, Geomembranes, and Related Products (Vol 3: Environmental applications, geosynthetics testing and related research)*. Singapore: Southeast Asia Chapter of the International Geotextile Society (SEAC-IGS), pp. 1165–1168.

Redmond, P.L. & Shackelford, C.D., 1994. Design and evaluation of a flow pump system for column testing. *Geotechnical Testing Journal*, 17(3), pp.269–281. Available at: https://doi.org/10.1520/GTJ10102J.

Rowe, R.K., 1998. Geosynthetics and the minimizations of contaminant migration through barrier systems beneath solid waste. In *Proceedings of the Sixth International Conference on Geosynthetics*. Atlanta, Georgia, USA, pp. 27–102.

Ruhl, J.L. & Daniel, D.E., 1997. Geosynthetic clay liners permeated with chemical solutions and leachates. *Journal of Geotechnical and Geoenvironmental Engineering*, 123(4), pp.369–381.

Sample-Lord, K.M. & Shackelford, C.D., 2018. Membrane behavior of unsaturated sodium bentonite. *Journal of Geotechnical and Geoenvironmental Engineering*, 144(1). Available at: https://doi.org/10.1061/(ASCE)GT.1943-5606.0001803.

Scalia IV, J., Bohnhoff, G.L., Shackelford, C.D., Benson, C.H., Sample-Lord, K.M., Malusis, M.A. & Likos, W.J., 2018. Enhanced bentonites for containment of inorganic waste leachates by GCLs. *Geosyntethics International*.

Scalia IV, J., Benson, C.H., Bohnhoff, G.L., Edil, T.B. & Shackelford, C.D., 2014. Long-term hydraulic conductivity of a bentonite-polymer composite permeated with agressive inorganic solutions. *Journal of Geotechnical and Geoenvironmental Engineering*, 140(3). Available at: https://doi.org/10.1061/(ASCE)GT.1943-5606.0001040.

Scalia IV, J. & Benson, C.H., 2010a. Effect of permeant water on the hydraulic conductivity of exhumed GCLs. *Geotechnical Testing Journal*, 33(3), pp.201–211. Available at: https://doi.org/10.1520/GTJ102609.

Scalia IV, J. & Benson, C.H., 2010b. Preferential flow in geosynthetic clay liners exhumed from final covers with composite barriers. *Canadian Geotechnical Journal*, 47(10), pp.1101–1111. Available at: https://doi.org/10.1139/T10-018.

Shackelford, C.D., Malusis, M.A., Majeski, M.J. & Stern, R.T., 1999. Electrical conductivity breakthrough curves. *Journal of Geotechnical and Geoenvironmental Engineering*, 125(4), pp.260–270. Available at: https://doi.org/10.1061/(ASCE)1090-0241(1999)125:4(260).

Shackelford, C.D., Benson, C.H., Katsumi, T., Edil, T.B. & Lin, L., 2000. Evaluating the hydraulic conductivity of GCLs permeated with non-standard liquids. *Geotextiles and Geomembranes*, 18(2–4), pp.133–161. Available at: https://doi.org/10.1016/S0266-1144(99)00024-2.

Shackelford, C.D., Lu, N., Malusis, M.A. & Sample-Lord, K.M., 2018 (manuscript in progress). Research Challenges Involving Coupled Flows in Geotechnical Engineering. In Springer-Verlag Berlin Heidelberg.

Shackelford, C.D., 2008. Selected issues affecting the use and performance of GCLs in waste containment applications. In M. Manassero & A. Dominijanni, eds. *Proceedings of the XXIV Edition of the Geotechnical Engineering Conference*. Torino, Italy, pp. 1–45.

Shackelford, C.D., 2014. The ISSMGE Kerry Rowe Lecture: The role of diffusion in environmental geotechnics. *Canadian Geotechnical Journal*, 51(11), pp.1219–1242. Available at: https://doi.org/10.1139/cgj-2013-0277.

Shackelford, C.D., 1994. Waste-soil interactions that alter hydraulic conductivity. *Hydraulic Conductivity and Waste Contaminant Transport in Soil, ASTM STP 1142*, pp.111–168.

Shackelford, C.D. & Redmond, P.L., 1995. Solute breakthrough curves for processed at low flow rates. *Journal of Geotechnical and Geoenvironmental Engineering*, 121(1), pp.17–32. Available at: https://doi.org/10.1061/(ASCE)0733-9410(1995)121:1(17).

Shackelford, C.D. & Sample-Lord, K.M., 2014. Hydraulic conductivity and compatibility of bentonite for hydraulic containment barriers. *From Soil Behavior Fundamentals to Innovations in Geotechnical Engineering*, pp.370–387. Available at: https://doi.org/10.1061/9780784413265.030.

Shan, H.-Y. & Daniel, D.E., 1991. Results of laboratory tests on a geotextile-bentonite liner material. In *Geosynthetics '91*. Atlanta, Georgia, USA, pp. 517–535.

Shan, H.Y. & Lai, Y.J., 2002. Effect of hydrating liquid on the hydraulic properties of geosynthetic clay liners. *Geotextiles and Geomembranes*, 20(1), pp.19–38.

Tang, L. & Sparks, D.L., 1993. Cation-exchange kinetics on montmorillonite using pressure-jump relaxation. *Soil Science Society of America Journal*, 57(1), pp.42–46.

Tian, Z., 2017. *Seepage Induced Consolidation Test Mine Tailings*. MS Thesis: Colorado State University.

Tong, S. & Shackelford, C.D., 2016. Standardized hydraulic conductivity testing of compacted sand-bentonite mixtures. *Geotechnical Testing Journal*, 39(6), p.20150204. Available at: https://doi.org/10.1520/GTJ20150204.

Trauger, R.J., Swan Jr., R.H. & Yuan, Z., 1997. Long-term shear strength behavior of a needlepunched geosynthetic clay liner. *Testing and Acceptance Criteria for Geosynthetic Clay Liners, STP11805S*, pp.103–120. Available at: https://doi.org/10.1520/STP11797S.

Vasko, S.M., Jo, H.-Y., Benson, C.H., Edil, T.B. & Katsumi, T., 2001. Hydraulic conductivity of partially prehydrated geosynthetic clay liners permeated with aqueous chloride solutions. In *Geosynthetics '01*. St. Paul, Minnesota, USA, pp. 685–699.

APPENDIX A GCL MANUFACTURING

The typical manufacturing process of a GCL roll is illustrated in Figure A.1. The bottom (carrier) geotextile is rolled on a conveyor belt and air-dried bentonite (granular or powdered) is poured onto the geotextile from an overhead hopper. The hopper aperture is automated to pour a certain pre-set mass bentonite per area. Bentonite placement can lead to heterogeneity in the bentonite loading across the GCL roll if the manufacturer does not take steps to ensure even distribution of bentonite (Heerten et al. 1992). The upper geotextile is then rolled on top of the poured bentonite. Stitching or needle punching is performed by barbed needles that are attached to panels. As the needles penetrated the cover geotextile the barbs grabbed fibers from the carrier geotextile and pull these fibers across the bentonite layer and affixed the fibers to the carrier geotextile. The joints of fibers at carrier geotextile can be opted to be thermal treated, or not. During manufacturing operations, the needles eventually wore off and become less efficient at grabbing fibers (relative to a new needles) and need to be replaced.

Figure A.2 presented the difference of stitched and needle-punched GCLs. Stitched GCLs are produced with needle plates with needles arranged at a specific distance (spacing) from one another. Fibers (or yarns) are stitched into the GCLs and are usually not intended to provide internal shear strength (Koerner 2005). In contrast, needle-punched GCLs are produced with barbed needles arranged in an irregular pattern. Needle-punched GCLs range from non-reinforced needle-punched (without improvement of internal shear strength from the fibers) to reinforced needle-punched (with needle punching fibers providing internal shear strength) in a wide range of peel-strengths.

REFERENCES

Heerten, G., von Maubeuge, K.P., Simpson, M. & Mills, C., 1992. Manufacturing quality control of geosynthetic clay liners-A manufacturers perspective. In R. M. Koerner & Y. G. Hsuan, eds. *MQC/MQA and CQC/CQA of Geosynthetics*. Philadelphia, PA: Industrial Fabrics Association International, pp. 86–95.

Koerner, R.M., 2005. Overview of geosynthetics. In *Designing With Geosynthetics*. Upper Saddle River, NJ: Pearson Prentice Hall, pp. 1–78.

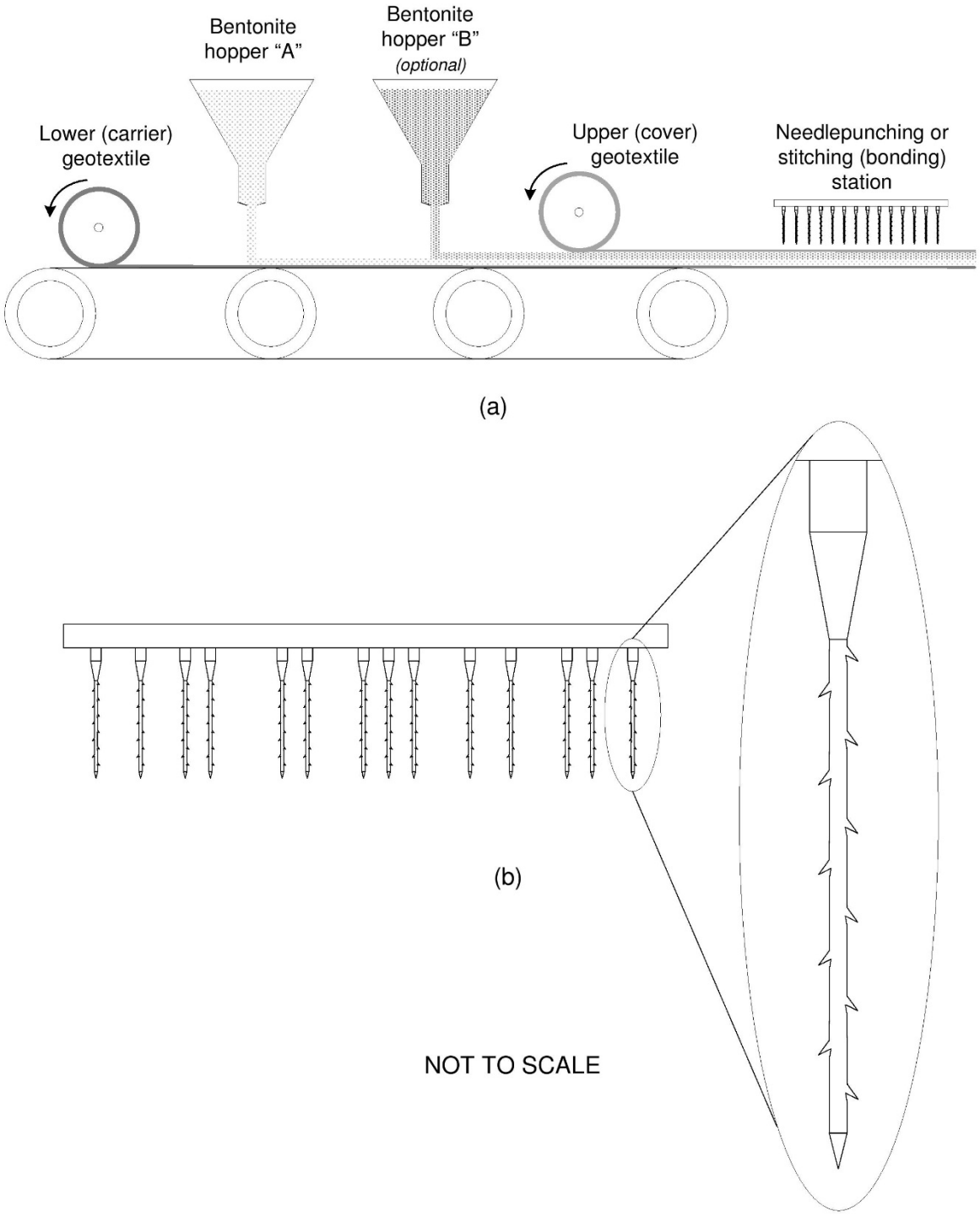

Figure A.1. (a) Manufacturing process of needle-punched GCL and (b) needle used for needle punching (redrawn after Koerner 2005)

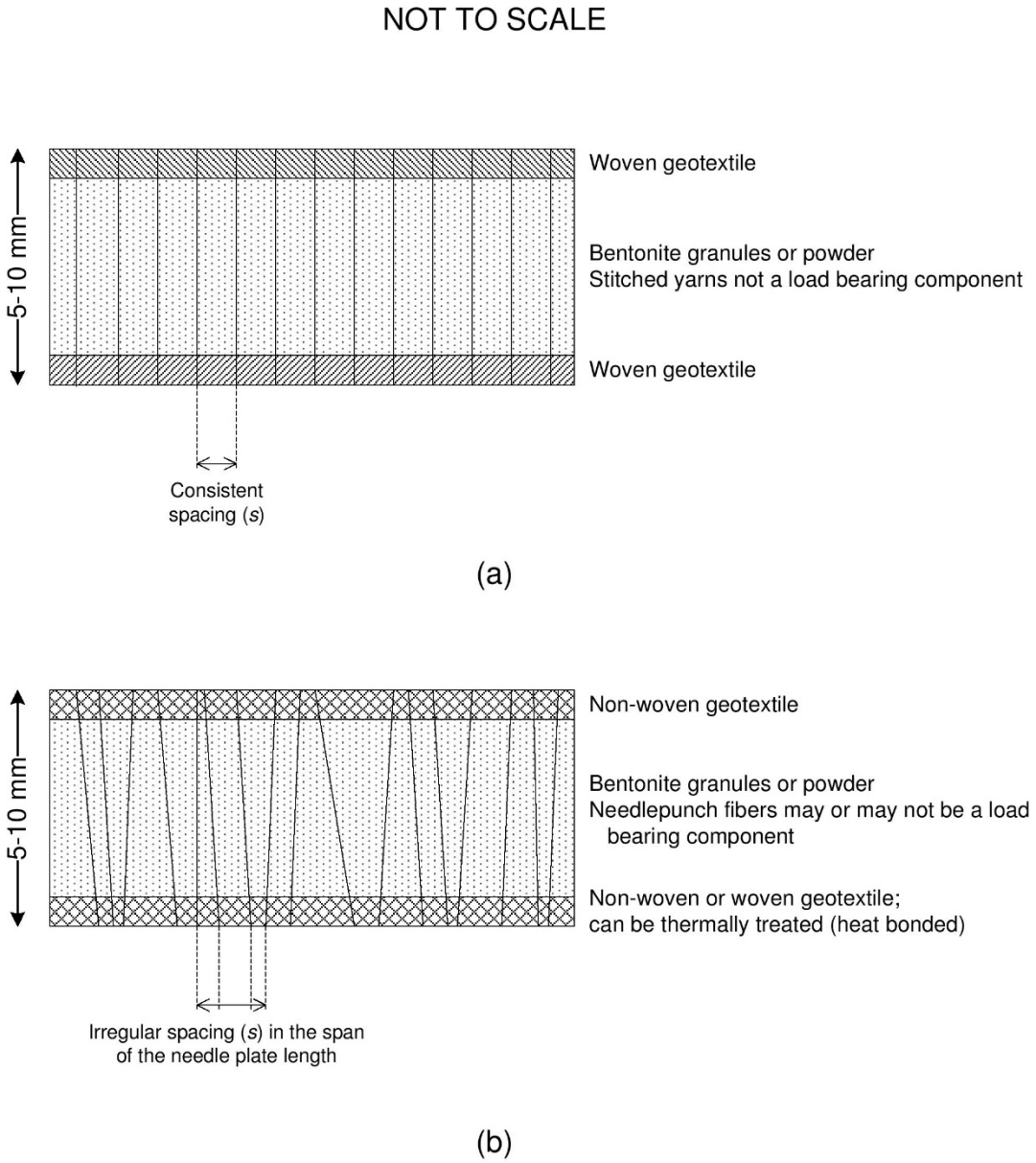

Figure A.2. Cross section sketch on the difference of stitched and needle-punched GCLs

APPENDIX B PREFERENTIAL FLOW PATHS VIA FIBER BUNDLES IN DYED SPECIMENS

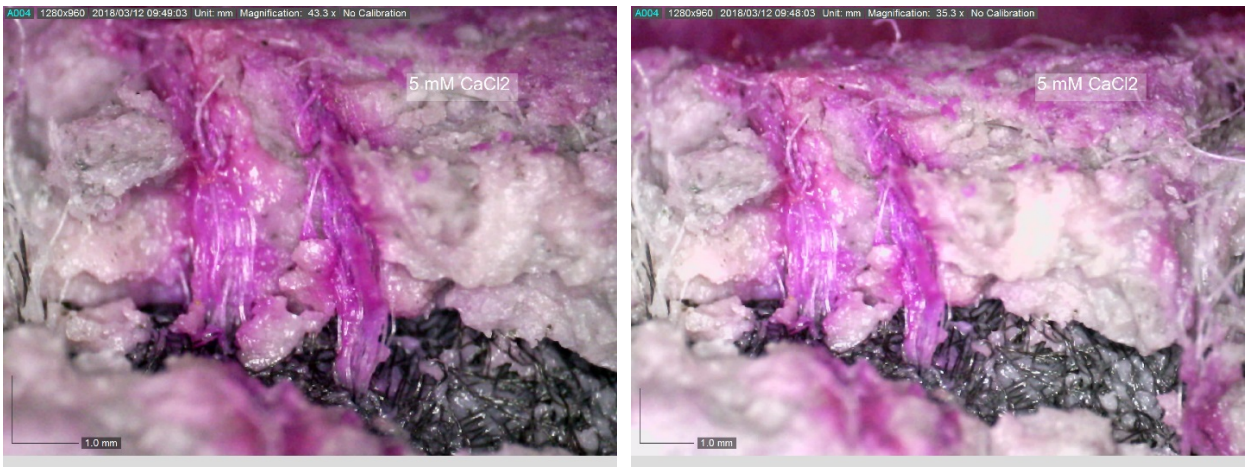

Figure B.1. Preferential flow paths present in Test Series 5 (5 mM $CaCl_2$) specimen

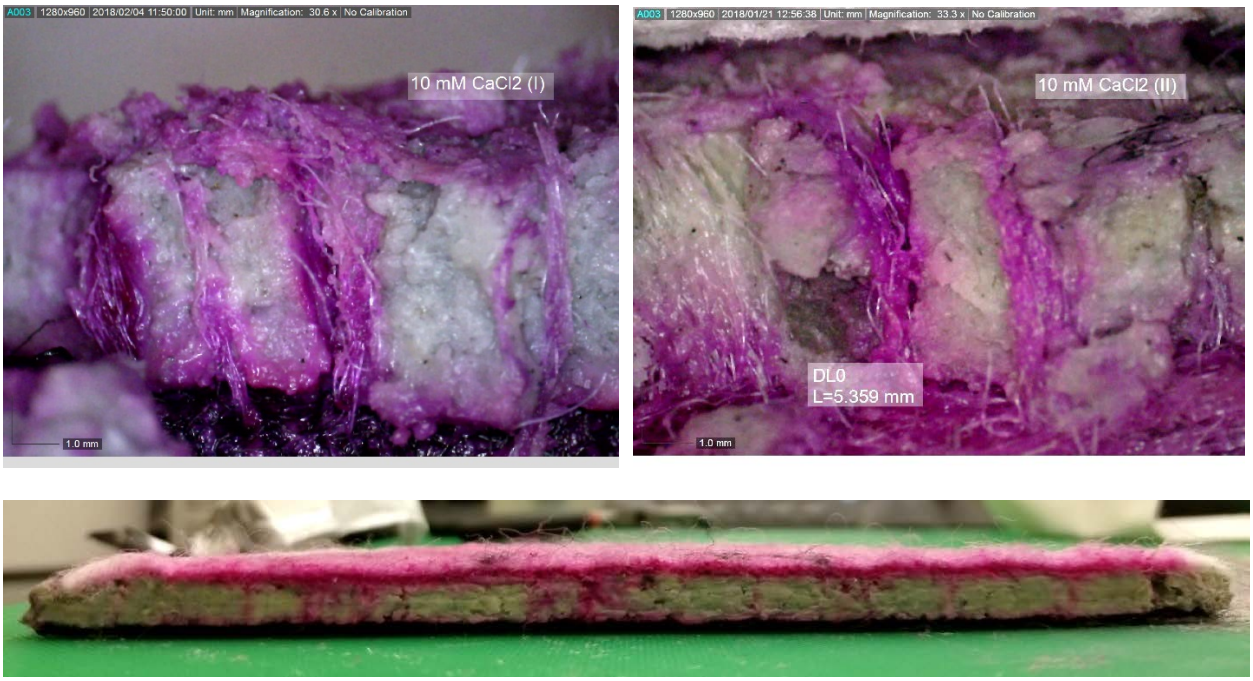

Figure B.2. (Color) Preferential flow paths present in Test Series 6 (10 mM $CaCl_2$) specimens

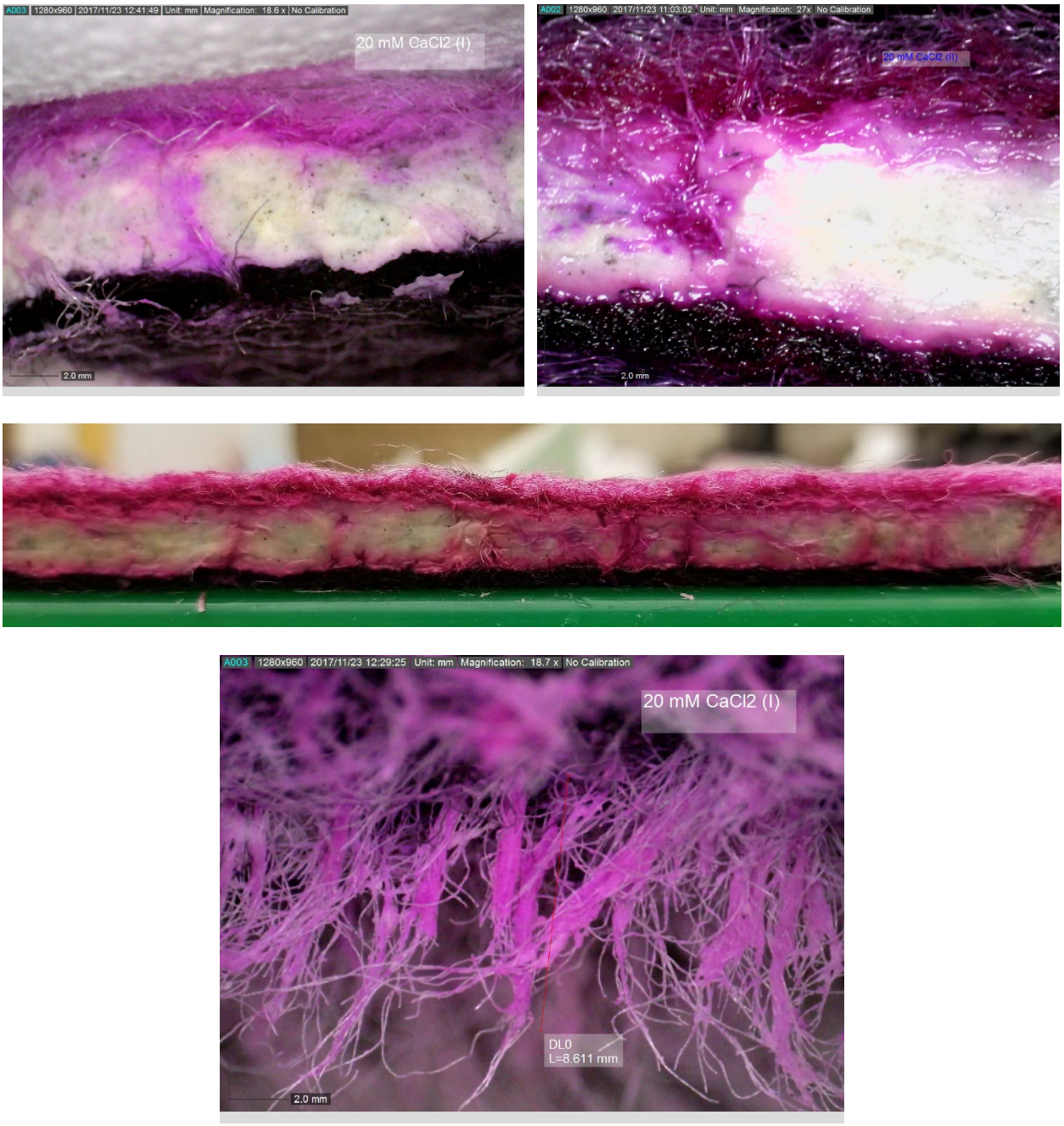

Figure B.3. (Color) Preferential flow paths present in Test Series 7 (20 mM $CaCl_2$) specimens

APPENDIX C HYDRAULIC CONDUCTIVITY MEASUREMENT OF NON-PREHYDRATED (NP) MOCK GCLs

In addition to manufactured needle-punched GCLs, mock (without needle punching) GCLs were also assembled in the laboratory from bulk granular and powdered sodium bentonite (Na-bentonite). These mock GCLs were used to investigate whether there was a distinct behavior between GCL with and without needle punching. Particle-size distributions for Na-bentonite extracted from the manufactured GCL as well as loose granular and powdered Na-bentonite used to create mock GCLs are presented in Figure C.1. Particle-size distributions for each material are reported for mechanical sieve (air dried) and hydrometer (wet). Granular Na-bentonites (from GCL and bulk) in air-dried condition classified as poorly graded sand, SP (ASTM D2487-17 2017) while bulk powdered bentonite classified as high plasticity clay, CH (ASTM D2487-17 2017).

Preparation of manufactured needle-punched GCL specimen (Test Series 8) was performed as described in CHAPTER 3. To prepare mock GCL (Test Series 9 and 10), bulk bentonite was carefully placed with the same mass per area as the needle-punched GCL. The procedure for assembly of bulk Na-bentonite within a flexible-wall permeameter was conducted per Scalia et al. (2014). Figure C.2 illustrated the schematic of the test setup. Unlike prehydrated specimen, non-prehydrated specimens were only continued until the achievement of termination criteria in ASTM D5084-16a (2016). All tests were permeated with conservative water (CW; see CHAPTER 3).

There are two sets of t, PVF, and k values presented in Table C.1. The values with the 5084 subscript (t_{5084}, PVF_{5084}, k_{5084}) pertain to those based on the hydraulic termination criteria in ASTM D5084-16a (2016). The values with the f subscript (t_f, PVF_f, k_f) pertain to those at the end of permeation. The values of S were determined following the procedure described by Conzelmann (2017). Measured S ranged from 103 % to 110 % and is in general agreement with Conzelmann et al. (2017) that specimens can be assumed to be saturated at the end of permeation without backpressure. The final w of the bentonite component of the terminated tests ranged from 102 % to 126 %. These tests were not extended until the attainment of chemical equilibrium. Test results for Test Series 8 and 9 are presented in Figure C.3 and test results for Test Series 10

are presented in Figure C.4. Test Series 10 have not attained hydraulic equilibrium at the time of writing (ongoing test).

Test Series 8: Geosynthetic clay liners

Figure C.3 illustrated that initial k values were high (~6×10^{-8} m/s), as expected from poorly graded sand material, during the initial stage of granule wetting, hydration, and swelling. The k_{5084} of both tests were essentially equal at ~2×10^{-10} m/s. Time needed to reach k_{5084} was 3-5 days (6-10 PVF). The k versus PVF graph illustrated unique behavior attributed to the continuous hydration process. A temporary plateau in k versus time (or versus PVF) was observed at which k_{5084} was determined. This plateau is hypothesized to result from water filling intergranular pores (at $Q_{in} > Q_{out}$) and then migrating by rate-limited osmosis into interparticle and interlayer pore spaces (at $Q_{in} \approx Q_{out}$), yielding swelling, and then further reducing k. The test was continued for several additional PVF until clear peak of *EC* ratio trend was obtained. The k_f measured was comparable to k_{5084} obtained for prehydrated specimens (~3×10^{-11} m/s; see CHAPTER 3). This decrease in k after k_{5084} was observed near the peak *EC* ratio at t = 4 day. Effluent *EC* progressed from $EC_{out} \approx EC_{in}$ initially, to a peak *EC* ratio at k_{5084} then finally decreased to a diffusion dominated *EC* ratio similar to prehydrated tests. Measured pH progressed upwards to a constant value of ~1.4$pH_{in.}$

Test Series 9: Non-needle punched (bulk) granular bentonite

The k of non-needle punched granular bentonite with respect to time displayed only minor variation from needle-punched GCL specimens. However, the slope of k with respect to PVF was leaner compared to needle-punched GCL specimens. This behavior is hypothesized to result from the absence of needle punching fiber bundles that act to distribute permeant liquid more quickly and therefore allow bentonite adjacent to the fibers to swell more rapidly. The k abruptly dropped approximately two orders of magnitudes from 10^{-9} to 10^{-11} m/s after ~5 days (< 14 PVF). This drop is believed to have been caused by blockage of intergranular pores due to bentonite swelling, yielded k_{5084} at ~1.2×10^{-11} m/s at ~29 days (< 13 PVF). The same progression of *EC* that was observed in Test Series 8 was also observed in Test Series 9, however the peak *EC* was higher and was achieved at a much later PVF than GCL specimens (Test Series 8).

First outlier with '?' in Figure C.3 was caused by inaccurate reading due to temporary loss of cell pressure that affects inflow. Upon disassembly, biological activity was observed on the specimen (Figure C.4). This condition had possibly contributed to the outliers from the k calculation (second and third '?' in Figure C.3). Due to biological clogging, decrease in k was observed and in turn increased of EC values by diffusion.

Test Series 10: Non-needle punched (bulk) powdered bentonite

At the time of writing, Test Series 10 had not producing outflow (after 12 days). Instead, cumulative inflow of Test Series 10 is plotted in Figure C.5 versus elapsed time, Test Series 8 and 9 are included for comparison. The initial inflow volume of Test Series 10 was significantly less than Test Series 8 (due to the absence of needle punching) and Test Series 9 (due to granular-form bentonite). Powder-form bentonite (see Figure C.1) created low permeability layer at the onset of flow.

REFERENCES

ASTM D2487-17, 2017. Standard Practice for Classification of Soils for Engineering Purposes (Unified Soil Classification System). *ASTM International, West Conshohocken, PA*, pp.1–10. Available at: https://doi.org/10.1520/D2487-17.

ASTM D5084-16a, 2016. Standard Test Methods for Measurement of Hydraulic Conductivity of Saturated Porous Materials Using a Flexible Wall Permeameter. *ASTM International, West Conshohocken, PA, USA*, pp.1–24. Available at: https://doi.org/10.1520/D5084-16A.

Conzelmann, J.T., Scalia IV, J. & Shackelford, C.D., 2017. Effect of backpressure saturation on the hydraulic conductivity of GCLs. In *Geotechnical Frontiers (GSP 276)*. pp. 227–235.

Petrov, R.J., Rowe, R.K. & Quigley, R.M., 1997. Selected factors influencing GCL hydraulic conductivity. *Journal of Geotechnical and Geoenvironmental Engineering*, 123(8), pp.683–695. Available at: https://doi.org/10.1061/(ASCE)1090-0241(1997)123:8(683).

Scalia IV, J., Benson, C.H., Bohnhoff, G.L., Edil, T.B. & Shackelford, C.D., 2014. Long-term hydraulic conductivity of a bentonite-polymer composite permeated with agressive inorganic solutions. *Journal of Geotechnical and Geoenvironmental Engineering*, 140(3). Available at: https://doi.org/10.1061/(ASCE)GT.1943-5606.0001040.

Shackelford, C.D., Benson, C.H., Katsumi, T., Edil, T.B. & Lin, L., 2000. Evaluating the hydraulic conductivity of GCLs permeated with non-standard liquids. *Geotextiles and Geomembranes*, 18(2–4), pp.133–161. Available at: https://doi.org/10.1016/S0266-1144(99)00024-2.

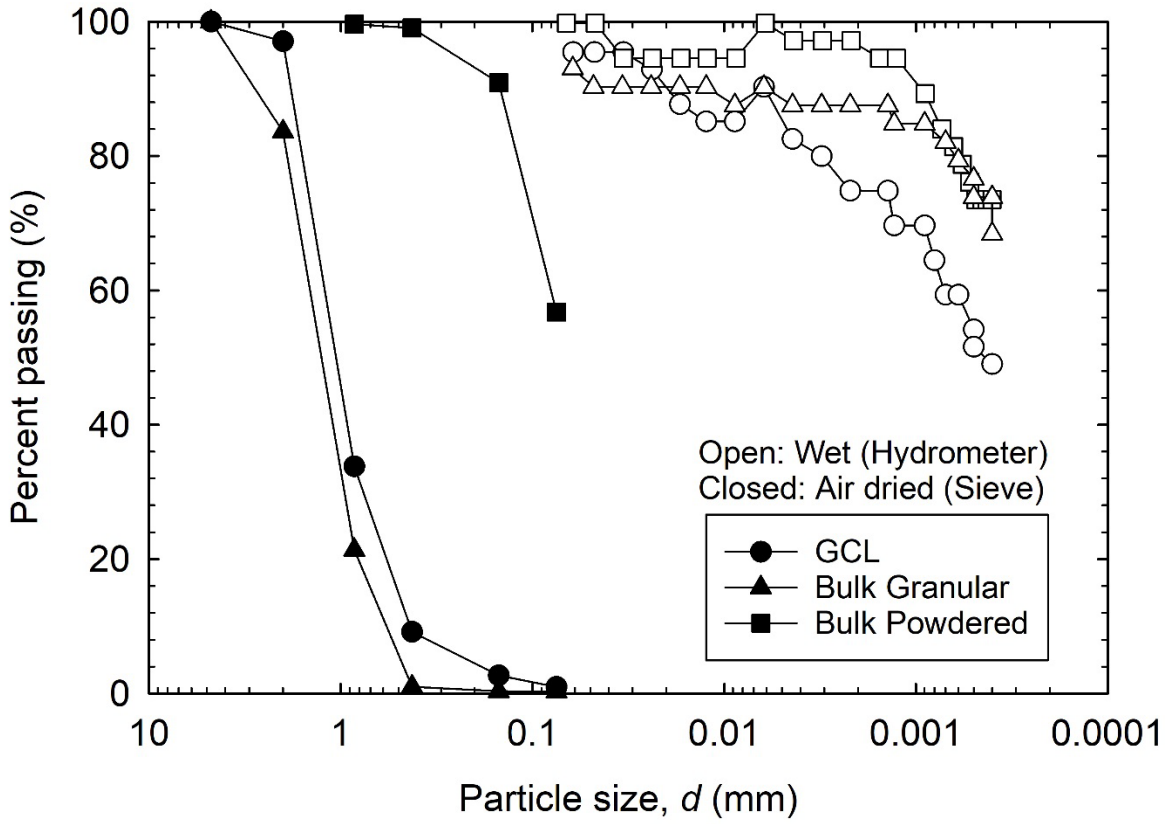

Figure C.1. Particle-size distributions for bentonites used for test with non-prehydrated specimen based on mechanical sieve (air dried) and hydrometer (wet) analyses

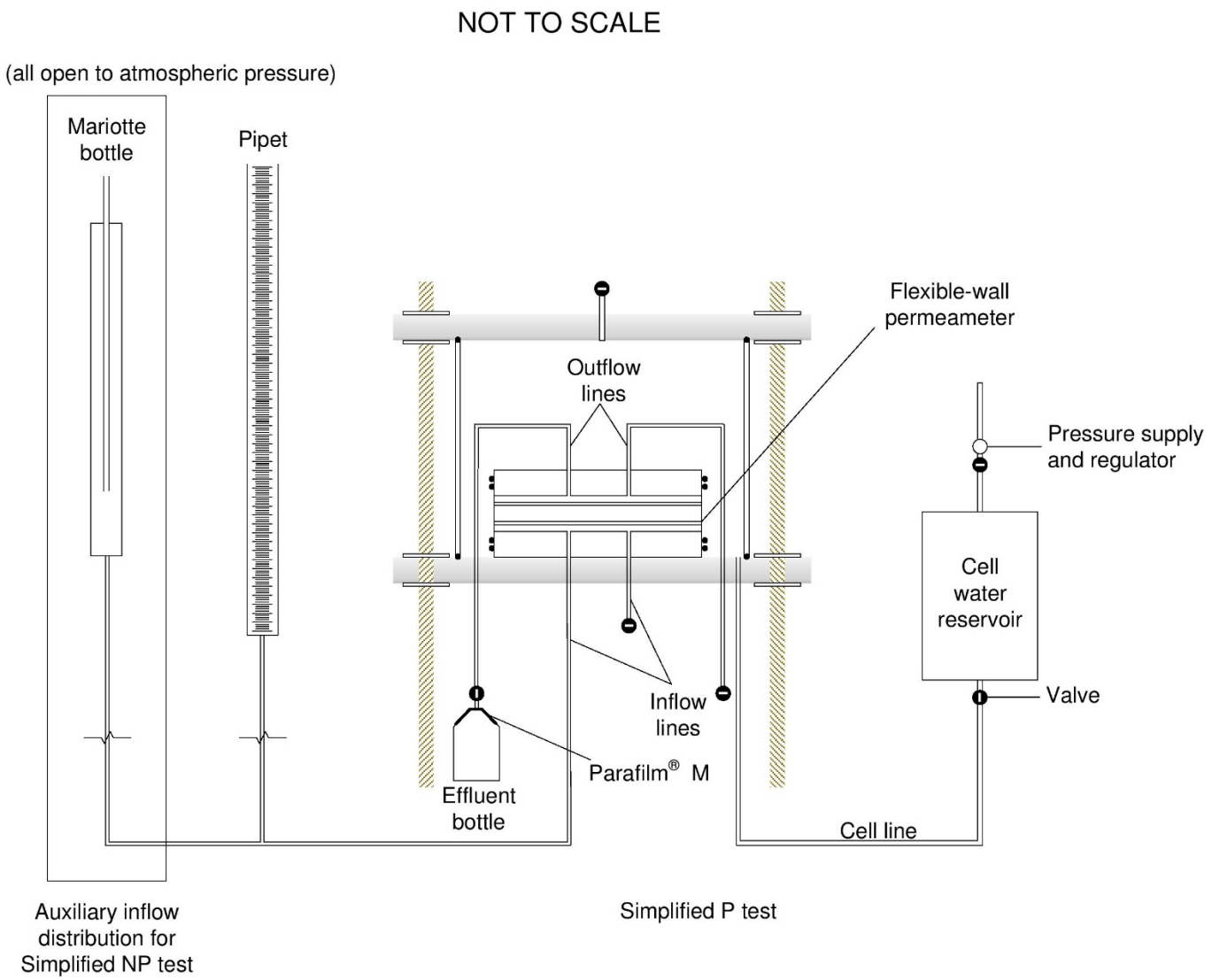

Figure C.2. Schematic of the test setup for hydraulic conductivity testing of by falling headwater, constant tailwater method for non-prehydrated (NP) specimens

Table C.1. (Color) Overall result of hydraulic conductivity test

Test Series	Test number[a]	Specimen	Values at termination criteria							
			ASTM D5084-16a (2016)			Final			*w*	*S*
			t_{5084} (d)[b]	PVF_{5084}	k_{5084} (m/s)	t_f (d)[b]	PVF_f	k_f (m/s)	(%)	(%)
8	8a	GCL	2.8	6.8	2.1×10^{-10}	21.86	8.8	2.5×10^{-11}	106	110
	8b		5.2	10.7	2.4×10^{-10}	28.79	14.1	3.2×10^{-11}	126	109
9	9	Bulk granular bentonite	29.11	11.9	1.2×10^{-11}	152.19	12.8	3.7×10^{-13}	102	103
10	10	Bulk powdered bentonite								

[a]Green color indicate tests are still running and have not meet chemical equilibrium criteria

[b]Reported time at which termination criteria was met elapsed since permeation

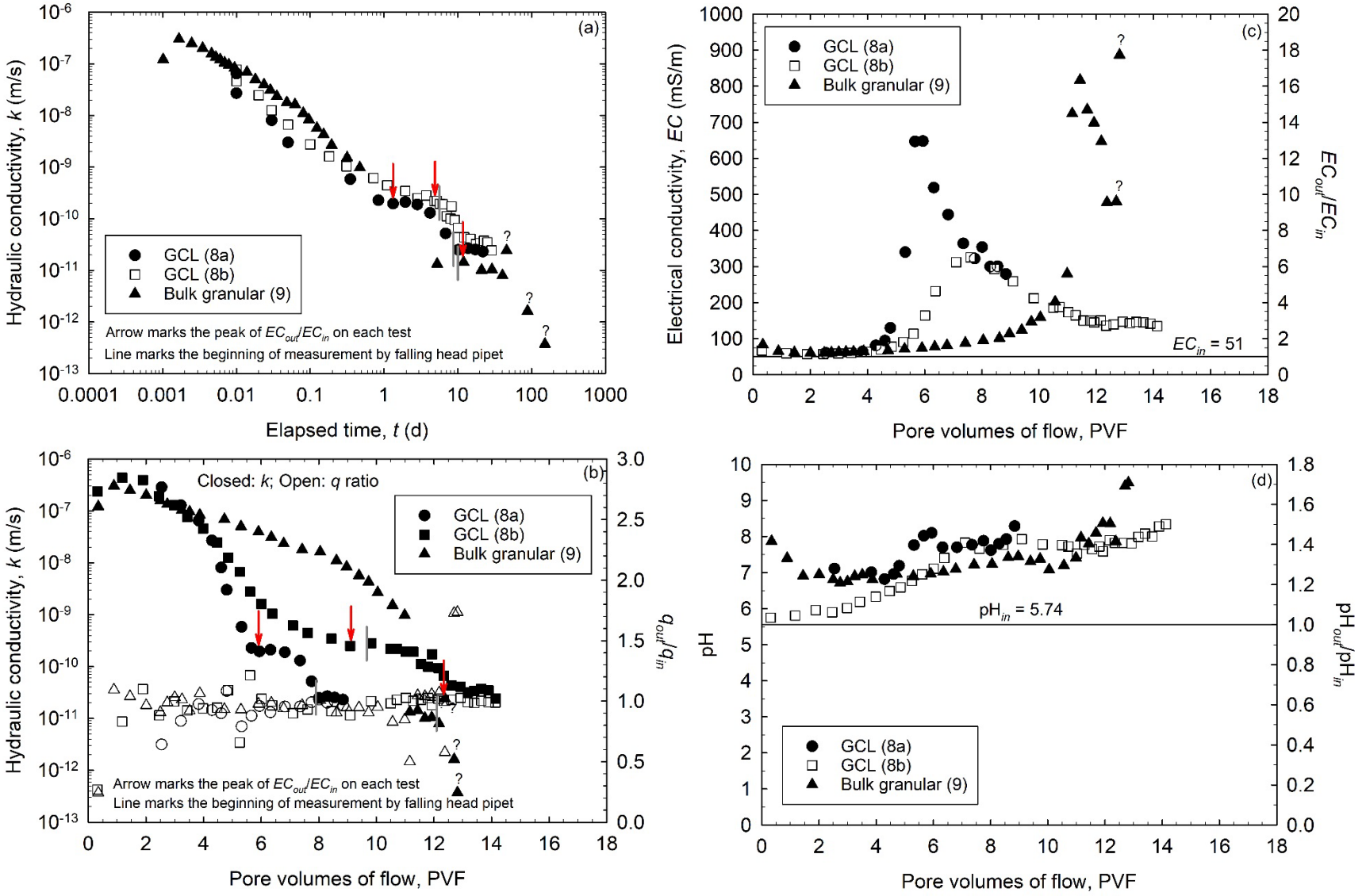

Figure C.3. (Color) Test results for non-prehydrated tests of needle-punched and non needle-punched GCLs with conservative water (Test Series 8-10): (a) hydraulic conductivity with respect to elapsed time on log scale, (b) hydraulic conductivity with respect to pore volumes of flow, (c) electrical conductivity, and (d) pH

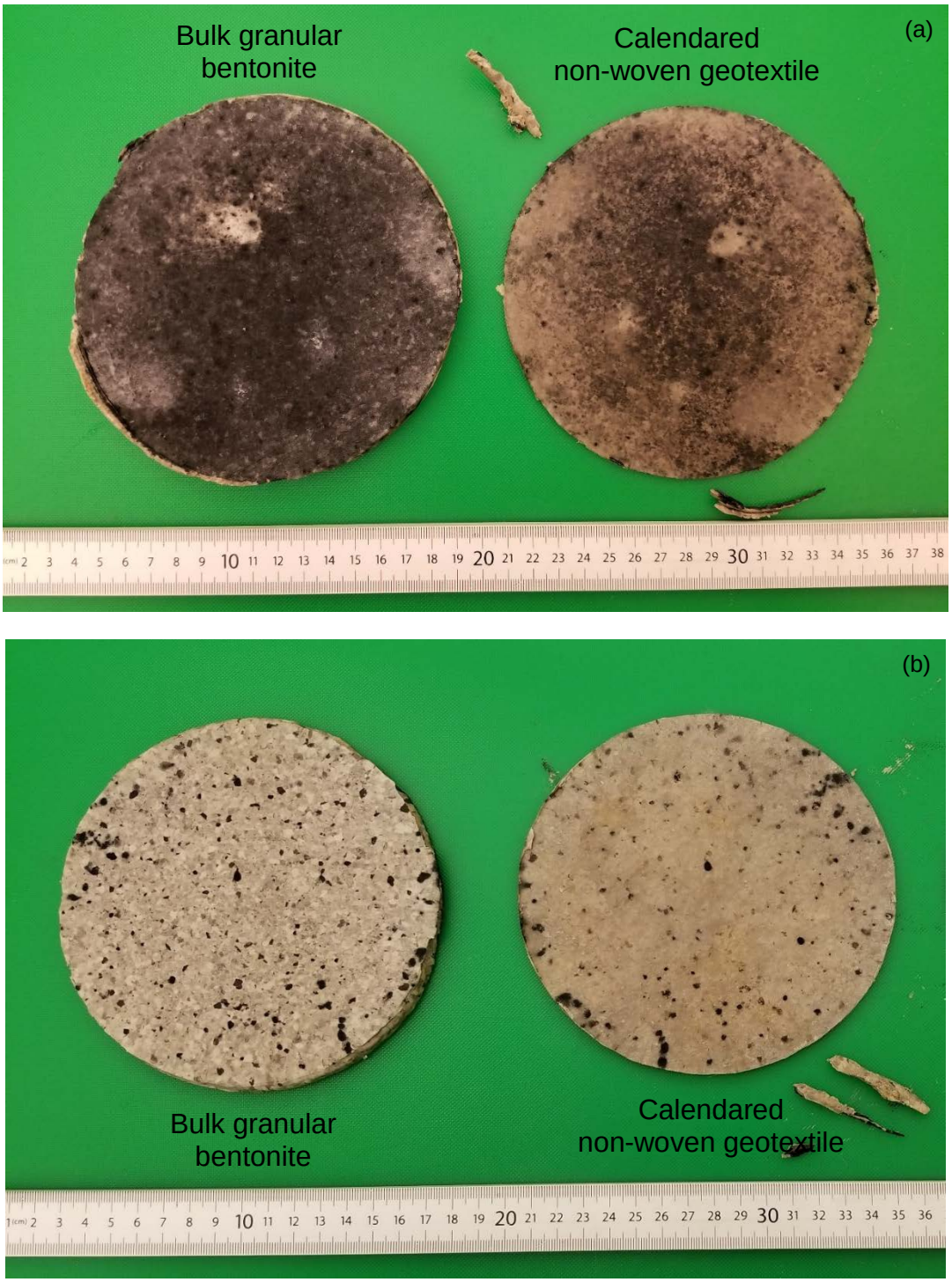

Figure C.4. (Color) Biological activity observed on the bulk granular bentonite specimen (Test 9): (a) and (b) showed each side of the extruded specimen

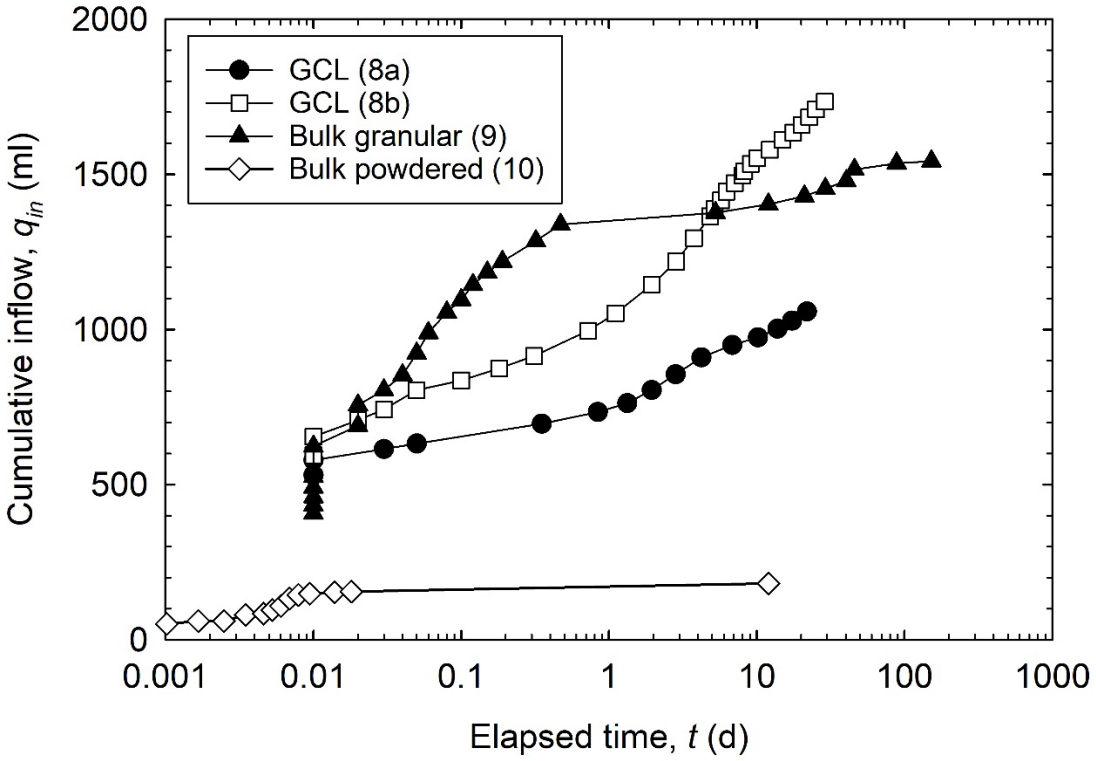

Figure C.5. Cumulative inflow intake over time for all non-prehydrated tests of needle-punched and non needle-punched GCLs with conservative water

APPENDIX D FLOW PUMP CALIBRATION

Flow pump calibration was performed to ensure the accuracy of the inflow applied to the specimens in Test Series 11 and 12. Figure D.1 presented the calibration curves for each syringe of Pump 3 (used for Test Series 12). Vertical axis labeled q_{pump} is the flow rate provided by the manufacturer, whereas horizontal axis labeled q_{actual} is the flow rate as measured. Resultant calibration factors were then incorporated for calculation in Test Series 12. Test Series 11 used Pump Nos 1 and 2 that had not been calibrated before testing. Therefore, the average calibration factor from Pump 3 were used temporarily for Pump 1 and 2 (i.e. Test Series 11) until pump-specific calibrations were performed at the termination of testing.

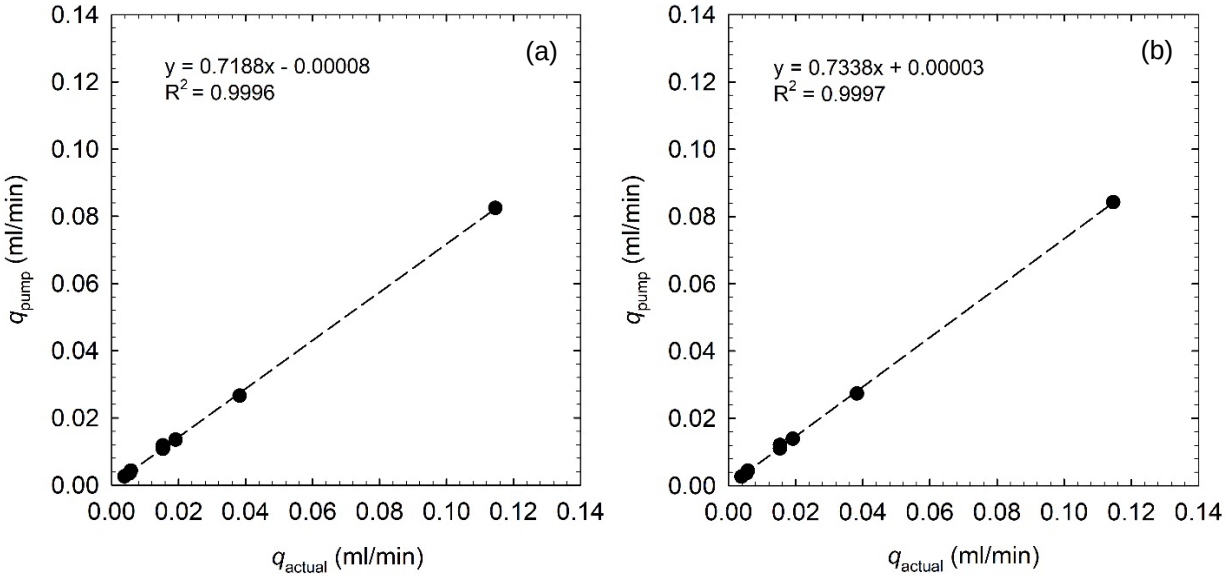

Figure D.1. Calibration curve of (a) Pump 3L for Test 12a and (b) Pump 3R for Test 12b

APPENDIX E DATA AND FIGURES WITH REPLICATE TESTS

For clarity, several result and discussion figures in CHAPTER 3 replicate test results for each test method were excluded. The following figures includes both test reported in CHAPTER 3 and the associated replicate tests.

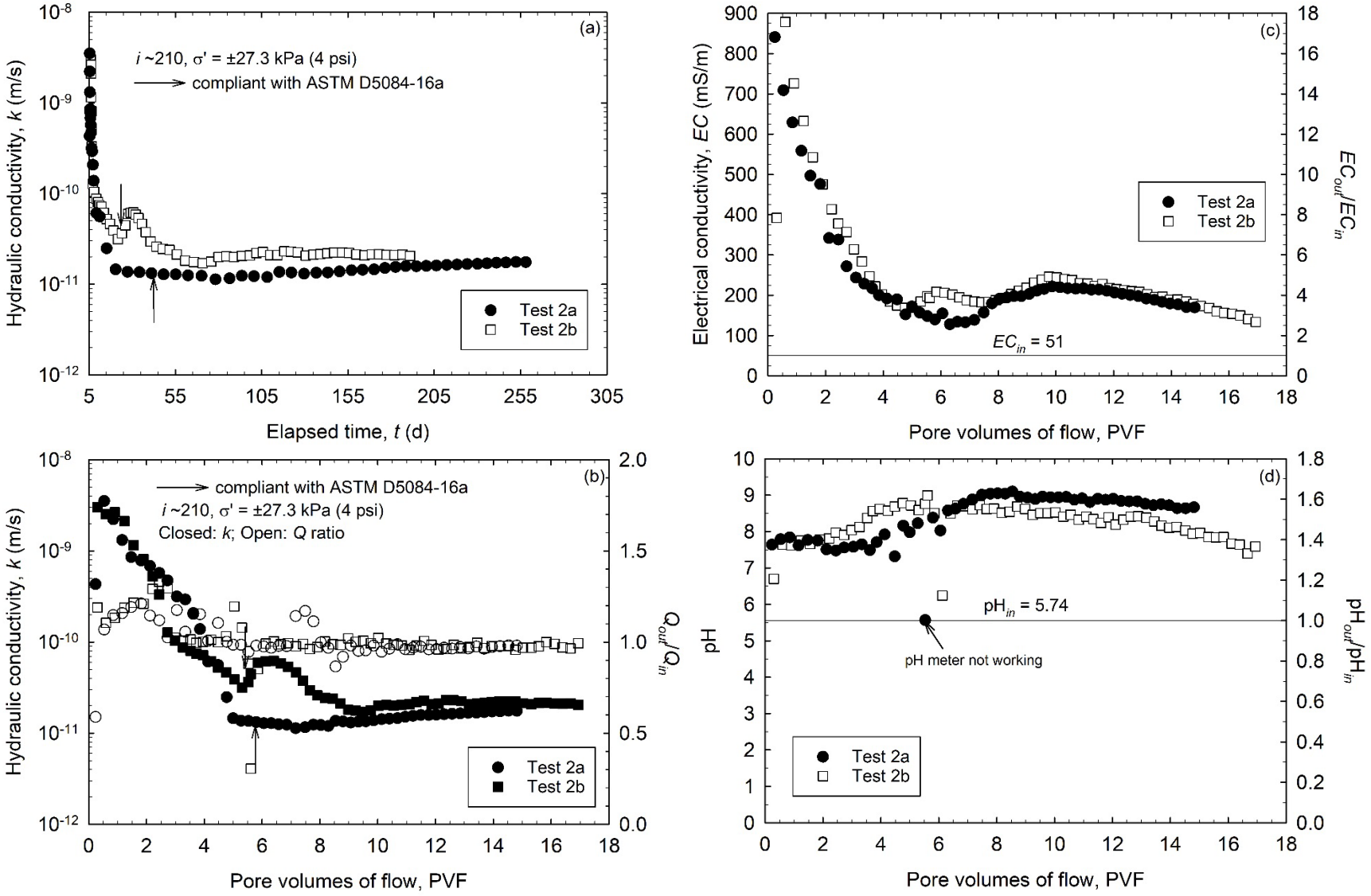

Figure E.1. Test results for falling headwater, constant tailwater method for prehydrated (Simplified P) tests with conservative water (Test Series 2): (a) hydraulic conductivity with respect to elapsed time, (b) hydraulic conductivity with respect to pore volumes of flow, (c) electrical conductivity, and (d) pH

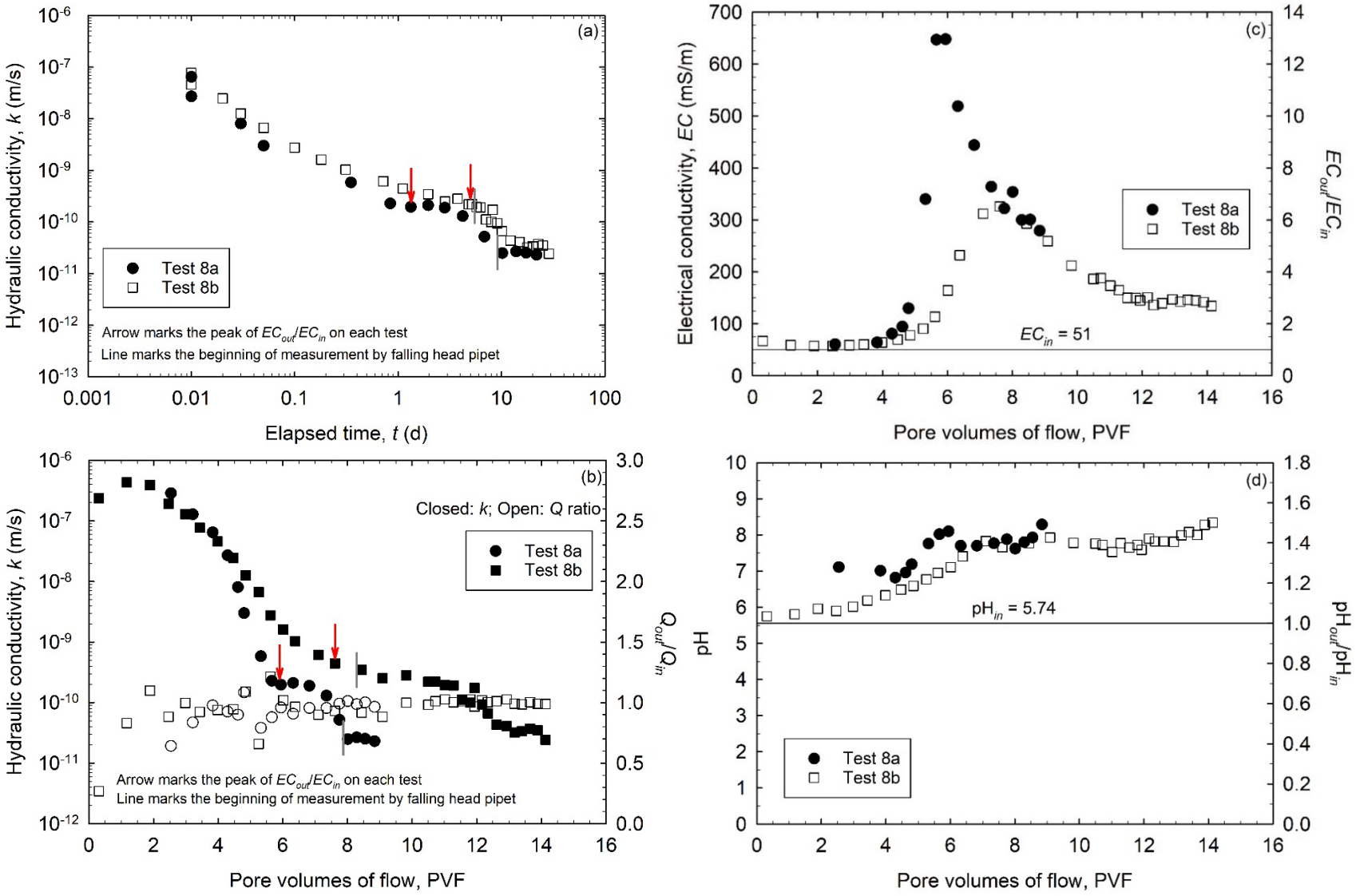

Figure E.2. (Color) Test results for non-prehydrated (Simplified NP) tests with conservative water (Test Series 8): (a) hydraulic conductivity with respect to elapsed time on log scale, (b) hydraulic conductivity with respect to pore volumes of flow, (c) electrical conductivity, and (d) pH

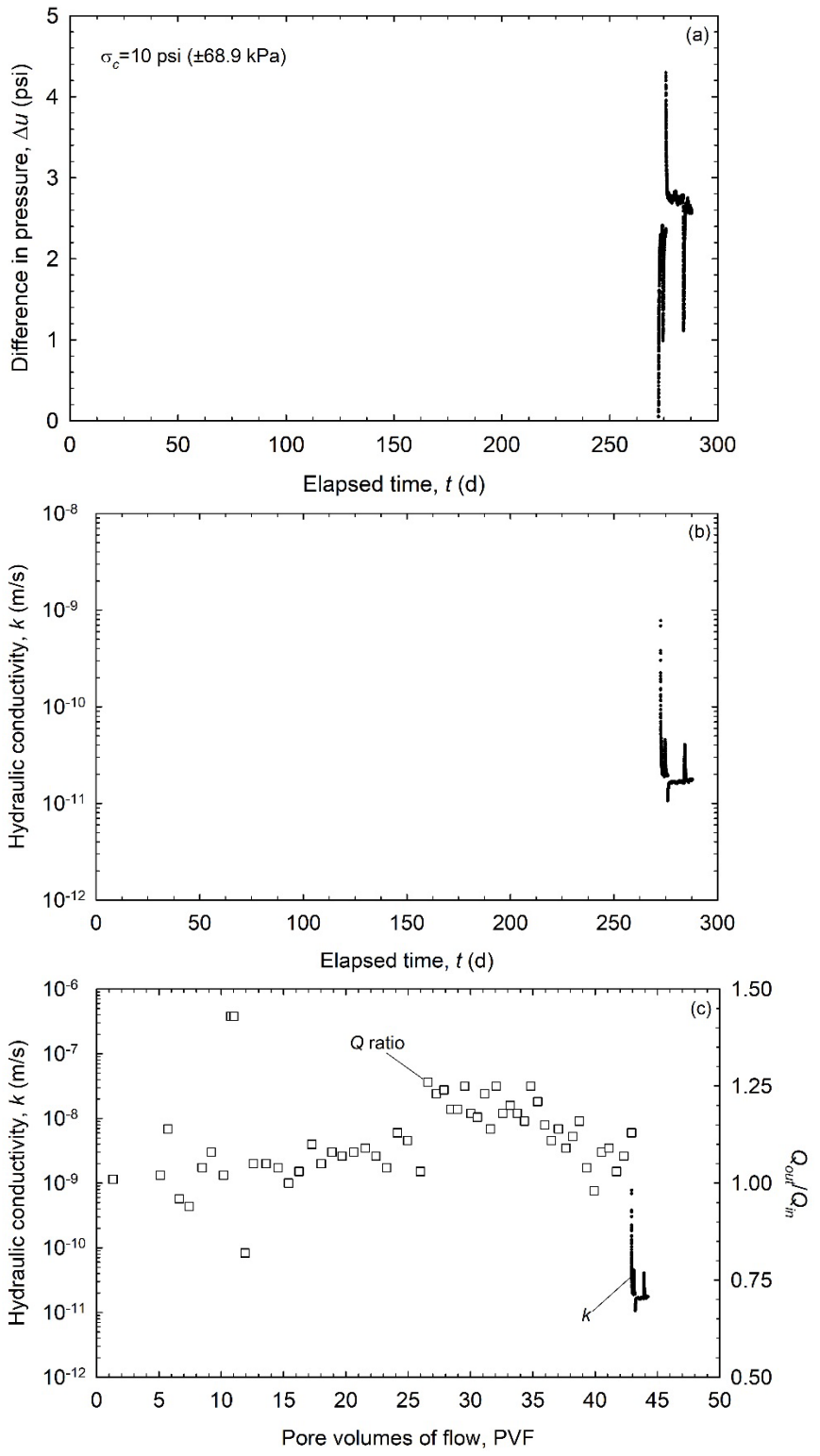

Figure E.3. Test results for constant rate-of-flow for prehydrated (Flow Pump P) test with conservative water by simultaneous infusing influent and withdrawing effluent (Test 11b): (a) difference in pore-water pressure with respect to elapsed time, (b) hydraulic conductivity and cell water reading with respect to elapsed time, and (c) hydraulic conductivity and volumetric flow ratio with respect to pore volumes of flow

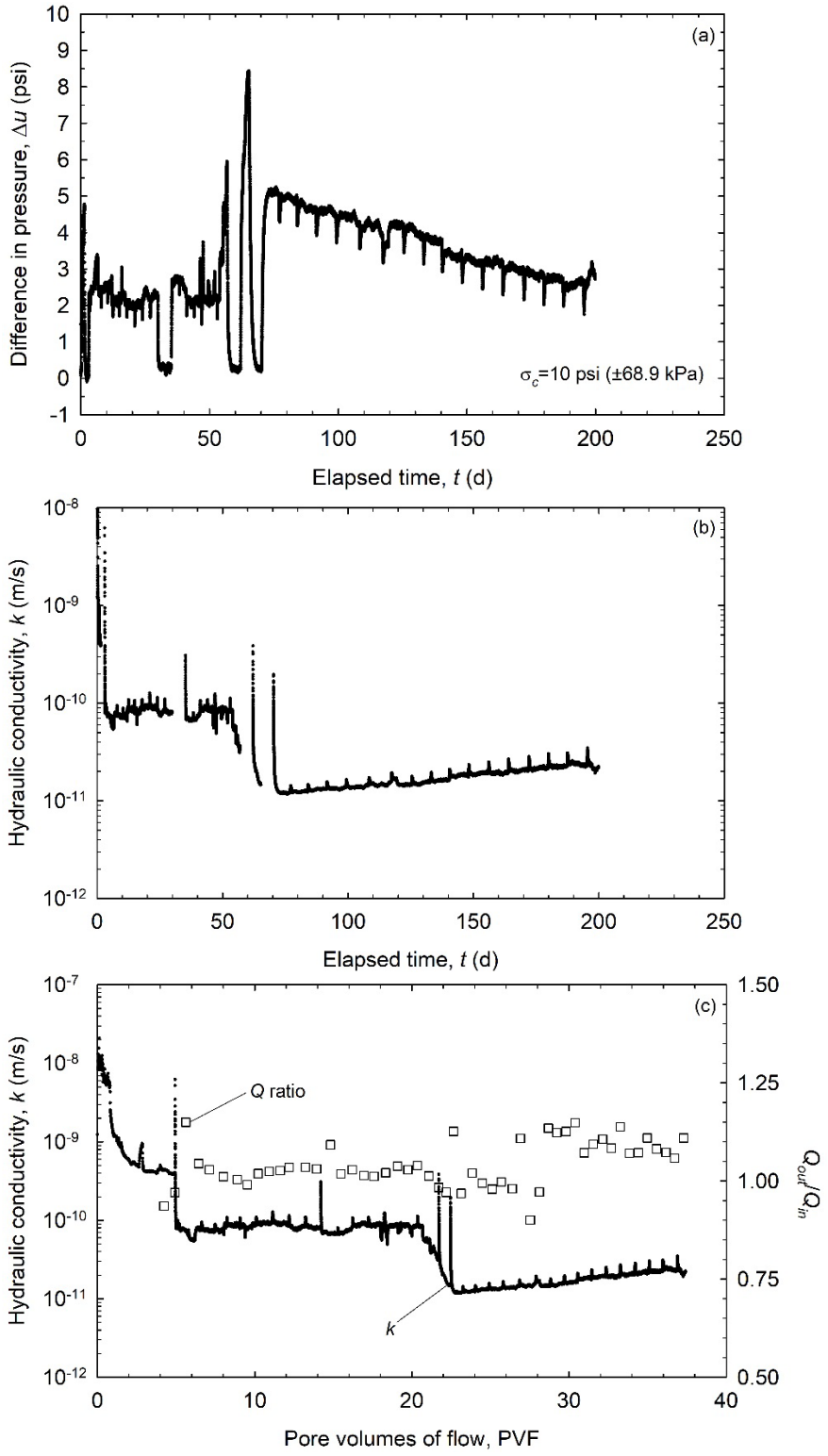

Figure E.4. Test results for constant rate-of-flow for prehydrated (Flow Pump P) test with conservative water by infusing influent only (Test 12b): (a) difference in pore-water pressure with respect to elapsed time, (b) hydraulic conductivity and cell water reading with respect to elapsed time, and (c) hydraulic conductivity and volumetric flow ratio with respect to pore volumes of flow

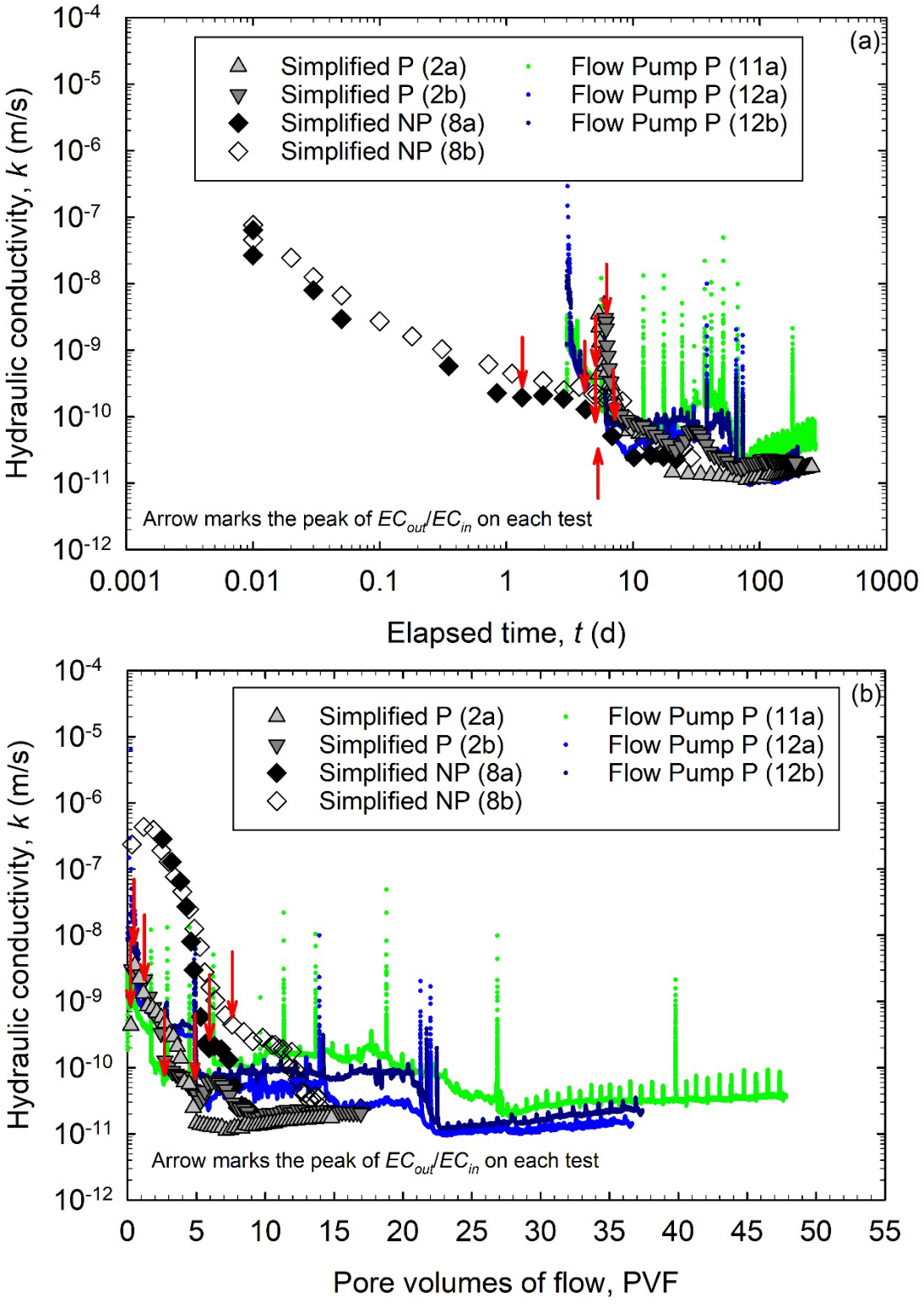

Figure E.5. (Color) Comparison of hydraulic conductivity from all test methods: (a) hydraulic conductivity with respect to elapsed time in log scale, (b) hydraulic conductivity with respect to pore volumes of flow. Test 11b data was not available for direct comparison.

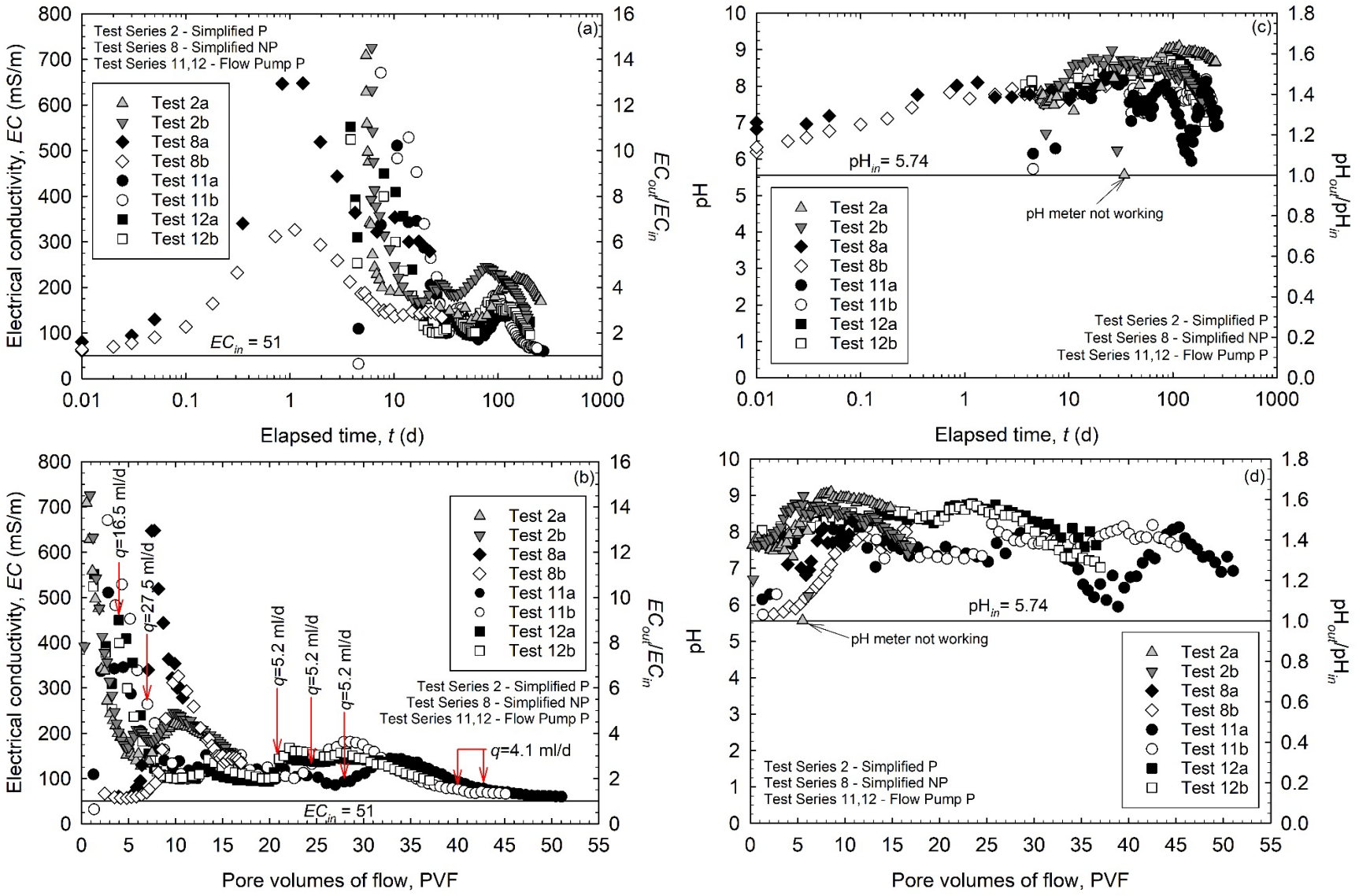

Figure E.6. (Color) Effect of diffusion illustrated by: (a) electrical conductivity versus elapsed time in log scale and (b) electrical conductivity versus pore volumes flow. Data on corresponding pH measurement provided in (c) and (d) for completeness